Electromagnetic scattering beyond the weak regime

Solving the problem of divergent Born perturbation series by Padé approximants

T.A. van der Sijs

Master of Science Thesis

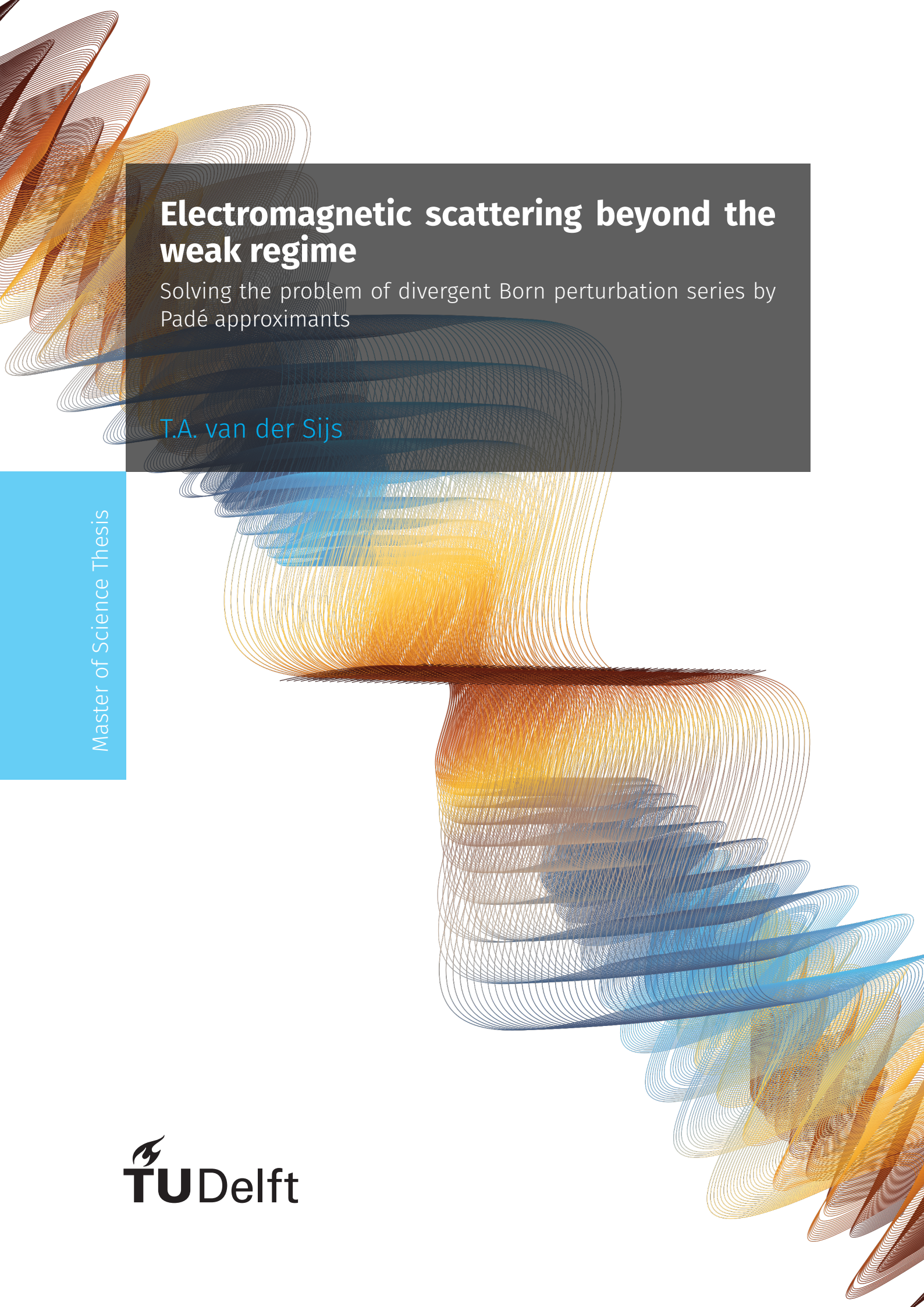

TU Delft

Electromagnetic scattering beyond the weak regime

Solving the problem of divergent Born perturbation series by Padé approximants

MASTER OF SCIENCE THESIS

For the degree of Master of Science in Applied Physics at Delft University of Technology

T.A. van der Sijs

September 9, 2020

Faculty of Applied Sciences (AS) · Delft University of Technology

Abstract

In many optical measurement methods one aims to retrieve the shape or physical properties of an unknown object by measuring how it scatters an incident optical field. Such an inverse problem is often approached by solving the corresponding direct scattering problem iteratively. Despite the existence of numerical methods, a perturbation approach could be a powerful way to solve those direct problems. In such an approach the field is expressed as a series, known as the Born series, in which the higher-order corrections represent multiple-scattering effects. This approach has the advantage that each term of the series has a clear physical meaning and that it can unveil much more about the scattering process than a purely numerical approach. Under (very) weak-scattering conditions the Born series converges and then often the first or first few terms of the series are sufficient to model the scattering. However, except under very special circumstances such as for x-rays where optical contrasts are extremely low, multiple scattering effects are very important and the Born series in general does not converge. Although multiple scattering could, in principle, allow resolving sub-wavelength details of the unknown object, this is in practice impeded by the divergent nature of the Born series.

In this thesis, we show how Padé approximation can be employed in electromagnetic problems to retrieve an accurate evaluation of the scattered field even under strong-scattering conditions. Padé approximants are rational functions that can offer improvements in two ways, namely, accelerating the rate of convergence of (already) converging series and analytic continuation of series outside its region of convergence. We apply the method to three scalar scattering problems. In one dimension we consider an infinitely thin slab and a slab of finite thickness, and in two dimensions an infinitely long cylinder. In particular, we study cases in the strong-scattering regime for which the Born series diverges. It will be shown that for all cases studied, Padé approximation retrieves an accurate result.

The presented method integrates multiple-scattering effects one by one and can therefore represent an important building block to the application of the Born series to direct and inverse problems, with potential applications in superresolution, optical metrology, and phase retrieval.

Table of Contents

Preface

When I started with this thesis, I had only a slight idea of what scientific research comprises, with only a bit of actual experience from my ten-week bachelor's end project. On one hand, the goal of the method researched in this thesis was clear from the start, since a proof of concept had already turned out promising. On the other hand, this thesis contained a subject that was new for the Optics group, which meant I had to take a deep dive into it. Doing this master's thesis has opened my eyes for scientific research, and I have consequently seized the opportunity to pursue a PhD in the Optics group.

The increased interest in doing research has been fueled by my supervisors Paul and Omar by being very enthusiastic about the subject, which made want to dig even more into the subject. I would like to thank Omar for his optimism and encouragement, and for always being open for discussion and taking time to explain some new concept to me, sharing any new insights and helping me attain a more rigorous understanding of optics and electromagnetism. I would like to thank Paul, first for giving me the opportunity of doing a master's thesis on a promising subject, and for, on one hand, thinking with a broad scope in our weekly meetings and coming up with new ideas on all fronts, and on the other hand also for thoroughly analyzing any derivation as well as scrutinizing my thesis, thereby even suggesting the smallest of improvements. Moreover, I would like to thank both Paul and Omar for all the opportunities for personal development, such as writing a scientific article and giving me the responsibility appertaining to the first author of an article.

Furthermore, I would like to thank the entire Optics group—office companions, support staff, and everyone else—and I am grateful for having been part of it in the past period and for participating in all (scientific) activities.

Finally, I would like to thank my parents Arjan and Liliana and my sister Amanda for their unquenchable support and interest at all times. Last of all, I want to thank everyone that I have encountered throughout the past seven years in Delft—university friends (including during my exchange period in Lund), my year-club, roommates, team members at Project MARCH—, who have enriched my life in whatever way possible in the past years.

Delft, University of Technology
September 9, 2020

T.A. van der Sijs

"Physics is really nothing more than a search for ultimate simplicity, but so far all we have is a kind of elegant messiness."

— *Bill Bryson, A Short History of Nearly Everything*

CHAPTER 1

Introduction

Electromagnetic scattering problems

Contactless measurement methods based on light are of growing relevance because of their non-invasiveness, speed, and integrability in industrial processes. The common denominator of these methods is the fact that when a known electromagnetic field, typically in the visible range, interacts with an unknown object, a scattered field is produced in which information about the object gets encoded. Applications often require that the scattered field (or its intensity only) is measured in the far-field regime, that is, at distances of many wavelengths from the object.

By knowing the laws of physics that govern the interaction, useful information about the object can be retrieved from measurements of the scattered field. To accomplish this, it is required to solve a nonlinear inverse problem, which is the counterpart of a direct scattering problem in which the object is actually known and one aims to determine the scattered field. The inverse problem can be formally formulated by means of the Lippmann-Schwinger equation. Inverse electromagnetic problems play a main role in modern technologies, of which the most important example probably is metrology in the semiconductor sector. The nonlinear nature of the inverse problem stems from the fact that the scattered field *inside* the object is unknown and depends strongly on the object itself (namely its geometry and/or its permittivity) [1]. These problems are usually difficult to solve due to their nonlinearity and in many cases methods to approach them rely on iteratively solving the direct problem starting from some prior knowledge of the object. In every iteration, the object is estimated anew and then used to update the scattered electromagnetic field by solving the direct scattering problem. This is repeated until the iteration converges. In other words, the goal is to find the best estimate of the object which is compatible with a set of measurements.

The advantage of this iterative approach is that direct problems are mathematically well-posed, contrary to inverse problems, and there exist many different numerical tools—Finite Element Methods, Finite Difference Time-Domain, Rigorous Coupled Wave Analysis, just to name a few—to solve them nowadays, even for very complex geometries [2, 3, 4]. Resorting to those numerical solvers has, however, the downside of losing a comprehensible connection

with the underlying physical mechanisms of the solution. Thus, in view of their application in solving inverse problems, an analytical approach to direct scattering problems is still highly valuable.

Limitations of perturbation theory

In the direct scattering problem, the Lippmann-Schwinger equation can be solved analytically for the scattered field by using perturbation theory. The electromagnetic field is expressed as a sum of different perturbation orders. The zero-th order represents the unperturbed solution, while the first-order correction is denoted as the Born approximation [5, 6, 7]. Each additional term of the series can be added to the previous terms, which leads to a possibly more accurate estimate of the exact solution. As we will recall in Section 2.2, breaking down the solution into different contributions allows keeping the connection with the physics of the problem as each term of the series has a clear physical meaning, making it a clear advantage of a perturbation approach over numerical solvers.

Generally, the presence of the scatterer alters the incident field *inside* the scatterer. Two regimes can be distinguished according to the strength of this interaction, which depends on the size of the object and the permittivity contrast: the weak-scattering and the strong-scattering regime. If the interaction is weak enough, the first-order Born approximation, also referred to as the single-scattering approximation, can already provide a satisfactory estimate of the solution and higher-order corrections can safely be neglected. In the weak-scattering regime in general, higher-order terms of the Born series can be computed additionally to achieve a higher accuracy. On the other hand, when the interaction between the field and the scatterer is strong, one must go beyond the Born approximation and take the higher-order terms, representing multiple-scattering effects, into account. However, what most standard books do not stress enough is that the Born series diverges under these strong-scattering conditions, which frustrates the benefit of the whole approach [8]. This makes it an unpractical approach for problems under such strong-scattering conditions. Thus, despite the fact that multiple-scattering effects could, in principle, allow resolving sub-wavelength details of the unknown object in inverse problems, this possibility is in practice impeded by the divergent nature of the Born series.

This problem of divergence has been originally encountered in particle physics, where different methods have been investigated to circumvent it, ranging from iterative methods [9], to transforming the original Lippmann-Schwinger equation from a Fredholm to a Volterra structure by renormalization [10] or using other transformation-based methods [11].

Padé approximation as a semi-analytical approach

Nonlinear resummation techniques constitute another category of techniques that have been investigated in particle scattering physics to alleviate the problem of divergence. Padé approximation is such a resummation method in which the terms of a divergent series are cast into a different representation in order to (hopefully) yield a converging result. Simply put, Padé approximants are rational functions that are able to represent poles, whereas power series, such as the Born series, are not, which is exactly the reason such a series breaks down at a certain point. Padé approximants have several properties that make them beneficial over power series as a way to represent functions. First, Padé approximation can speed up the

rate of convergence of a (slowly) converging series, which is also seen in its relation to the Shanks transform as will be further discussed in Section 3.4. Secondly, Padé approximants can analytically continue a power series outside its region of convergence, such that they can yield useful results in cases where the original power series (strongly) diverges.

As explained earlier, it would be extremely useful to have a semi-analytical approach that integrates multiple-scattering effects for solving direct scattering problems in the area of optical metrology techniques [12, 13, 14, 15, 16, 17]. Padé approximation shows this potential of incorporating multiple-scattering effects.

In the literature on scattering, Tani applied Padé approximants to the K-matrix in potential scattering [18, 19, 20], whereas Gammel applied the method to neutron-deuteron scattering [21]. Chisholm more generally considered the application of the Padé method to a certain type of linear integral equations [22]. In more specific works, the method was applied to a Yukawa potential [23], to an exponential potential [24], to three-body problems [25], and to elastic particle scattering [26]. In two works by Baker, a broad overview of knowledge of Padé approximants is compounded, including applications in (particle) scattering physics [27, 28].

Objective

In this thesis, we investigate the method of Padé approximants as a way to overcome the problem of divergence of the Born series in electromagnetic scattering problems. Our goal is to show that one can still make use of the information provided by the terms of the divergent Born series and obtain accurate results out of perturbative methods, even in the strong-scattering regime. We will consider one-dimensional (1D) and two-dimensional (2D) scalar scattering problems, for which a closed-form expression for the analytical solution can be found. This can be used for comparison when assessing the method of Padé approximants. We will both consider cases under weak- as well as strong-scattering conditions. For the former the aim is to study the effects of series acceleration by Padé approximant, whereas for the latter we want to investigate whether Padé approximants can be used to obtain an accurate evaluation of the field from a divergent series.

Outline of this thesis

In Chapter 2 we start by laying out the scalar direct scattering problem and its perturbative solution. We introduce Padé approximants and how they can be applied to this problem in Chapter 3.

The Padé method is first applied in Chapter 4 to the simple, though unrealistic problem of an infinitely thin 1D slab. Its simplicity allows us to treat the problem completely analytically, such that we can get a more intuitive grasp on how the method works. In Chapter 5 we elaborate on this approach, by applying it to the 1D case of a slab placed in a vacuum, where we implement some of the calculations numerically. Subsequently, we extend the procedure to a 2D problem in Chapter 6: that of an infinitely long cylinder. We conclude the thesis in Chapter 7 and discuss the implications of this new approach.

Parts of the findings in this study have already been published by us in an article in Physical Review Research, a new open-access journal [29].

CHAPTER 2

Electromagnetic scattering theory

2.1 Electromagnetic scattering

Electromagnetic scattering is the interaction between light and matter. An incoming wave is distorted by an object, called the scatterer. Electromagnetic scattering theory describes phenomena such as the scattering of sunlight by molecules and aerosols in the atmosphere and is used in optical imaging—in particular in near-field optics—, with applications such as measuring the quality of optical coatings and detecting defects. Electromagnetic scattering theory has many similarities with quantum scattering, which often involves the scattering of particles, and acoustic scattering. Scattering is a phenomenon that is closely related to diffraction. In fact, diffraction is in a sense a result of scattering or can be seen as a particular type of scattering.

In practical applications, we are often interested in inverse scattering problems which concern determining the properties of an object instead of determining the outgoing scattered waves. Inverse scattering problems are however *ill-posed* problems because they are very difficult to solve. Often inverse problems are tackled in an iterative way, where at each iteration the corresponding direct problem is solved. In this thesis we focus on a new method to solve the direct scattering problem. This method requires very little memory and is computationally fast. Moreover, since it is intrinsically linked to multiple scattering, it is very suitable for studying the influence of multiple scattering on the resolution that can be obtained in solving inverse problems.

Since we aim this study to be a proof of concept of the application of Padé approximants to direct problems in electromagnetic scattering, we limit ourselves to scalar scattering problems, which are less complex and moreover less computationally expensive when doing numerical calculations. Therefore, we will only treat scalar electromagnetic wave theory in this chapter.

2.1.1 Maxwell's equations

We assume that the reader has a basic knowledge of electrodynamics and we will therefore not go into the details of the general theory, but we will mention which assumptions we

make and consequently which physical quantities are relevant and to which extent Maxwell's equations can be simplified. First, we only consider complex time-harmonic fields, which depend on time by a factor $\mathrm{e}^{-i\omega t}$, with $\omega > 0$ the angular frequency. For brevity, we leave out this factor in all equations. Secondly, we assume that the permeability of all materials considered in this thesis is that of vacuum, i.e, $\mu = \mu_0$ such that $\mu_r = 1$, because at optical frequencies by far most materials are nonmagnetic. With these two considerations in mind, Maxwell's equations in matter reduce to

$$\nabla \cdot \mathbf{H} = 0, \tag{2.1a}$$
$$\nabla \times \mathbf{E} = i\omega\mu_0 \mathbf{H}, \tag{2.1b}$$
$$\nabla \cdot \mathbf{D} = \rho, \tag{2.1c}$$
$$\nabla \times \mathbf{H} = \mathbf{J} - i\omega \mathbf{D} \tag{2.1d}$$

with the constitutive relations

$$\mathbf{D} = \varepsilon \mathbf{E}, \tag{2.2a}$$
$$\mathbf{J} = \kappa \mathbf{E}. \tag{2.2b}$$

We use κ for the conductivity since σ will be used as a perturbation parameter. The permittivity ε can spatially vary, that is, $\varepsilon(\mathbf{r}) = \varepsilon_r(\mathbf{r})\varepsilon_0$, and the relative permittivity ε_r has a (possibly) complex value with positive imaginary part.

2.1.2 Waves in vacuum

The wave equation in vacuum for a scalar field U, which can be any component of the $\mathbf{E}$ or $\mathbf{H}$ field, reads

$$\nabla^2 U(\mathbf{r}, t) - \frac{1}{c^2}\frac{\partial^2}{\partial t^2} U(\mathbf{r}, t) = 0, \tag{2.3}$$

where $\mathbf{r}$ is the position vector (depending on the dimensionality of the problem at hand), t is time and c is the light velocity in vacuum. The time-independent equation, which holds for time-harmonic monochromatic fields and is known as the Helmholtz equation, reads

$$\nabla^2 U(\mathbf{r}) + k_0^2 U(\mathbf{r}) = 0, \tag{2.4}$$

which can be in either one, two or three dimensions. The wave number in vacuum k_0 is related to ω by $k_0 = \omega\sqrt{\varepsilon_0\mu_0}$. The Green's function of the Helmholtz equation satisfies

$$\nabla^2 G_0(\mathbf{r}; \mathbf{r}') + k_0^2 G_0(\mathbf{r}; \mathbf{r}') = -\delta(\mathbf{r} - \mathbf{r}'), \tag{2.5}$$

where the subscript 0 is used to indicate that it is the free-space Green's function. Note that we define it with a minus sign on the right-hand side[1]. Table 2.1 lists $G_0(\mathbf{r}; \mathbf{r}')$ for one, two and three dimensions, which can for instance be found in Ref. [30].

[1] It is equally fine to define it with the plus sign, in which case $G_0(\mathbf{r}; \mathbf{r}')$ is the same up to an overall minus sign. Also, an extra minus sign would appear in equations such as Eq. (2.9) as a result.

Table 2.1: Free-space Green's function of the Helmholtz equation. $H_0^{(1)}$ is the outward radiating Hankel function of the first kind.

1D	$G_0(z;z') = \dfrac{i}{2k_0}\mathrm{e}^{ik_0\lvert z-z'\rvert}$
2D	$G_0(\mathbf{r};\mathbf{r}') = \dfrac{i}{4}H_0^{(1)}(k_0\lvert\mathbf{r}-\mathbf{r}'\rvert)$
3D	$G_0(\mathbf{r};\mathbf{r}') = \dfrac{\mathrm{e}^{ik_0\lvert\mathbf{r}-\mathbf{r}'\rvert}}{4\pi\lvert\mathbf{r}-\mathbf{r}'\rvert}$

2.1.3 The scattering problem as a boundary value problem for the Helmholtz equation

The incident field $U_i(\mathbf{r})$ is defined as the field that would be present if there were no objects, i.e., if only the homogeneous background medium is present. This field thus satisfies the homogeneous Helmholtz equation (2.4). When there are scattering objects, a secondary field, called the scattered field $U_s(\mathbf{r})$, is generated. The total field $U(\mathbf{r})$ is the sum of the incident and scattered field and satisfies the scalar Helmholtz equation in the presence of scattering objects:

$$\nabla^2 U(\mathbf{r}) + k_0^2 \varepsilon_r(\mathbf{r}) U(\mathbf{r}) = 0. \tag{2.6}$$

The total field also satisfies the boundary condition that $U(\mathbf{r}) - U_i(\mathbf{r}) = U_s(\mathbf{r})$ is propagating outward for large r, namely,

$$\lim_{r\to\infty} r\left(\frac{\partial U^s(\mathbf{r})}{\partial r} - ik_0 U(\mathbf{r})\right) = 0. \tag{2.7}$$

The properties of the scattering objects are defined through the spatially varying relative permittivity $\varepsilon_r(\mathbf{r})$. The wave number in matter k is therefore also spatially varying, because it equals $\sqrt{\varepsilon_r(\mathbf{r})}k_0$. We note however that the scalar Helmholtz equation for each component of the electromagnetic field is equivalent to Maxwell's equations only in homogeneous media.

We are interested in the behaviour of scattering by a d-dimensional bounded object, whose domain is denoted by Ω, located in a background medium in d-dimensional space consisting of vacuum or air. It is therefore useful to reformulate the problem as

$$\nabla^2 U(\mathbf{r}) + k_0^2 U(\mathbf{r}) = -k_0^2 \Delta\varepsilon_r(\mathbf{r}) U(\mathbf{r}), \qquad \mathbf{r} \in \mathbb{R}^d, \tag{2.8}$$

where the permittivity contrast $\Delta\varepsilon_r(\mathbf{r}) = \varepsilon_r(\mathbf{r}) - 1$ is introduced, which is the difference between the local relative permittivity of the object and that of vacuum or air[2]. This equation for the total field is an inhomogeneous version of Eq. (2.4), though the right-hand side depends on the field $U(\mathbf{r})$ itself and is therefore not simply solvable by means of the free-space Green's function. In the formulation of the scalar scattering problem in terms of the Helmholtz equation it is implicitly assumed that at interfaces where the permittivity has a jump, both $U(\mathbf{r})$ and its normal derivative are continuous. In the case of a perfect conductor, the electric field

[2]For other background media, it would suffice to introduce $\Delta\varepsilon_r(\mathbf{r}) = \varepsilon_{r,2}(\mathbf{r}) - \varepsilon_{r,1}$, the subscripts 1 and 2 denoting the background medium and object medium.

does not penetrate the scatterer such that the tangential components of the electric field must be 0. Because we consider $U(\mathbf{r})$ as one of these components, we take as boundary condition for the case of a perfect conductor: $U(\mathbf{r}) = 0$ on the boundary.

2.1.4 Integral formulation of the scattering problem

The Helmholtz equation for the total field $U(\mathbf{r})$ has an equivalent integral form that follows from Eqs. (2.5) and (2.8), which is the Lippmann-Schwinger equation:

$$U(\mathbf{r}) = U_i(\mathbf{r}) + k_0^2 \int_\Omega G_0(\mathbf{r};\mathbf{r}')\Delta\varepsilon_r(\mathbf{r}')U(\mathbf{r}')\,\mathrm{d}\mathbf{r}'. \tag{2.9}$$

This representation is valid for all $\mathbf{r}$. The integral depends on the total field $U(\mathbf{r})$ inside the scatterer, which implies that Eq. (2.9) is an integral equation for $U(\mathbf{r})$. Hence, if Eq. (2.9) is solved for $U(\mathbf{r})$ *inside* Ω, the result can be substituted in the right-hand side of Eq. (2.9) to obtain $U(\mathbf{r})$ for any $\mathbf{r}$, also outside of Ω.

The Lippmann-Schwinger equation is a Fredholm integral equation of the second kind. Moreover, it is linear in both the permittivity contrast and the field *separately*, but it is bilinear in both. The latter property shows that the inverse problem of retrieving $\Delta\varepsilon_r(\mathbf{r})$ from a set of solutions $U(\mathbf{r})$ is a nonlinear problem. Equation (2.9) can also be written in terms of the scattered field $U_s(\mathbf{r}) = U(\mathbf{r}) - U_i(\mathbf{r})$:

$$U_s(\mathbf{r}) = k_0^2 \int_\Omega G_0(\mathbf{r};\mathbf{r}')\Delta\varepsilon_r(\mathbf{r}')\left[U_i(\mathbf{r}') + U_s(\mathbf{r}')\right]\mathrm{d}\mathbf{r}', \tag{2.10}$$

which subsequently can be split in an integral with the known U_i (and can therefore be calculated), and an integral with the unknown U_s:

$$U_s(\mathbf{r}) = k_0^2 \int_\Omega G_0(\mathbf{r};\mathbf{r}')\Delta\varepsilon_r(\mathbf{r}')U_i(\mathbf{r}')\,\mathrm{d}\mathbf{r}' + k_0^2 \int_\Omega G_0(\mathbf{r};\mathbf{r}')\Delta\varepsilon_r(\mathbf{r}')U_s(\mathbf{r}')\,\mathrm{d}\mathbf{r}'. \tag{2.11}$$

2.1.5 Types of scattering problems

Depending on the application, some parameters of a scattering problem are known while others are unknown and the combination of these determines the type of scattering problem. In a direct scattering problem, the goal is to determine how the object scatters the incident field, while the properties (being the geometry and permittivity) of the object are known. This is in general a well-posed type of problem since the integral operator belongs to the class of compact operators [1]. In an inverse problem the scattered field (usually far away from the object) is detected for a certain set of given incident fields and the permittivity (and linked to that the geometry) of the object have to be determined from these data. In contrast to the direct problem, the inverse problem is non-linear since the integral depends on the permittivity contrast both directly and through the unknown scattered field in the interior of the object. This constitutes a category of ill-posed problems and the inverse problem is therefore often severely affected by noise among others. Better results can be obtained with a priori information. Typically, inverse problems require solving the direct problem iteratively to get an iterated estimate of the scattered field.

2.1.6 Similarities with quantum scattering

The mathematics of electromagnetic scattering according to the Helmholtz equation are in many ways very similar to that of quantum scattering [31]. Since in Chapters 4 to 6 we will be treating problems that have an analytical solution, it could be instructive to consider their quantum-mechanical counterparts while taking the similarities and differences into account. Making it more concrete, when we consider the time-independent Schrödinger equation

$$-\frac{\hbar^2}{2m}\nabla^2\psi(\mathbf{r}) + V(\mathbf{r})\psi(\mathbf{r}) = E\psi(\mathbf{r}) \tag{2.12}$$

for a wave function $\psi(\mathbf{r})$ and rewrite it as

$$[\nabla^2 + k_0^2]\psi(\mathbf{r}) = Q(\mathbf{r})\psi(\mathbf{r}), \tag{2.13}$$

we see that it has the same form as the Helmholtz equation in matter [32]. In the Schrödinger equation we have $k_0 = \sqrt{2mE}/\hbar$ and $Q(\mathbf{r}) = k_0^2 V(\mathbf{r})/E$, while in the Helmholtz equation $k_0 = \omega/c$ and $Q(\mathbf{r}) = -k_0^2\Delta\varepsilon_r(\mathbf{r})$. The permittivity contrast is in this comparison analogous to the potential $V(\mathbf{r})$ by $-E\Delta\varepsilon_r(\mathbf{r}) \leftrightarrow V(\mathbf{r})$, and in Ref. [33] the authors even consider to refer to it as the 'light potential'.

2.2 Direct scattering: A perturbation approach

As mentioned, in a direct scattering problem one knows (or assumes to know) the object and its properties as well as the chosen incident field, and the goal is to calculate the scattered field. In a limited number of cases, the analytical solution can be found and calculating the scattered field is straightforward. In other cases one can discretize Maxwell's equations and use the FDTD method, or one has to revert to the Lippmann-Schwinger equation which is difficult to handle due to its implicit nature. The problem with a numerical solver is however that one has to rely on the obtained results even though it more or less acts like a black box.

Perturbation theory, which is most often known from its application in quantum mechanics, is an analytical approach in which a problem that is very difficult to solve, is converted to an, often, infinite sequence of more simple problems. In practice, however, it is impossible to solve this infinite number of problems and it therefore does not eventually yield the exact solution. This is not directly a disadvantage compared to other methods, because those are often approximations as well, for instance because of the use of finite-sized grids. Perturbation theory forms the basis of the method that is set forth in this thesis and we will treat the concept in this section.

2.2.1 Born approximation

The Lippmann-Schwinger equation is difficult to handle due to its implicit nature, but a simple idea can circumvent this. One can assume that the interaction between the object and the field is so weak that the incident field is not distorted by it and that therefore the field inside the object is equal to the incident field. It is furthermore assumed that the scattered field does

not excite any secondary sources inside the scatterer. Hence, we take $U(\mathbf{r}) \approx U_i(\mathbf{r})$ for $\mathbf{r} \in \Omega$ in the integrand of the Lippmann-Schwinger equation:

$$U(\mathbf{r}) \approx U_i(\mathbf{r}) + k_0^2 \int_{\mathbf{r}'} G_0(\mathbf{r};\mathbf{r}')\Delta\varepsilon_r(\mathbf{r}')U_i(\mathbf{r}')\,\mathrm{d}\mathbf{r}'. \tag{2.14}$$

This is called the first Born approximation. Basically, it is assumed that $|U_s(\mathbf{r})| \ll |U_i(\mathbf{r})|$ which for an incident plane wave (with unit amplitude) means that the scattered field must be much smaller than unity.

Validity of the first Born approximation The validity of this approximation is limited to cases of weak interaction, which means that the permittivity contrast and the size of the scatterer relative to the wavelength are small. Two different criteria determine the validity of the approximation, one for the low- and the other for the high-frequency limit [34]. These are, respectively:

$$k_0^2 a^2 \left|\varepsilon_r(\mathbf{r}) - 1\right| \ll 1 \quad \text{for } k_0 a \ll 1, \tag{2.15a}$$
$$k_0 a \left|\varepsilon_r(\mathbf{r}) - 1\right| \ll 1 \quad \text{for } k_0 a \gg 1, \tag{2.15b}$$

where a is the diameter of the scatterer Ω, or more intuitively, the radius of the smallest circle or sphere that encloses the scatterer. The most important observation is that the validity of the first Born approximation not only depends on the permittivity contrast, but also on the size of the scatterer relative to the wavelength. In other references, criteria are often of a similar form [35, 36], though the argumentation on which they are based are different, such as the requirement that the phase change of the incident field when propagating through the scatterer should not exceed π [37]. In the case of Ref. [38], a criterion is derived specifically when using the first-order Born approximation for reconstruction of the scatterer by diffraction tomography. It is empirically derived based on the requirement that the average relative error of the reconstructed refractive index should not exceed $25\,\%$.

The first Born approximation works well for a variety of scattering problems in elementary particles, but is only of limited practical use in electromagnetic problems, because conditions (2.15a) or (2.15b) are hardly ever satisfied in practice. In Ref. [38] the first-order Born approximation is used in a diffraction tomography algorithm to reconstruct the permittivity of an infinitely long homogeneous cylinder. There, the approximation works reasonably well (i.e., the average relative error of the electric field is below $25\,\%$) for differences in refractive index between cylinder and background that are maximum 0.016. This corresponds to permittivity contrasts of up to 2.56×10^{-4} [38], which is very low compared to those of metals or semiconductors in practical applications.

Improvements Several variations to the classical Born approximation have been developed to deal with the convergence problem. An example is Ref. [39], where a modified Born series is constructed by adding an imaginary component to the wave number of the background medium so that the Green's function in a homogeneous medium decays with distance. This is compensated by an imaginary term in the (in our notation) permittivity contrast $\Delta\varepsilon_r$, but results in a converging Born series. However, this method appears to converge slowly for strong scatterers. Other examples include the quasi-linear and the higher-order generalized Born approximation [40, 41], and others [42, 11].

2.2.2 Perturbation series

The first Born approximation can in principle be iterated for an indefinite number of times to get an increasingly accurate result that (hopefully) converges to the exact solution. Effectively, the same is achieved when we introduce a power series expansion of the field in terms of a perturbation parameter σ

$$U^{(\sigma)}(\mathbf{r}) = \sum_{\ell=0}^{\infty} U_\ell(\mathbf{r})\sigma^\ell. \tag{2.16}$$

σ is an additional parameter that we introduce by inserting it in front of the permittivity contrast. The value of σ of interest is therefore $\sigma = 1$. The expansion is performed simultaneously with an introduction of σ in the Helmholtz equation and in the Lippmann-Schwinger equation:

$$\nabla^2 U(\mathbf{r}) + k_0^2 U(\mathbf{r}) = -\sigma k_0^2 \Delta\varepsilon_r(\mathbf{r}) U(\mathbf{r}), \tag{2.17}$$

$$U(\mathbf{r}) = U_i(\mathbf{r}) + \sigma k_0^2 \int_{\mathbf{r}'} G_0(\mathbf{r};\mathbf{r}')\Delta\varepsilon_r(\mathbf{r}')U(\mathbf{r}')\,\mathrm{d}\mathbf{r}'. \tag{2.18}$$

The object is therefore perceived as a perturbation superimposed on the background where σ is the variable strength of the perturbation. Since the strength of the perturbation is also determined by the permittivity contrast, the expansion is in that sense actually in terms of the permittivity contrast. To proceed, the expansion (2.16) is substituted in Eq. (2.18) and we obtain:

$$\sum_{\ell=0}^{\infty} U_\ell(\mathbf{r})\sigma^\ell = U_i(\mathbf{r}) + \sum_{\ell=0}^{\infty} \sigma^{\ell+1} k_0^2 \int_{\mathbf{r}'} G_0(\mathbf{r};\mathbf{r}')\Delta\varepsilon_r(\mathbf{r}')U_\ell(\mathbf{r}')\,\mathrm{d}\mathbf{r}'. \tag{2.19}$$

When equating the terms with equal powers of σ, we get:

$$U_0(\mathbf{r}) = U_i(\mathbf{r}), \tag{2.20a}$$

$$U_1(\mathbf{r}) = k_0^2 \int_\Omega G_0(\mathbf{r};\mathbf{r}')\Delta\varepsilon_r(\mathbf{r}')U_0(\mathbf{r}')\,\mathrm{d}\mathbf{r}', \tag{2.20b}$$

$$U_2(\mathbf{r}) = k_0^2 \int_\Omega G_0(\mathbf{r};\mathbf{r}')\Delta\varepsilon_r(\mathbf{r}')U_1(\mathbf{r}')\,\mathrm{d}\mathbf{r}', \tag{2.20c}$$

$$\vdots$$

$$U_{\ell+1}(\mathbf{r}) = k_0^2 \int_\Omega G_0(\mathbf{r};\mathbf{r}')\Delta\varepsilon_r(\mathbf{r}')U_\ell(\mathbf{r}')\,\mathrm{d}\mathbf{r}', \tag{2.20d}$$

where the incident field, which should satisfy the unperturbed equation, is the zero-th order term. The perturbation approach is thus a method to recurrently calculate higher-order corrections.

By introducing the Lippmann-Schwinger operator $\mathcal{L}$ defined as

$$\mathcal{L}f(\mathbf{r}) = k_0^2 \int_\Omega G_0(\mathbf{r};\mathbf{r}')\Delta\varepsilon_r(\mathbf{r}')f(\mathbf{r}')\,\mathrm{d}\mathbf{r}', \tag{2.21}$$

we can also write the Born series as a summation of repeated applications of $\mathcal{L}$ to the incident field, namely

$$U^{(\sigma)}(\mathbf{r}) = U_i(\mathbf{r}) + \sigma\mathcal{L}U_i(\mathbf{r}) + \sigma^2\mathcal{L}\mathcal{L}U_i(\mathbf{r}) + \dots. \tag{2.22}$$

When a sufficient number N of terms have been calculated to get a meaningful result, the series is truncated and σ is set to 1 to get the partial sum

$$U^{(1)[N]}(\mathbf{r}) = U_i(\mathbf{r}) + U_1(\mathbf{r}) + U_2(\mathbf{r}) + ... + U_N(\mathbf{r}), \tag{2.23}$$

which then is a series approximation of the exact solution $U(\mathbf{r})$. However, this is under the condition that the series converges, a condition that we will discuss in the next section.

The $\ell = 1$ term is referred to as the single-scattering term, which means that the incident wave excites the dipoles inside the object, but these dipoles do not interact. The $\ell > 1$ terms describe the phenomenon referred to as multiple scattering and each term is a higher order of multiple scattering. The $\ell = 2$ term can be interpreted as the result of the incident wave being scattered twice by the dipoles inside the object during two scattering events. In other words, the first scattering event excites a secondary source which in turn radiates a wave which then can be scattered maximum once by another dipole in the object. The $\ell = 3$ term describes the case of maximum three scattering events, and so on. The first-order Born approximation is therefore a single-scattering approximation, where multiple-scattering effects are neglected. It can be shown that when multiple scattering is neglected and only the first Born approximation is applied, the information about the relative permittivity function $\Delta\varepsilon_r(\mathbf{r})$ that can be recovered from measurements of the scattered far field is limited to details of size larger than half the wavelength [15]. Multiple-scattering effects are in some sense equivalent to illumination by a near field and therefore by taking multiple scattering into account it can happen that higher spatial frequency information is encoded in the far field. However, resolution enhancement due to multiple scattering is only significant under very special (resonant) circumstances.

Note that in order to calculate the $(\ell + 1)$-th term in the series it is only necessary to know the previous term $U_\ell(\mathbf{r})$ inside the scatterer, since the integration domain is Ω. Therefore, one option is to calculate the terms only for all $\mathbf{r} \in \Omega$ and then use Eq. (2.23) as an approximation to the total field inside the scatterer, if the Born series converges. Then $U(\mathbf{r})$ for $r \notin \Omega$ can be found with the Lippmann-Schwinger equation (2.9). The other option is to calculate each term in Eq. (2.23) separately for all $\mathbf{r}$ of interest.

To put the Born series in a broader perspective, it is in fact a Liouville-Neumann series which is a type of series used to solve Fredholm integral equations of the second kind. Furthermore, the Born series is an expansion of the field, but similar expansions can also be obtained for the Green's function, which we discuss in Appendix A.2.

Integrability requirements A small note is made about the integrability of the Lippmann-Schwinger integrals in Eq. (2.20). One of the requirements for the existence of the integrals is that $\Delta\varepsilon_r(\mathbf{r})$ should be of compact support on Ω, which is obviously satisfied because an object always has a bounded volume. Secondly, the terms in the Born series are bounded as long as the potential is less singular than r^{-2} at any point inside the object, according to Ref. [19]. In Chapter 4 we study a scattering problem in which $\Delta\varepsilon_r(\mathbf{r})$ contains a singularity, but in practice $\Delta\varepsilon_r(\mathbf{r})$ has no singularities. An exception is a perfect conductor, where you get an integral equation on the boundary of the conductor. Such a case is outside our scope in this study.

Born series for a homogeneous object

In the case of a homogeneous object, the permittivity is constant throughout Ω, simplifying the calculation of the Born series. We define $U'_\ell(\mathbf{r})$ for $\ell > 0$ by taking $\Delta\varepsilon_r(\mathbf{r})$ outside the integrals in Eq. (2.20). Then $\Delta\varepsilon_r$ can be included in sigma, such that the series solution becomes

$$U(\mathbf{r}, \sigma) = \sum_{\ell=0}^{\infty} (\sigma \Delta\varepsilon_r)^\ell U'_\ell(\mathbf{r}). \tag{2.24}$$

The terms $U'_\ell(\mathbf{r})$ are thus calculated by setting $\Delta\varepsilon_r = 1$ in the integrals in Eq. (2.20). An important consequence is that the perturbation orders can be calculated for a certain Ω independent of the permittivity of the object, provided it is homogeneous. Only afterwards each term is scaled with a factor that depends on the medium, so that the whole computation of the integrals therefore need only be performed once for different materials.

2.2.3 Convergence of the Born series

In Section 2.2.1 we have discussed the validity of the first Born approximation and its dependence on the wavelength and object size and material. While for the first Born approximation the validity criterion is based on the question which error is acceptable, it is in principle possible with the Born series to keep calculating higher-order terms until a desired accuracy is achieved. The validity of the Born series is however determined by its region of convergence. Since the Born series is in fact a Taylor series, the series always converges at most in some disc in the complex plane around the point around which the function is expanded, which in our case is $\sigma = 0$. The radius of the disc is determined by the distance to the nearest pole in the complex plane of the expanded function. Since the Born series arises by repeated application of the Lippmann-Schwinger integral operator Eq. (2.21), the convergence condition can be said to be that the operator norm of $\mathcal{L}$ should not exceed 1. As a side note, $\mathcal{L}$ is a Fredholm operator. If the Born series converges, it is considered to be in the weak-scattering regime, while cases of divergent series are in the strong-scattering regime. Like the validity of the first Born approximation, the smaller the object (relative to the wavelength) and the lower the permittivity contrast, the better the Born series converges. Typically, objects that are of a material of practical interest correspond to cases in the strong-scattering regime, even for objects the size of about a wavelength. Hence for almost all cases of interest the Born series does not converge and is not of use. Many cases in which semiconductors, metals or dielectrics are used suffer from this problem.

Convergence metric

As we aim to use the Padé method to get useful results for (strongly) diverging Born series, we need a metric that indicates whether a certain case is in the weak- or strong-scattering regime (and by a certain case we mean an object and a specific material). Also, if it is in the strong-scattering regime, we want to know how strong the scattering is. For instance, the validity criterion for the first Born approximation is an indication of whether the scattering is weak enough for the first Born approximation to be accurate.

When calculating the Born series numerically, we can easily calculate a high number of terms in the series and observe whether the terms increase in size and moreover deduce thereof the

degree of convergence or divergence of the series. To this end, we introduce the parameter $\Gamma^{(n)}_{\text{Born}}$, where the superscript (n) denotes that it is a numerically deduced parameter. We define it as:

$$\Gamma^{(n)}_{\text{Born}} = \left(\frac{A_{\ell_{\text{max}}}}{A_0} \right)^{1/\ell_{\text{max}}}, \tag{2.25}$$

where ℓ_{max} is the highest-order term of the Born series that is computed and A_ℓ is the maximum over the scatterer of the absolute value of the Born term of order ℓ, that is, $A_\ell = \max_{\mathbf{r}\in\Omega} |U_\ell(\mathbf{r})|$. The parameter $\Gamma^{(n)}_{\text{Born}}$ is an estimate of how many times larger or smaller a term of order ℓ is than the term of order $\ell - 1$. If $\Gamma^{(n)}_{\text{Born}} < 1$, it is an indication that the Born series may converge. For it to be a guarantee for the convergence, one should take the limit $\ell_{\text{max}} \to \infty$, which in practice is of course not possible. Furthermore, if $\Gamma^{(n)}_{\text{Born}} > 1$, it is an indication that the Born series diverges, but this is not with certainty the case for all points, because A_ℓ is the maximum over $r \in \Omega$. Even when $\ell_{\text{max}} \to \infty$, it is not certain that the series diverges for all points. To be sure, one should do the test for $|U_\ell(\mathbf{r})|$ instead of A_ℓ and with $\ell_{\text{max}} \to \infty$.

In Chapters 5 and 6 we also introduce the parameter $\Gamma^{(a)}_{\text{Born}}$ as another indicator of the degree of divergence of the Born series, where the superscript (a) indicates that it is deduced from analytical expressions of the Born series.

2.2.4 Perturbation solution of the Green's function

Similar to the expansion of the field $U(\mathbf{r})$ in Section 2.2.2, we can perform a perturbation expansion of the full Green's function $G(\mathbf{r};\mathbf{r}')$. The corrections to the free-space Green's function $G_0(\mathbf{r};\mathbf{r}')$ are also calculated with a recurrence relation, namely, Eq. (A.9). We refer to Appendix A for more details on this expansion.

CHAPTER 3

Padé approximation

3.1 Introduction

The Born series is of practical use for weak scattering, because then the series converges to the correct solution. In strong-scattering cases, however, the series diverges and the terms in Eq. (2.16) often grow exponentially with ℓ. Also, even if the Born series converges, it might converge very slowly and one would need to calculate many higher-order terms to get a reliable answer which can be computationally expensive. The method of Padé approximants can help overcome both issues.

First, concerning the problem of divergence, Padé approximation is a so-called resummation method with which one aims to assign a finite value to a diverging series by making use of its properties and detecting (latent) patterns in its terms. Padé approximants are used to find an analytic continuation of the diverging series—in our case the Born series—outside the region of convergence. In short, these approximants are able to represent the poles of the approximated function and which are the cause for the breakdown of the Taylor series. Of interest are the questions whether a sequence of Padé approximants converges to the exact solution and how one can determine the error of a certain approximant.

Secondly, Padé approximation is a method to speed up the convergence of a slowly converging series, such that with an equal amount of terms, a more accurate answer is retrieved. It is closely related to continued fractions, the Shanks transform and the ε-algorithm which are also methods to accelerate the summation of series.

3.1.1 Padé rational function

A Padé approximant is a rational function, i.e., a fraction where both the numerator and denominator are polynomials of certain degrees M and N respectively:

$$P_N^M(\sigma) = \frac{Q_M(\sigma)}{R_N(\sigma)} = \frac{\sum_{m=0}^{M} A_m^{(M)} \sigma^m}{\sum_{n=0}^{N} B_n^{(N)} \sigma^n}, \tag{3.1}$$

where $A_m^{(M)}$ and $B_n^{(N)}$ are coefficients that are to be determined. The approximant P_N^M is said to be of order $[M/N]$ and the superscripts $^{(M)}$ and $^{(N)}$ of the coefficients denote that they correspond to the approximant of that order (and are thus not necessarily equal to the coefficients of other approximants). A rational function is perhaps the simplest function that can have singularities and that is the main motivation of approximating a function (with possible singularities) by such approximants. Note that we can set $B_0^N = 1$ in the denominator without loss of generality, since we can divide both the numerator and denominator by a constant factor [8]. Hence, we choose to use approximants with $B_0^M = 1$ from now on. The approximant of order $[M/N]$ is then of the form

$$P_N^M(\sigma) = \frac{\sum_{m=0}^{M} A_m^{(M)} \sigma^m}{1 + \sum_{n=1}^{N} B_n^{(N)} \sigma^n}, \tag{3.2}$$

which has $M + N + 1$ coefficients instead of $M + N + 2$. The main idea of the Padé approximant is that it approximates a function $f(\sigma)$ by equating it to the first $M + N + 1$ terms of its series expansion in the part of the complex plane where both representations, i.e., the Padé approximant and the Taylor series, exist (assuming that there is a region of overlap in the complex plane where both representations are valid). In other words, the difference between the series expansion of the function $f(\sigma)$ and the approximant $P_N^M(\sigma)$ are the terms of order higher than σ^{M+N+1} (after multiplying $f(\sigma)$ and $P_N^M(\sigma)$ by the denominator $R_N(\sigma)$). Formulating it mathematically, we have:

$$f(\sigma)R_N(\sigma) - Q_M(\sigma) = O(\sigma^{M+N+1}) \quad \text{for } \sigma < R_0, \tag{3.3}$$

where R_0 is the radius of convergence of the Taylor series. The coefficients $A_m^{(M)}$ and $B_n^{(N)}$ are found by equating the coefficients of equal powers on the left-hand side of Eq. (3.3), which we will discuss in more depth in Section 3.2.

In our case, we intend to find an approximation for the field $U(\mathbf{r})$ by using its expansion, the Born series. Alternatively, the series expansion of the full Green's function, as discussed in Appendix A, can be used to find an approximation to it, which has been done in Ref. [43] for instance. It is important to note that P_N^M is a function of σ since its aim is to approximate a function of σ, but it is also a function of $\mathbf{r}$ through the dependence of $U(\mathbf{r})$. In fact, we get a different approximant $P_N^M(\sigma)$ for each point $\mathbf{r}$ considered and therefore $A_m^{(M)}$ and $B_n^{(N)}$ are functions of $\mathbf{r}$. Throughout this chapter this dependence on $\mathbf{r}$ will be omitted for brevity however.

As mentioned in Section 2.2.2, the total field can be approximated by using the Born series in two ways. The same two options apply to Padé approximation. The first option is to calculate the Born series only for points inside the scatterer and to calculate Padé approximants for each of those points. The approximation can then be used inside the integral in the Lippmann-Schwinger equation to find the total field for any point outside (and for that matter also for any point inside) the scatterer. The second option is to calculate the terms in the Born series for points both inside and outside the scatterer and to compute the Padé approximants for each of those points *separately*. The first option implies that it is only necessary to use Padé approximants inside the scatterer. In both approaches enough points inside the scatterer should be considered to get an accurate result.

Symmetric approximants

We will only consider the special case of symmetric Padé approximants in this thesis. These are approximants of which the numerator and denominator are polynomials of equal degree, i.e., the approximants of order $[N/N]$. The P_N^N approximants thus have $2N+1$ unknown coefficients.

Padé sequence

A sequence of Padé approximants of increasing order is known as a Padé sequence. For example, the symmetric approximants of order $[N/N]$ can form a sequence for $N = 0, 1, 2, 3, \ldots$. The idea is that this sequence is determined such that for increasing N the approximants converge to $f(\sigma)$. Rigorous mathematical theory on the convergence of Padé approximants is limited. We will discuss convergence properties in Section 3.3.

3.1.2 Comparison to other resummation methods

Other resummation methods include Borel summation and Euler summation. However, these are not considered actual alternatives because these methods require the knowledge of *all* terms of a series in order to obtain an analytic continuation of the series outside its region of convergence [8]. An example for which Borel and Euler summation work is a geometric series. In electromagnetic scattering (or in general in perturbation) problems it does not occur in practice that all terms in the perturbation series are known. A rare exception is the problem we discuss in Chapter 4, for which the Born series results to be a geometric series.

Moreover, as already mentioned, Padé approximation can additionally be used for series acceleration of convergent series. In other words, a more accurate result can be obtained from a fixed number of terms of the Taylor series compared to when the terms are simply summed as a partial sum. Interestingly, this means that latent information about the exact solution is extracted more efficiently from these terms. Many compelling examples are presented in Ref. [8]. Series acceleration is discussed in more detail in Section 3.4.

3.2 Applying Padé approximation

In this section, we will show how to compute Padé approximants from a power series. We will discuss symmetric approximants in particular, since in the literature it is often (empirically) found that symmetric approximants appear to approximate the solution best [28, Ch. I.1.3].

3.2.1 System of equations and Cramer's rule

The approximant of order $[M/N]$ for a series $U(\sigma)$ is computed by equating the coefficients of terms with the same power of σ in Eq. (3.3), such that we get a system of equations for the

coefficients $A_m^{(M)}$ and $B_n^{(N)}$, which is

$$\begin{aligned}
A_0^{(M)} &= U_0, \\
A_1^{(M)} &= U_1 + U_0 B_1^{(N)}, \\
A_2^{(M)} &= U_2 + U_1 B_1^{(N)} + U_0 B_2^{(N)}, \\
&\vdots = \vdots \\
A_M^{(M)} &= U_M + U_{M-1} B_1^{(N)} + \ldots + U_0 B_M^{(N)}, \\
0 &= U_{M+1} + U_M B_1^{(N)} + \ldots + U_{M-N+1} B_N^{(N)}, \\
&\vdots = \vdots \\
0 &= U_{M+N} + U_{M+N-1} B_1^{(N)} + \ldots + U_M B_N^{(N)}.
\end{aligned} \tag{3.4}$$

These are $M+N+1$ equations for the $M+N+1$ coefficients, of which the last N equations only have the $B_n^{(N)}$ as unknowns, while in the first $M+1$ equations both the $A_m^{(M)}$ and $B_n^{(N)}$ are unknowns. The last N equations of the system can be solved for $B_n^{(N)}$ by Cramer's rule, which states that $B_n^{(N)} = \det(T_n)/\det(T)$, where

$$T = \begin{bmatrix} U_M & U_{M-1} & \cdots & U_{M-N+1} \\ U_{M+1} & U_M & \cdots & U_{M-N+2} \\ \vdots & \vdots & \ddots & \vdots \\ U_{M+N-1} & U_{M+N-2} & \cdots & U_M \end{bmatrix} \tag{3.5}$$

and where T_n is obtained by replacing the n-th column of T by $[U_{M+1} U_{M+2} \ldots U_{M+N}]^T$. The computed values of $B_n^{(N)}$ can be substituted in the first $N+1$ equations of Eq. (3.4) to obtain the $A_m^{(M)}$ coefficients. According to Ref. [27], the expressions of the denominator and numerator that follow from the solution can be simplified to

$$Q_M(\sigma) = \det \begin{vmatrix} U_{M-N+1} & U_{M-N+2} & \cdots & U_{M+1} \\ \vdots & \vdots & \ddots & \vdots \\ U_M & U_{M+1} & \cdots & U_{M+N} \\ \sum_{j=N}^{M} U_{j-N}\sigma^j & \sum_{j=N-1}^{M} U_{j-N+1}\sigma^j & \cdots & \sum_{j=0}^{M} U_j \sigma^j \end{vmatrix}, \tag{3.6}$$

$$R_N(\sigma) = \det \begin{vmatrix} U_{M-N+1} & U_{M-N+2} & \cdots & U_{M+1} \\ \vdots & \vdots & \ddots & \vdots \\ U_M & U_{M+1} & \cdots & U_{M+N} \\ \sigma^N & \sigma^{N-1} & \cdots & 1 \end{vmatrix}. \tag{3.7}$$

Cramer's rule is computationally very inefficient, so numerically it is better to solve the system of equations with a linear solver that uses LU factorization for instance. This is further discussed in Section 3.6.

3.2.2 Expressions for symmetric approximants

Although the linear systems for the Padé coefficients are in practice small systems which can be solved by many standard numerical methods, we will explicitly show how to find the symmetric Padé approximants $[N/N]$ by solving the system of equations step by step. Such an approach can namely be of interest when we calculate the Born series and Padé approximants analytically, because it may reveal some underlying properties that can be grasped more intuitively in such a way. We will treat the steps for $N = 0, 1, 2$ as well as provide a general formula for any symmetric approximant of order N.

Case N=0

The first case is simple, because we only need the first term in the Born series, which is just the incident field:

$$P_0^0(\sigma) = A_0^{(0)} = U_0 = U_i. \tag{3.8}$$

Case N=1

Now we have the three unknowns $A_0^{(1)}$, $A_1^{(1)}$ and $B_1^{(1)}$ in the approximant $[1/1]$, which reads

$$P_1^1(\sigma) = \frac{A_0^{(1)} + A_1^{(1)}\sigma}{1 + B_1^{(1)}\sigma}. \tag{3.9}$$

Following Eq. (3.3), we have

$$A_0^{(1)} + A_1^{(1)}\sigma + O(\sigma^3) = (U_0 + U_1\sigma + U_2\sigma^2)(1 + B_1^{(1)}\sigma), \tag{3.10a}$$

$$A_0^{(1)} + A_1^{(1)}\sigma + O(\sigma^3) = U_0 + (U_1 + U_0B_1^{(1)})\sigma + (U_2 + U_1B_1^{(1)})\sigma^2 + U_2B_1^{(1)}\sigma^3. \tag{3.10b}$$

By equating the coefficients of the terms with equal powers of σ on the left- and right-hand side, we find a system of three equations for the coefficients of P_1^1, which reads

$$A_0^{(1)} = U_0, \tag{3.11a}$$

$$A_1^{(1)} = U_1 + U_0B_1^{(1)}, \tag{3.11b}$$

$$0 = U_2 + U_1B_1^{(1)}. \tag{3.11c}$$

First we can solve Eq. (3.11c) for $B_1^{(1)}$ after which we calculate $A_1^{(1)}$ to find

$$B_1^{(1)} = -\frac{U_2}{U_1}, \tag{3.12a}$$

$$A_0^{(1)} = U_0, \tag{3.12b}$$

$$A_1^{(1)} = U_1 - U_0\frac{U_2}{U_1}. \tag{3.12c}$$

The symmetric Padé approximant $[1/1]$ is therefore

$$P_1^1(\sigma) = \frac{U_0 + (U_1 - U_0\frac{U_2}{U_1})\sigma}{1 - \frac{U_2}{U_1}\sigma} = U_0 + U_1\sigma + U_2\sigma^2\frac{U_1}{U_1 - U_2\sigma}. \tag{3.13}$$

Comparing this to the truncation of the Born series after U_2, which simply is $U_{\text{Born},2} = U_0 + U_1 + U_2$, we see that the second-order correction in P_2^2 is not simply U_2, but is a nonlinear function of U_1 and U_2.

Case N=2

Similarly, for $N = 2$ we have a system of equations for the five unknown coefficients, which is

$$A_0^{(2)} = U_0, \tag{3.14a}$$
$$A_1^{(2)} = U_1 + U_0 B_1^{(2)}, \tag{3.14b}$$
$$A_2^{(2)} = U_2 + U_1 B_1^{(2)} + U_0 B_2^{(2)}, \tag{3.14c}$$
$$0 = U_3 + U_2 B_1^{(2)} + U_1 B_2^{(2)}, \tag{3.14d}$$
$$0 = U_4 + U_3 B_1^{(2)} + U_2 B_2^{(2)}. \tag{3.14e}$$

We first solve Eqs. (3.14d) and (3.14e) for $B_1^{(2)}$ and $B_2^{(2)}$ by elimination, which gives

$$B_1^{(2)} = \frac{-U_3 U_2 + U_4 U_1}{U_2^2 - U_3 U_1}, \tag{3.15a}$$
$$B_2^{(2)} = \frac{-U_2 U_4 + U_3^2}{U_2^2 - U_3 U_1}. \tag{3.15b}$$

We substitute these values in Eqs. (3.14a) to (3.14c) to directly find $A_m^{(2)}$. For P_2^2 we thus obtain, after simplifying the expression slightly,

$$P_2^2(\sigma = 1) = \frac{(U_0 + U_1 + U_2)(U_2^2 - U_3 U_1) + (U_0 + U_1)(-U_3 U_2 + U_4 U_1) + U_0(-U_2 U_4 + U_3^2)}{U_2^2 - U_3 U_1 - U_3 U_2 + U_4 U_1 - U_2 U_4 + U_3^2}. \tag{3.16}$$

General case

For a certain order N, the $2N + 1$ coefficients of the approximant P_N^N are found from the system in Eq. (3.4). The $B_n^{(N)}$ coefficients can be solved with Cramer's rule, as described in Section 3.2.1, where now $M = N$ such that

$$T = \begin{bmatrix} U_N & U_{N-1} & \cdots & U_1 \\ U_{N+1} & U_N & \cdots & U_2 \\ \vdots & \vdots & \ddots & \vdots \\ U_{2N-1} & U_{2N-2} & \cdots & U_N \end{bmatrix}. \tag{3.17}$$

Actually, T is a Toeplitz matrix. We define $\Delta = \det(T)$ and $\Delta_n = \det(T_n)$. As a result,

$$B_n^{(N)} = \frac{\Delta_n}{\Delta}, \tag{3.18}$$
$$A_m^{(N)} = U_m + \sum_{\ell=0}^{m-1} U_\ell B_{m-\ell} = U_n + \sum_{\ell=0}^{m-1} U_\ell \frac{\Delta_\ell}{\Delta}, \tag{3.19}$$

where the expression for $A_m^{(N)}$ results from substituting the $B_n^{(N)}$ in the first $N + 1$ equations of Eq. (3.4). Having found the coefficients, the approximant is

$$P_N^N(\sigma) = \frac{\sum_{m=0}^{N} A_m^{(N)} \sigma^m}{1 + \sum_{n=1}^{N} B_n^{(N)} \sigma^n} = \sum_{\ell=0}^{N} U_\ell \sigma^\ell \frac{\Delta + \sum_{m=1}^{N-\ell} \Delta_m \sigma^m}{\Delta + \sum_{n=1}^{N} \Delta_n \sigma^n}. \tag{3.20}$$

Finally, we can set $\sigma = 1$ to obtain the approximant for the value of the permittivity contrast of interest.

3.2.3 Approximants for scattering by a homogeneous object

In Section 2.2.2 it was mentioned that when scattering by a homogeneous object is considered, the Born series is of the form (2.24), where the terms $U'_\ell(\mathbf{r})$ can be calculated independently from the permittivity of the object. Consequently, we can calculate new coefficients $A'^{(M)}_m$ and $B'^{(N)}_n$ in terms of these $U'_\ell(\mathbf{r})$ instead of $U_\ell(\mathbf{r})$, such that the approximant is

$$P^M_N(\sigma\Delta\varepsilon_r) = \frac{\sum_{m=0}^{M} A'^{(M)}_m (\sigma\Delta\varepsilon_r)^m}{\sum_{n=0}^{N} B'^{(N)}_n (\sigma\Delta\varepsilon_r)^n}. \tag{3.21}$$

This works because the series is in powers of $\sigma\Delta\varepsilon_r$ and therefore it can be viewed as if $\Delta\varepsilon_r$ is incorporated in the perturbation parameter σ. Now, $A'^{(M)}_m$ and $B'^{(N)}_n$ are independent of the material properties and once they have been calculated for a certain approximant $[M/N]$, the approximant (3.2) becomes simply a rational function of $\Delta\varepsilon_r$ (after setting $\sigma = 1$). The approximant can then easily be found for any material. This suggests that for a homogeneous object the material properties and the geometry of the object, i.e., a certain Ω, are uncoupled.

3.2.4 Padé table

It can be enlightening to arrange the approximants of different orders in a so-called Padé table:

$$\begin{array}{cccc} [0/0] & [0/1] & [0/2] & \cdots \\ [1/0] & [1/1] & [1/2] & \cdots \\ [2/0] & [2/1] & [2/2] & \cdots \\ \vdots & \vdots & \vdots & \ddots \end{array}. \tag{3.22}$$

The approximants along the diagonal are the symmetric approximants for which $M = N$. The approximants of order $[M/0]$ in the first column are partial sums of the Taylor series, because the denominator is just 1 and the numerator is equal to that partial sum as a result.

Stairstep sequence

The diagonal approximants $[N/N]$ and off-diagonal approximants $[N+1/N]$ form a so-called stairstep sequence, which is the following: $[0/0]$, $[1/0]$, $[1/1]$, $[2/1]$, $[2/2]$, $[3/2]$, ... In some cases, such a stairstep sequence converges monotonically to the solution and might therefore be of interest to error estimation of Padé approximants. It is therefore further discussed in Section 3.5.

Padé table cross rule

An approximant $[L/M]$ in a Padé table can be expressed in terms of the four Padé approximants that neighbour the $[L/M]$ approximant in the table. This identity, also known as Wynn's cross rule, reads [28, Ch. I.3]:

$$([L\text{-}1/M]-[L/M])^{-1}+([L+1/M]-[L/M])^{-1} = ([L/M\text{-}1]-[L/M])^{-1}+([L/M+1]-[L/M])^{-1}. \tag{3.23}$$

We can also write this equation equation as follows

$$(N-C)^{-1}+(S-C)^{-1}=(W-C)^{-1}+(E-C)^{-1}, \tag{3.24}$$

where C is the $[L/M]$ approximant and N, S, W and E are the neighbouring approximants, referring to the relative position to C in the Padé table (3.22) in the following way:

$$\begin{array}{ccccc} & [L-1/M] & & & N \\ [L/M-1] & [L/M] & [L/M+1] & \rightarrow & W \quad C \quad E \\ & [L+1/M] & & & S \end{array}. \tag{3.25}$$

With this cross rule, the lower triangular part of the Padé table (3.22) can be calculated from the first column $[n/0]$ and by using the initialization $[n/\text{-}1]=\infty$, $n=0,1,2,\ldots$. Similarly, the upper triangular part of the Padé table can be calculated from the first row $[0/n]$ with the initialization $[-1/n]=0$, $n=0,1,2,\ldots$.

Although we limit ourselves to symmetric approximants, this rule can help to speed up calculating a full Padé table in the case that one wants to do a more extensive search for the most accurate approximant in the table. Even in the case of symmetric approximants, the rule might offer a speed up in calculation, since in the regular way a system of equations has to be solved for each Padé approximant for each considered point in space. The cross rule does not involve solving these linear systems, except for the first row $[0/n]$.

3.3 Convergence

General convergence properties

The convergence of a sequence of Padé approximants is quite poorly understood and rigorous mathematical theory of convergence is mainly limited to so-called Stieltjes series. A Stieltjes series is the series expansion of a Stieltjes function $f(z)$, that is defined as [8, 28, Ch. I.5]:

$$f(z)=\int_0^\infty \frac{\phi(u)}{1+zu}\,\mathrm{d}u, \tag{3.26}$$

where the weight function $\phi(u)$ is nonnegative for $u>0$ and approaches zero so rapidly as $u\rightarrow\infty$ that the moment integrals

$$f_j=\int_0^\infty u^j\,\mathrm{d}\phi(u), \quad j=0,1,2,\ldots \tag{3.27}$$

exist for all positive integers j. The Stieltjes series then reads

$$f(z)=\sum_{j=0}^{\infty} f_j(-z)^j. \tag{3.28}$$

If one can proof that the series at hand is a Stieltjes series, it can be directly said that any diagonal sequence of approximants $[M+J/M]$ converges to the correct solution as M tends to infinity [8].

Convergence in potential scattering problems

Theory on convergence is more elaborate for specific categories of problems. In Ref. [22] the convergence of diagonal Padé approximants to the solution of linear integral equations with a finite-rank operator is shown. Moreover, Tani has a set of two papers that discusses the analytic continuation of the Born series by Padé approximants in scattering by a potential [19, 20]. Other relevant literature on the convergence of Padé approximants in scattering theory is Refs. [44, 45, 46]. A counterexample of a Fredholm integral equation of the second kind for which the Padé method fails is found in Ref. [47].

3.4 Acceleration of summations

As mentioned in Section 3.1.1, Padé approximants can also be employed as a method to accelerate the summation of series. This is not unexpected, since Padé approximants are intimately linked to the Shanks transformation.

Connection with Shanks transformation

The Shanks transform is a method for the acceleration of a series. The sequence of partial sums A_n of a series A is transformed to a new sequence $S\{A_n\}$, which is defined as

$$S\{A_n\} = \frac{A_{n+1}A_{n-1} - A_n^2}{A_{n+1} + A_{n-1} - 2A_n}. \tag{3.29}$$

It follows that if N elements of the original sequence A_n are considered, the transform $S\{A_n\}$ contains $N-2$ elements. The transform is based on the assumption that A_n has a transient term that is exponentially decaying and vanishes for $n \to \infty$. The aim of the method is to eliminate this transient and thereby speed up convergence. Although the considered sequence may already converge (exponentially), the Shanks transform can still reduce the error by a few orders of magnitude, while using the same terms of the sequence. The transformation can be iterated, even multiple times, to achieve further acceleration and after applying the transform m times the resulting sequence $S^m\{A_n\}$ has $2m$ elements less than A. However, instabilities can result from applying the Shanks transform too often.

The generalized Shanks transformation $S_k\{A_n\}$ is an extension of the regular Shanks transform. The subscript k denotes the order of the transformation and the first-order transform $S_1\{A_n\}$ is the regular Shanks transform (3.29). Here, the relation to Padé approximants is seen in the fact that the n-th element of the k-th order Shanks transformation $S_k\{A_n\}$ is equal to the $[(n+k)/k]$ approximant of A. Hence we have,

$$[L/M] = S_M\{A_{L-M}\}. \tag{3.30}$$

This means in particular that the sequence resulting from the first-order Shanks transform $S_1\{A_n\}$ is equal to the second row of the Padé table consisting of the $[L/1]$ approximants. The formulas for the generalized transformation can for example be found in Ref. [8].

Connection with the ε-algorithm

The ε-algorithm is a method for recursively calculating the Shanks transform $S_k\{A_n\}$ of a sequence A_n. The algorithm is as follows [28]:

$$\varepsilon_{-1}^{(n)} = 0, \qquad \varepsilon_0^{(n)} = A_n, \qquad n = 0, 1, 2, \ldots \tag{3.31a}$$

$$\varepsilon_{m+1}^{(n)} = \varepsilon_{m-1}^{(n+1)} + \left[\varepsilon_m^{(n+1)} - \varepsilon_m^{(n)}\right]^{-1}, \qquad n, m = 0, 1, 2, \ldots, \tag{3.31b}$$

where the quantities $\varepsilon_m^{(n)}$ are related to the Shanks transformation through $\varepsilon_{2k}^{(n)} = S_k\{A_n\}$. When considering the relation between Padé approximants and the Shanks transformation in the previous paragraph, the relation $\varepsilon_{2k}^{(n)} = [(n+k)/k]$ also holds. The ε-algorithm can thus be used to recursively calculate the entries in a Padé table.

3.5 Error estimation and determining the best approximant

3.5.1 Error estimation

If the case the original perturbation series converges and the solution is known, the computed Padé approximants can be compared to it to determine the approximation error. Since in this thesis we consider scattering problems for which the Born series is possibly (strongly) divergent, the error of the approximation can not be estimated by comparison with the original series. Therefore, we have chosen to consider problems for which a closed-form analytical solution is available on purpose. In the respective chapters that are dedicated to these problems we discuss the relevant error metrics. In short, one can consider the accuracy of the approximant at a certain point in space, or the weighted relative error in the spatial domain of interest of the approximation.

Furthermore, in Part II of Ref. [28], an error bound is derived for the Padé approximants of the solution $f(\mathbf{r})$ of integral equations of the type

$$f(\mathbf{r}) = g(\mathbf{r}) + \lambda \int K(\mathbf{r}; \mathbf{r}') f(\mathbf{r}) \, \mathrm{d}\mathbf{r}'. \tag{3.32}$$

The Lippmann-Schwinger equation for electromagnetic scattering, discussed in Chapter 2, belongs to this category of equations. However, this error bound is only valid within the circle of convergence of the series expansion and is therefore useless for divergent series.

On a different note, in Ref. [8] Bender and Orszag mention cases where a stairstep sequence of Padé approximants converges monotonically. More specifically, the sequence of P_N^N approximants approaches the solution monotonically from above, while the sequence of P_N^{N+1} does it from below. Therefore, the P_N^N and P_N^{N+1} for a certain N form an interval for the solution, which gives an error bound of the approximants. For increasing N this error decreases. Whether the optical scattering problems have this property is not clear and is a subject for further research.

3.5.2 Determining the best approximant

The problems studied in Chapters 4 to 6 are specifically chosen because a closed-form analytical solution can be found, by which it is straightforward to determine which Padé function is the best approximation. However, for more complex geometries of which no analytical solution is known, determining which approximant is most accurate has to be done without a priori knowledge. In that case, if one is using the diagonal Padé approximants, one could calculate the difference between two consecutive diagonal approximants P_N^N and P_{N+1}^{N+1} and determine for which N this difference is minimum. Such a minimum would point to a stagnation in improvement of the approximations. This method amounts to determining N_{best} such that

$$e_{\text{consec},N} = \int_\Omega \left| P_N^N(\mathbf{r}) - P_{N-1}^{N-1}(\mathbf{r}) \right|^2 \mathrm{d}\mathbf{r} \tag{3.33}$$

is minimum.

3.6 Implementation of the Padé approximants

Once a sufficient number of terms in the original perturbation series have been calculated numerically for all desired points in space, the Padé coefficients are calculated from the series' terms with a MATLAB routine. The routine uses the first $2N+1$ terms of the Born series to calculate the $[N/N]$ symmetric Padé approximant.

The $B_n^{(N)}$ Padé coefficients can be found either by Cramer's rule, as decribed in Section 3.2.2, or by using a linear solver to solve the system of equations. Numerically, the linear solver is faster and therefore we use the MATLAB `linsolve` function. When the system of N equations that determine $B_n^{(N)}$ are put in matrix form, the matrix is a Toeplitz matrix. Therefore, we construct it from the terms of the Born series with the MATLAB `toeplitz` function.

3.6.1 Computational complexity

To get an idea of the complexity of the Born-Padé method, we make a rough estimate of the computational complexity in this section. In this estimate we consider the computation for points inside the scatterer only, since in the finite difference or finite element method the domain of computation would also be as small as possible. This estimate includes the calculation of the Born series and subsequently of the Padé approximants. The estimation is done for a general implementation for any geometry for which a Fourier transform is used to calculate the convolution integrals that occur in the terms of the Born series.

After all terms up to and including U_ℓ have been computed, to compute the next term $U_{\ell+1}$ the term $U_\ell(\mathbf{r})$ is Fourier transformed, multiplied by the (analytically known) Fourier transform of the Green's function, and then back Fourier transformed. In this process, any Fourier transform that has to be computed numerically is of course done by the Fast Fourier Transform (FFT). It has a complexity of $\sim n^d \log_2(n^d)$, where n is the number of grid points along one dimension and d is the dimensionality of the problem. Hence, considering that the FFT is performed twice per term, and that in order to compute a Padé approximant of order N we need $2N$ terms in the Born series besides the incident field, the complexity is $\sim 4Nn^d \log_2(n^d)$.

The second part of the routine consists of calculating the coefficients of the Padé approximants from the system of $2N+1$ equations. For all grid points, the $B^{(N)}$ coefficients are solved from N equations, while the $A^{(N)}$ coefficients are found by substitution of $B^{(N)}$ in the other $N+1$ equations. The computational complexity of solving the system of N equations by Gaussian elimination is approximately $\frac{2}{3}N^3$ operations. The coefficients have to be calculated for each of the n^d points on the grid, which is done by looping over the grid points.

These two parts make the overall complexity of the method

$$\sim Nn^d \left[\log_2(n) + N^2\right], \tag{3.34}$$

where constant factors are left out. Of course, once $2N+1$ terms in the Born series have been calculated, all Padé approximants of order lower than N can be calculated from these terms as well, such that the first part does not need to be repeated.

For comparison, the finite difference or finite element method require solving a sparse linear system. Solving it with the conjugate gradient method has a computational complexity of $\sim n_{\text{tot}}^{1+1/d}$ for a total of n_{tot} elements. Saying that n_{tot} is approximately n^d with n the number of grid points along one dimension, the complexity becomes $\sim n^{d+1}$.

As an example, we consider a 3D problem (i.e., $d = 3$) in which we choose $n = 30$ grid points along one dimension and $N = 10$ for the order of the Padé approximant. The number of operations for the Padé method is thus approximately 2.70×10^6, whereas for the finite difference or finite element method it is approximately 0.81×10^6. For this particular example it means that the Padé method would require more operations.

However, an important note is that the accuracy of the Padé method does not depend on the spacing between the points on which the approximant is calculated. Therefore, the second part of the routine can be done with less grid points than the first part, once the terms of the Born series have been calculated. In that case, the computational complexity is

$$\sim Nn^d \log_2(n) + n_P^d N^3, \tag{3.35}$$

where n_P is the number of grid points along one dimension when computing the Padé approximants. For instance, when using $n_P = n/2$ in the above example, the number of operations would reduce to

Additionally, the Padé method has the advantage that the Padé coefficients only need to be calculated once for different materials when dealing with a homogeneous scatterer, which we discuss in Section 2.2.2.

CHAPTER 4

One-dimensional infinitely thin slab

4.1 Scattering by an infinitely thin slab

Here we start with the application of the methods to specific problems. The first scattering problem is a first and simple illustration of the method of Padé approximants, namely scattering by an infinitely thin slab in one dimension. As we will discuss in this chapter, this toy problem provides a simple, though effective example of the efficacy of the Padé approach in electromagnetic scattering problems. Since most of the analysis of this specific problem can be done with analytical expressions, it provides a way to understand the essence of how, if and why the approach works.

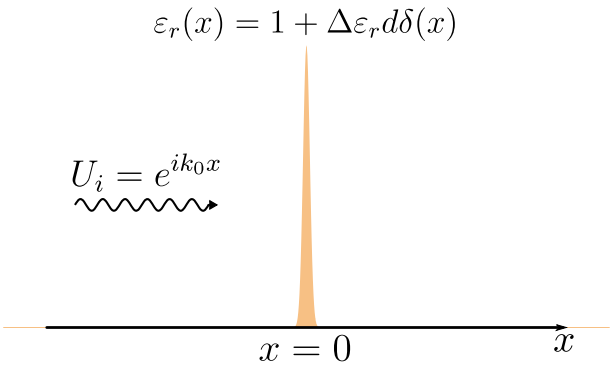

Figure 4.1: Geometry of the one-dimensional problem of an infinitely thin slab which is modeled as a Dirac delta function. The incident field U_i is a plane wave.

In the problem, the x-axis is chosen perpendicular to the slab. Furthermore, since we consider a 1D problem, the incident and hence also the total field depend only on x. The permittivity of the infinitely thin slab is modeled as a Dirac delta function $\delta(x)$ located at $x = 0$ in one-dimensional space and has a nominal thickness d in order to obtain correct dimensions. See Fig. 4.1. The analogous problem of quantum-mechanical scattering by a delta potential is often encountered in textbooks on quantum mechanics as a beginner's problem on how to

solve the Schrödinger equation with boundary conditions [32, 48]. Hence, the mathematics is (unsurprisingly) similar. In the electromagnetic scattering problem, the field satisfies the 1D Helmholtz equation, with vacuum as the background medium and the Dirac delta function as the perturbation, which reads

$$\frac{\mathrm{d}^2}{\mathrm{d}x^2}U(x) + k_0^2[1 + \Delta\varepsilon_r d\delta(x)]U(x) = 0. \tag{4.1}$$

Here, $\Delta\varepsilon_r$ is the permittivity contrast and denotes the weight of the delta function. We specifically choose to treat the case of a plane wave $U_i(x) = \mathrm{e}^{ik_0 x}$ as the incident field throughout this chapter. The free-space Green's function of the Helmholtz equation in 1D is, as listed in Table 2.1,

$$G_0(x;x') = \frac{i}{2k_0}\mathrm{e}^{ik_0|x-x'|}, \tag{4.2}$$

while the full Green's function of the problem satisfies

$$\left[\frac{\mathrm{d}^2}{\mathrm{d}x^2} + k_0^2\right] G(x;x') = -\delta(x-x') - \Delta\varepsilon_r d\delta(x)G(x;x'). \tag{4.3}$$

The reason this case is simpler than the 1D slab with finite thickness is that here we distinguish only between two regions, $x < 0$ and $x > 0$ (with one interface), instead of three regions (with two interfaces) and thus only one boundary condition has to be satisfied, instead of two. One could think of another scattering problem with only one interface, which is that of a semi-infinite scatterer, i.e., where $\Delta\varepsilon_r(x)$ is 0 for $x < 0$ and a nonzero constant for $x > 0$ (and corresponds to the quantum-mechanical analogy of a step-potential). However, the object is then unbounded on one side, which impedes the application of the Padé method, since it would require integration over a semi-infinite domain when calculating terms in the Born series.

We start with the analytical solution of the problem using different approaches in Section 4.2, after which we compute the Born series for this case in Section 4.3 and apply the method of Padé approximation to the obtained perturbation series. Additionally, in Section 4.3.4 we also apply the Padé method to find the full Green's function of this problem as an alternative. Lastly, we conclude the study of this toy problem with some key remarks in Section 4.4.

4.2 Analytical approach

We will discuss two methods for finding the analytical solution to the 1D Helmholtz equation in this problem and compute the Green's function of the infinitely thin slab as well. This will give a good overview of the several possible ways in which the Padé method can be applied to these type of problems. First, from the point of view of differential equations, the Helmholtz equation can be solved by employing boundary conditions at the interface $x = 0$ of the two regions. On the other hand, this is one of the rare cases where the solution can also be found directly from the integral form of the governing equations, i.e., from either the Lippmann-Schwinger equation for the field or the Dyson equation for the Green's function.

4.2.1 Analytical solution

Solution by boundary conditions

The analytical solution to the delta-function scattering problem for an incoming plane wave is well-known from the literature, such as Refs. [32, 48], where the solution to the quantum-mechanical version of the problem is presented. The usual approach is by writing the field as $U(x) = U_i(x)+U_s(x)$ and substituting the known incident field $U_i(x) = \mathrm{e}^{ik_0x}$ in the Helmholtz equation in Eq. (4.1) [1]. The result is an equation for the unknown scattered field:

$$\frac{\mathrm{d}^2}{\mathrm{d}x^2}U_s(x) + k_0^2U_s(x) = -k_0^2\Delta\varepsilon_r d\delta(x)[\mathrm{e}^{ik_0x} + U_s(x)]. \tag{4.4}$$

Because for $x \neq 0$ Eq. (4.4) is equal to the Helmholtz equation in vacuum, the solutions in the two regions $x < 0$ and $x > 0$ are simply linear combinations of plane waves $\mathrm{e}^{\pm ik_0x}$. The radiation condition at infinity requires that the scattered field propagates outward for $|x| \to \infty$, which means that $U_s(x) = A_-\mathrm{e}^{-ik_0x}$ for $x < 0$ and $U_s(x) = A_+\mathrm{e}^{ik_0x}$ for $x > 0$, with A_- and A_+ constants that are to be determined.

Subsequently, two boundary conditions are imposed. First, the field $U(x)$ is continuous at the origin and since $U_i(x)$ is already continuous there, it follows for $U_s(x)$ that $A_- = A_+ \equiv A$. Secondly, the derivative of the total field $U(x)$ makes a jump at $x = 0$, such that

$$\left.\frac{\mathrm{d}U(x)}{\mathrm{d}x}\right|_{x=+0} - \left.\frac{\mathrm{d}U(x)}{\mathrm{d}x}\right|_{x=-0} = -k_0^2\Delta\varepsilon_r dU(0). \tag{4.5}$$

Hence,

$$(ik_0 - ik_0A) - (ik_0 + ik_0A) = -k_0^2\Delta\varepsilon_r d(1 + A), \tag{4.6a}$$

$$A = -\frac{k_0\Delta\varepsilon_r d}{2i + k_0\Delta\varepsilon_r d}. \tag{4.6b}$$

Finally, the total field is:

$$U(x) = \mathrm{e}^{ik_0x} - \mathrm{e}^{ik_0|x|}\frac{k_0\Delta\varepsilon_r d}{2i + k_0\Delta\varepsilon_r d}, \tag{4.7}$$

where the first and second term correspond to $U_i(x)$ and $U_s(x)$, respectively. The reflection and transmission coefficients r and t are

$$r = \frac{k_0\Delta\varepsilon_r}{2i + k_0\Delta\varepsilon_r d} \quad \text{and} \quad t = \frac{2i}{2i + k_0\Delta\varepsilon_r d}. \tag{4.8}$$

Solution through the Lippmann-Schwinger equation

The solution can also be found by using the Lippmann-Schwinger equation for the scattered field, Eq. (2.10), which for one dimension and this potential can be evaluated as

$$U_s(x) = k_0^2\Delta\varepsilon_r d\int_{x'} G_0(x;x')\delta(x')U(x')\,\mathrm{d}x' \tag{4.9a}$$

$$= k_0^2\Delta\varepsilon_r dG_0(x;0)[U_i(0) + U_s(0)]. \tag{4.9b}$$

[1] To be specific, we use that $[\nabla^2 + k_0^2]U_i(x) = 0$.

We see that the scattered field depends on $U_s(0)$, the field itself in $x = 0$. We can proceed by setting $x = 0$ and solving for $U_s(0)$, yielding

$$U_s(0) = \frac{k_0^2 \Delta\varepsilon_r d G_0(0;0) U_i(0)}{1 - k_0^2 \Delta\varepsilon_r d G_0(0;0)} = -\frac{k_0 \Delta\varepsilon_r d}{2i + k_0 \Delta\varepsilon_r d}, \tag{4.10}$$

where we used that $U_i(0) = 1$ and $G_0(0;0) = i/(2k_0)$. Substituting this into Eq. (4.9b), we find that the scattered field is

$$U_s(x) = -\mathrm{e}^{ik_0|x|} \frac{k_0 \Delta\varepsilon_r d}{2i + k_0 \Delta\varepsilon_r d}. \tag{4.11}$$

This agrees with Eq. (4.7), once we add the incident field to it.

Solution by first computing the Green's function of the infinitely thin slab

The scattered field can also be calculated directly from the incident field if the full Green's function of the problem, which satisfies Eq. (4.3), is known. It can be found from the Dyson equation (A.7), which is the integral form of Eq. (4.3) and is an equation of the same type as the Lippmann-Schwinger equation. Therefore, the procedure for finding $G(x;x')$ is similar to the one for solving $U_s(x)$ from the Lippmann-Schwinger equation in Section 4.2.1 [49]. Using the notation of the Dyson equation as in Eq. (A.7), we have $V(x) = -k_0^2 \Delta\varepsilon_r d\delta(x)$ and therefore $G(x;x')$ satisfies

$$G(x;x') = G_0(x;x') + k_0^2 \Delta\varepsilon_r d \int_{x_1} G_0(x;x_1)\delta(x_1) G(x_1;x') \,\mathrm{d}x_1 \tag{4.12a}$$

$$= G_0(x;x') + k_0^2 \Delta\varepsilon_r d G_0(x;0) G(0;x'), \tag{4.12b}$$

where $G(x;x')$ (and $G(0;x')$) are to be determined. Again, by setting $x = 0$, we can solve for $G(0;x')$ in terms of the known free-space $G_0(x;x')$, which yields

$$G(0;x') = \frac{G_0(0;x')}{1 - k_0^2 \Delta\varepsilon_r d G_0(0;0)}. \tag{4.13}$$

Substituting this in Eq. (4.12b) gives

$$G(x;x') = G_0(x;x') + k_0^2 \Delta\varepsilon_r d \frac{G_0(x;0) G_0(0;x')}{1 - k_0^2 \Delta\varepsilon_r d G_0(0;0)} \tag{4.14a}$$

$$= \frac{i}{2k_0} \mathrm{e}^{ik_0|x-x'|} - \frac{i}{2k_0} \mathrm{e}^{ik_0(|x|+|x'|)} \frac{k_0 \Delta\varepsilon_r d}{2i + k_0 \Delta\varepsilon_r d}, \tag{4.14b}$$

where the known free-space Green's function was used. As discussed in Appendix A.1, $G(x;x')$ contains all information about how the system reacts to an incident field and we can therefore compute the scattered field directly from the incident field as follows,

$$U_s(x) = \int_{x'} G(x;x') k_0^2 \Delta\varepsilon_r d\delta(x') U_i(x') \,\mathrm{d}x' \tag{4.15a}$$

$$= k_0^2 \Delta\varepsilon_r d G(x;0) U_i(0) \tag{4.15b}$$

$$= k_0^2 \Delta\varepsilon_r d \left[\frac{i}{2k_0} \mathrm{e}^{ik_0|x|} - \frac{i}{2k_0} \mathrm{e}^{ik_0|x|} \frac{k_0 \Delta\varepsilon_r d}{2i + k_0 \Delta\varepsilon_r d} \right] \tag{4.15c}$$

$$= -\mathrm{e}^{ik_0|x|} \frac{k_0 \Delta\varepsilon_r d}{2i + k_0 \Delta\varepsilon_r d}, \tag{4.15d}$$

which agrees with the solutions found from both the method of boundary conditions and the Lippmann-Schwinger equation.

4.2.2 Examples

We provide two examples for which we take a wavelength of $\lambda = 400\,\mathrm{nm}$, a nominal thickness $d = 100\,\mathrm{nm}$ and two values for the permittivity contrast, namely $\Delta\varepsilon_r = 0.3$ and $\Delta\varepsilon_r = 0.3{+}0.3i$. The field is shown in Fig. 4.2 for both cases. Concerning reflection and transmission, the coefficients are $|r|^2 = 0.470$ and $|t|^2 = 0.530$ for the former case, and $|r|^2 = 0.381$ and $|t|^2 = 0.215$ for the latter. Notice that in the second case, the two coefficients do not add up to 1 since the permittivity contrast has an imaginary part that results in damping,

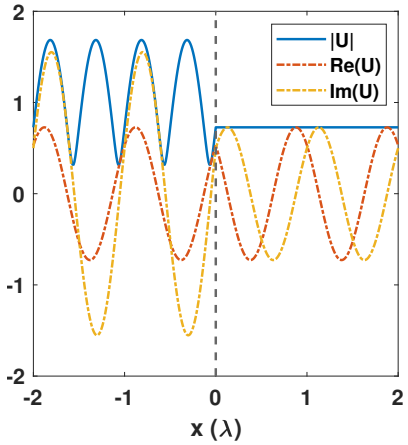

(a) Analytical solution for $\Delta\varepsilon_r = 1.2$.

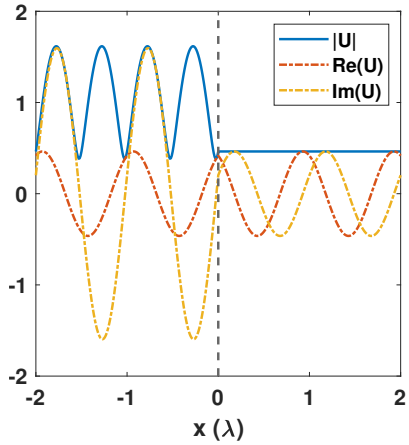

(b) Analytical solution for $\Delta\varepsilon_r = 1.2 + 1.2i$.

Figure 4.2: Analytical solution of the problem of scattering by an infinitely thin slab for $\lambda = 400\,\mathrm{nm}$, $d = 100\,\mathrm{nm}$ and two distinct values of $\Delta\varepsilon_r$. The blue line corresponds to the absolute value of the field, while the orange and yellow dashed lines correspond to the real and imaginary part, respectively. The grey dashed line indicates the position of the delta function.

4.2.3 Discussion of the analytical solution

The reflection coefficient r of the scattered field (4.8), has a pole $\Delta\varepsilon_r = -2i/(k_0 d)$ in the complex plane. This already suggests that a series expansion of r in terms of $k_0\Delta\varepsilon_r d/2i$, yielding a geometric series, would only converge for $|k_0\Delta\varepsilon_r d/2i| < 1$ [10]. Hence, we see that the series expansion is limited in how well it represents the actual solution to the problem, which motivates to find a representation that works better for strong-scattering cases, i.e., cases for which the permittivity contrast satisfies $|\Delta\varepsilon_r| > 2/(k_0 d)$. The analytical solution is in that sense a good representation for all cases except for $\Delta\varepsilon_r = -2i/(k_0 d)$.

The pole $k_0 = -2i/(\Delta\varepsilon_r d)$ is also known as a quasi-normal wave number (which in this case is complex) and the solution corresponding to it is called a quasi-normal mode [50]. It is possible to find this quasi-normal mode, which is of the form

$$U(x) = c\,G_0(x;0), \tag{4.16}$$

where c is an arbitrary constant [51].

4.3 Perturbation approach

As explained in Section 2.2.2, the total field $U(x)$ can be found by applying perturbation theory which yields the Born series (2.16). The terms of the series, which are corrections to the unperturbed solution, i.e., the incident field, are computed by the recurrence relation (2.20). When the terms are computed, simply summing them (while setting $\sigma = 1$) would work for converging series, but not for diverging ones. Since the perturbation series in general diverges, we will apply the Padé method in Section 4.3.3.

4.3.1 Calculation of the Born series

The first term in the Born series is the incident field, that is, $U_0(x) = \mathrm{e}^{ik_0 x}$, and then the recurrence relation Eq. (2.20) yields the higher-order terms [10, 52]:

$$\begin{aligned} U_1(x) &= k_0^2 \Delta\varepsilon_r d \int_{-\infty}^{+\infty} G_0(x;x')\delta(x')\mathrm{e}^{ik_0 x'}\,\mathrm{d}x' = k_0^2\Delta\varepsilon_r d G_0(x;0) \\ &= \frac{ik_0\Delta\varepsilon_r d}{2}\mathrm{e}^{ik_0|x|}, \end{aligned} \tag{4.17a}$$

$$\begin{aligned} U_2(x) &= k_0^2 \Delta\varepsilon_r d \int_{-\infty}^{+\infty} G_0(x;x')\delta(x')\frac{ik_0\Delta\varepsilon_r d}{2}\mathrm{e}^{ik_0|x'|}\,\mathrm{d}x' \\ &= \frac{ik_0^3}{2}G_0(x;0) = \left(\frac{ik_0\Delta\varepsilon_r d}{2}\right)^2 \mathrm{e}^{ik_0|x|}, \end{aligned} \tag{4.17b}$$

$$U_3(x) = \left(\frac{ik_0\Delta\varepsilon_r d}{2}\right)^3 \mathrm{e}^{ik_0|x|}, \tag{4.17c}$$

and so on, so that in general, for every $\ell > 0$:

$$U_\ell(x) = \left(\frac{ik_0\Delta\varepsilon_r d}{2}\right)^\ell \mathrm{e}^{ik_0|x|}. \tag{4.18}$$

The perturbation series is thus

$$U^{(\sigma)}(x) = \mathrm{e}^{ik_0 x} + \mathrm{e}^{ik_0|x|}\sum_{\ell=1}^{\infty}\left(\frac{ik_0\Delta\varepsilon_r d}{2}\right)^\ell \sigma^\ell. \tag{4.19}$$

We see that this power series converges if $|ik_0\Delta\varepsilon_r d\sigma/2| < 1$ (or $|\Delta\varepsilon_r\sigma| < 2/(k_0 d)$). This result was already predicted based on the analytical solution discussed in Section 4.2.1. The convergence criterion can be used to characterize the transition between the weak- and strong-scattering regime, where $|ik_0\Delta\varepsilon_r d\sigma/2| < 1$ corresponds to the weak regime and $|ik_0\Delta\varepsilon_r d\sigma/2| > 1$ to the strong regime.

4.3.2 Analytic continuation

We observe that the calculated Born series contains a geometric series, which allows us to rewrite it as a rational function [10], namely

$$U^{(\sigma)}(x) = \mathrm{e}^{ik_0x} + \mathrm{e}^{ik_0|x|}\frac{\frac{ik_0\Delta\varepsilon_r d}{2}\sigma}{1-\frac{ik_0\Delta\varepsilon_r d}{2}\sigma} = \mathrm{e}^{ik_0x} - \mathrm{e}^{ik_0|x|}\frac{k_0\Delta\varepsilon_r d\sigma}{2i+k_0\Delta\varepsilon_r d\sigma}. \tag{4.20a}$$

If we set the perturbation parameter σ to 1 to obtain the solution to the original problem, we exactly retrieve the analytical solution. This suggests that the Born series contains all necessary information to derive a useful expression although the series diverges when you choose to simply sum all the terms in a certain set of cases. Replacing the series by a rational function is in a sense an analytic continuation of the series from a disc with radius $2/k_0$ centered at $\Delta\varepsilon_r = 0$ (which corresponds to the unperturbed problem) to the full complex plane with exception of the pole at $\Delta\varepsilon_r = -2i/(k_0 d)$.

4.3.3 Padé approximation

The procedure for calculating the Padé approximants was explained in Section 3.2. We consider only symmetric Padé approximants, i.e., those of order $[N/N]$. Applying the procedure, for $N = 0$ and $N = 1$ we obtain the expressions

$$P_0^0(\sigma = 1, x) = \mathrm{e}^{ik_0x}, \tag{4.21a}$$

$$P_1^1(\sigma = 1, x) = \mathrm{e}^{ik_0x} - \mathrm{e}^{ik_0|x|}\frac{k_0\Delta\varepsilon_r d}{2i+k_0\Delta\varepsilon_r d}. \tag{4.21b}$$

The $N = 0$ order is simply the incident field, for which only the $\ell = 0$ term in the series was used. On the other hand, the $N = 1$ order exactly returns the analytical solution, for which three terms, $\ell = 0, 1, 2$, were used. More details on the calculation can be found in Appendix B. Interestingly, only three terms are required to retrieve the exact solution, whereas in Section 4.3.2 all terms had to be known to be able to analytically continue the geometric series. Apparently, the analytical solution only contains one pole and the $[1/1]$ approximant is sufficient to represent that pole.

Higher-order approximants When calculating the next order $N = 2$, we encounter the problem that the determinants Δ and Δ_n are 0, which means the system is singular. As a result the coefficients $B_n^{(2)}$ and $A_n^{(2)}$ are undetermined. This is a so-called degenerate approximant, and this indeed always happens for $[N/2]$ approximants of a geometric series [28, Ch. 2.4]. Symmetric approximants of order $N > 2$ suffer from the same problem and so does any Padé approximant $[M/N]$ with $M > N$. On the other hand, the Padé approximants $[N-1/N]$ for $N > 1$ reduce to the exact solution, in the absence of noise [53].

Comparison to partial sums The alternative to the $N = 2$ approximant, is simply summing the $\ell = 0, 1, 2$ terms, which gives the second Born approximation:

$$U_{\text{Born},2}(x) = \mathrm{e}^{ik_0x} + \mathrm{e}^{ik_0|x|}\left[\frac{ik_0\Delta\varepsilon_r d}{2} + \left(\frac{ik_0\Delta\varepsilon_r d}{2}\right)^2\right]. \tag{4.22}$$

Obviously, this is not equally effective, but for small values of $k_0\Delta\varepsilon_r d$ it could be a good approximation. A quantification of the accuracy of the (second) Born approximation could be made with a numerical comparison with the analytical solution.

4.3.4 Perturbation approach for Green's function

A perturbation solution can also be found for the Green's function of the problem, as discussed in Section 2.2.4, by means of an expansion of the Dyson equation, the integral equation that the Green's function must satisfy. The terms of the series are determined by a recurrence relation as well, namely Eq. (A.9). Using the free-space Green's function as the zero-th order term in the series, we obtain for $\ell > 0$

$$G_{\ell+1}(x;x') = k_0^2\Delta\varepsilon_r d\int_{x_1} G_0(x;x_1)\delta(x_1)G_\ell(x_1;x')\,\mathrm{d}x_1 \tag{4.23a}$$

$$= k_0^2\Delta\varepsilon_r d G_0(x;0)G_\ell(0;x') \tag{4.23b}$$

$$= \frac{ik_0\Delta\varepsilon_r d}{2}\mathrm{e}^{ik_0|x|}G_\ell(0;x') = \left(\frac{ik_0\Delta\varepsilon_r d}{2}\right)^\ell \mathrm{e}^{ik_0|x|}G_0(0;x'), \tag{4.23c}$$

which is of a similar form as the perturbation series of $U(x)$. The full perturbation solution is

$$G^{(\sigma)}(x;x') = \frac{i}{2k_0}\mathrm{e}^{ik_0|x-x'|} + \frac{i}{2k_0}\mathrm{e}^{ik_0(|x|+|x'|)}\sum_{\ell=1}^{\infty}\left(\frac{ik_0\Delta\varepsilon_r d}{2}\right)^\ell \sigma^\ell. \tag{4.24}$$

Notably, if one takes the first order approximation (so up to the $\ell = 1$ term), and proceeds to calculate $U_s(x)$ with it, it turns out it gives the same result as the first-order Born approximation of the field $U(x)$ itself, i.e., the $\ell = 0, 1$ terms of Eq. (4.19).

Using the same procedure as we did in Section 4.3.3 for $U(x)$, we can calculate the Padé approximants for the Green's function Q_N^N. The order $[1,1]$ approximant is

$$Q_1^1(x;x',\sigma=1) = \frac{i}{2k_0}\mathrm{e}^{ik_0|x-x'|} - \frac{i}{2k_0}\mathrm{e}^{ik_0(|x|+|x'|)}\frac{k_0\Delta\varepsilon_r d}{2i + k_0\Delta\varepsilon_r d} \tag{4.25}$$

which exactly agrees with the analytical result in Section 4.2. Obviously, the scattered field that can be calculated with it, as in Section 4.2, is the same.

As we see, the application of Padé approximants in these electromagnetic scattering problems is not only limited to the field, but also works well for the Green's function. The approximated Green's function can in turn be used to find an approximation to the field.

4.4 Discussion

We discussed the relatively simple case of scattering by an infinitely thin slab because this example contains all the main features of the problem we intend to address in this thesis. This problem is approached both analytically and by a perturbation method, for which the Born series is calculated. It is both possible to find an analytic continuation to the Born series (which is a rare case) and to obtain analytical expressions for the Padé approximants from the

Born series. The problem of an infinitely thin slab is special in that the Padé approximant P_1^1 gives the exact analytic solution. An important distinction between the analytic continuation of the Born series and the Padé approximation is that for the former all terms had to be known to obtain the exact solution, whereas for the latter only three terms are sufficient to calculate the $[1/1]$ approximant, which already returns the exact solution. This can be explained by the fact that the analytical solution only contains one pole and the $[1/1]$ approximant is sufficient to represent that pole.

The methods have been applied to both the field itself and the full Green's function and while their approximations return the same expressions for the scattered field, the approximation of the Green's function is independent of the incident field and is therefore of more general use.

Attempts to calculate higher-order symmetric Padé approximants $[N/N]$ show that these are so-called degenerate approximants [28]. Apparently, when there is only one pole to represent, the higher Padé approximants are not only superfluous but can not even be computed due to singularities that occur in the system of equations for determining the Padé coefficients. Padé approximants of order $[M/N]$ with $M > N$ also suffer from this probem

Other toy problems

Other toy problems in one or more dimensions can be considered for further study of the Padé approximant method in simple cases with analytical solutions. A few are proposed here.

Two infinitely thin slabs in one dimension The application of Padé approximants on simple scattering problems could extended to the case of two infinitely thin slabs (represented by two delta functions) for instance, since the analytical solution is well-known for the quantum-mechanical case, such as presented in Ref. [54].

Point source in more dimensions The problem of a permittivity function given by a delta function could be extended to higher-dimensional cases. Many of the equations from the one-dimensional case, also hold for the cases in two and three dimensions. An important problem that would be encountered is that in 1D the Green's function is analytical, while in two and three dimensions it contains a singularity as $\mathbf{r} \to \mathbf{r}'$, which in the 2D case is a logarithmic singularity [49]. With regularization techniques it is possible to take care of the singularity and get a meaningful result [55].

Delta function ring in two dimensions A more interesting alternative in two dimensions would be a delta function ring, described by $\Delta\varepsilon_r(\mathbf{r}) = \Delta\varepsilon_r\delta(r - R)$. Here, the singularity in the Green's function poses no problem and a similar approach can be used as in the infinitely thin slab case.

CHAPTER 5

One-dimensional slab

5.1 Scattering by a slab

In this chapter we turn our attention to another, but more practical, one-dimensional problem: that of scattering by a slab of finite thickness d by a perpendicularly incident wave. Although it is not in itself a very physical problem, it is more realistic compared to the toy problem in Chapter 4.

The incident field is a plane wave $U_i(z) = \mathrm{e}^{ik_0 z}$ incoming from the left and scattered by a slab of thickness d and permittivity $\varepsilon_0\varepsilon_r$ and surrounded by vacuum (with permittivity ε_0). The relatively permittivity ε_r of the slab can be a complex number with non-negative imaginary part. The geometry of the problem is shown in Fig. 5.1. Since the left side of the slab is

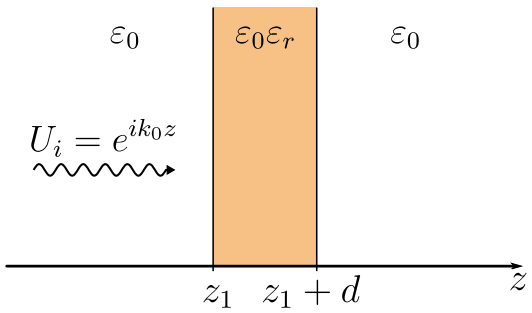

Figure 5.1: Geometry of the 1D problem of scattering by a slab with finite thickness d. The field $U_i(z)$ is a perpendicularly incident plane wave and the background is vacuum and the permittivity of the slab is $\varepsilon_0\varepsilon_r$. The left surface of the slab is at z_1.

located at $z = z_1$, we distinguish three domains $z < z_1$, $z_1 < z < z_1 + d$ and $z > z_1 + d$. The relative permittivity contrast in the three domains reads

$$\Delta\varepsilon_r(z) = \begin{cases} 0 & \text{for } z < z_1, \\ \varepsilon_r - 1 & \text{for } z_1 \leq z \leq z_1 + d, \\ 0 & \text{for } z > z_1 + d. \end{cases} \tag{5.1}$$

The total field $U(z)$ is a component of the electromagnetic field that is perpendicular to z and therefore satisfies the inhomogeneous 1D Helmholtz equation:

$$\frac{\mathrm{d}^2}{\mathrm{d}z^2}U(z) + k_0^2 U(z) = -k_0^2 \Delta\varepsilon_r(z) U(z), \tag{5.2}$$

as well as the boundary conditions that both $U(z)$ and $\mathrm{d}U(z)/\,\mathrm{d}z$ are continuous at the two interfaces $z = z_1$ and $z = z_1 + d$. In the case of TM polarization, $U_i(z)$ is either the x- or y-component of the electric field, and the boundary conditions would hold for E_x or E_y, respectively. For TE polarization, the boundary conditions would similarly hold for either H_x or H_y, depending on whether $U_i(z)$ is the H_x or the H_y component. The free-space Green's function for this equation is:

$$G_0(z; z') = \frac{i}{2k_0} \mathrm{e}^{ik_0|z-z'|}, \tag{5.3}$$

and was listed in Table 2.1.

Although this problem is simple enough to compute all terms of the Born series analytically, it would be very tedious to calculate a high number of terms in the Born series by hand. In this chapter we therefore numerically implement the computation of the Born series and of the Padé approximants. We start with the analytical solution of the scattering problem in Section 5.2.1. There we also calculate the analytical expressions for the lowest-order terms of the Born series for comparison with numerical calculations. In Section 5.3 we discuss the numerical implementation of the Born series and of the Padé approximation for this problem. Lastly, we show results for this one-dimensional problem in Section 5.4. The numerical implementation in this chapter can also be used for other 1D scalar scattering problems with other geometries or permittivity contrasts, including non-constant functions.

5.2 Analytical approach

5.2.1 Analytical solution of the scattering problem

Due to its simplicity, the problem of scattering by a 1D slab has an analytical solution, which will be used to determine the accuracy of the method of Padé approximation. We start by considering the incident field $U_i(z) = \mathrm{e}^{ik_0 z}$, which is a solution to the homogeneous 1D Helmholtz equation

$$\mathrm{d}^2 U(z)/\,\mathrm{d}z^2 + k_0^2 U(z) = 0. \tag{5.4}$$

The total field $U(z) = U_i(z) + U_s(z)$ is found by solving the Helmholtz equation (5.2) in each of the three domains $z < z_1$, $z_1 \leq z \leq z_1 + d$ and $z > z_1 + d$. The solutions are then connected by imposing the boundary conditions, i.e., the continuity of both $U(z)$ and $\mathrm{d}U(z)/\,\mathrm{d}z$, at the two interfaces. The radiation condition at infinity requires that the scattered field propagates outward for $|z| \to \infty$, which means that $U_s(z) = \alpha_1 \mathrm{e}^{-ik_0 z}$ for $z < z_1$ and $U_s(x) = \alpha_3 \mathrm{e}^{ik_0 z}$ for $z > z_1 + d$, with α_1 and α_3 some constants.

We will provide here the analytical solution for the case $z_1 = 0$. The general solution for any z_1 is included in Appendix C. If we denote by $\Delta\varepsilon_r$ the scalar value of the relative permittivity

contrast of the slab and by $n = \sqrt{\Delta\varepsilon_r}$ the refractive index, the analytical solution of this problem reads

$$U(z) = \begin{cases} \mathrm{e}^{ik_0 z} + r_s \mathrm{e}^{-ik_0 z} & \text{for } z < 0, \\ A_+ \mathrm{e}^{ik_0 n z} + A_- \mathrm{e}^{-ik_0 n z} & \text{for } 0 \le z \le d, \\ t_s \mathrm{e}^{ik_0 z} & \text{for } z > d, \end{cases} \tag{5.5}$$

where r_s and t_s are the reflection and transmission coefficients of the slab and where

$$A_\pm = \frac{(n \pm 1) + r_s(n \mp 1)}{2n}. \tag{5.6}$$

The reflection and transmission coefficients read:

$$r_s = r_1 + \frac{t_1 t_2 e^{ik_0 n d}}{1 + r_2 r_1}, \tag{5.7a}$$

$$t_s = \frac{t_1 t_2 r_2 e^{ik_0 n d}}{1 + r_2 r_1}. \tag{5.7b}$$

Here, r_1, t_1, r_2 and t_2 are the Fresnel coefficients of the two interfaces, 1 and 2 corresponding to z_1 and $z_1 + d$, respectively. These Fresnel coefficients are

$$r_1 = -r_2 = \frac{1-n}{1+n} \quad \text{and} \quad t_1 = t_2 = \frac{2\sqrt{n}}{1+n}. \tag{5.8}$$

The reflection r_s is 0 when $n = m\pi/(k_0 d)$ with m an integer.

5.2.2 Born series

While all terms of the Born series can be computed numerically, in this section we are also providing analytical expressions for the first three terms of the series. This is useful for comparison with numerical calculations. Furthermore, an analytical expression of a few orders of the perturbation series helps to identify the transition between the weak- and strong-scattering regime and the physical parameters which control that transition.

The perturbation expansion of the Lippmann-Schwinger equation gives the Born series

$$U^{(\sigma)}(z) = \sum_{\ell=0}^{\infty} U_\ell(z) \sigma^\ell, \tag{5.9}$$

of which the terms can be determined with the integral recurrence relation (2.20). Specifically for the 1D problem, this relation reads

$$U_{\ell+1}(z) = k_0^2 \int_{z_1}^{z_1+d} G_0(z; z') \Delta\varepsilon_r U_\ell(z') \, \mathrm{d}z' \quad \text{for } \ell = 0, 1, 2, \ldots, \tag{5.10}$$

with $U_0(z) = U_i(z)$. Since the slab is homogeneous, we can write

$$U_{\ell+1}(z) = \frac{ik_0 \Delta\varepsilon_r}{2} \int_{z_1}^{z_1+d} \mathrm{e}^{ik_0|z-z'|} U_\ell(z') \, \mathrm{d}z' \quad \text{for } \ell = 0, 1, 2, \ldots, \tag{5.11a}$$

$$= \frac{ik_0 \Delta\varepsilon_r}{2} \cdot \begin{cases} \mathrm{e}^{-ik_0 z} \int_{z_1}^{z_1+d} \mathrm{e}^{ik_0 z'} U_\ell(z') \, \mathrm{d}z' & \text{for } z < z_1, \\ \mathrm{e}^{ik_0 z} \int_{z_1}^{z} \mathrm{e}^{-ik_0 z'} U_\ell(z') \, \mathrm{d}z' + \mathrm{e}^{-ik_0 z} \int_{z}^{z_1+d} \mathrm{e}^{ik_0 z'} U_\ell(z') \, \mathrm{d}z' & \text{for } z_1 \le z \le z_1 + d, \\ \mathrm{e}^{ik_0 z} \int_{z_1}^{z_1+d} \mathrm{e}^{-ik_0 z'} U_\ell(z') \, \mathrm{d}z' & \text{for } z > z_1 + d, \end{cases} \tag{5.11b}$$

where we have substituted Eq. (5.3). In Eq. (5.12) we provide the analytical expressions of the first three terms of the Born series, $U_0(z), U_1(z), U_2(z)$, calculated using Eq. (5.11b) for an incident field that is a plane wave. Each of the terms is expressed as a linear combination of the plane waves $\mathrm{e}^{\pm ik_0 z}$ in each of the three intervals.

$$U_0(z) = \mathrm{e}^{ik_0 z} \quad \text{for all } z. \tag{5.12a}$$

$$U_1(z) = \frac{\Delta\varepsilon_r}{4} \times \begin{cases} \mathrm{e}^{-ik_0 z}\mathrm{e}^{2ik_0 z_1}\left[\mathrm{e}^{2ik_0 d} - 1\right] & \text{for } z < z_1, \\ \mathrm{e}^{+ik_0 z}\left[2ik_0(z - z_1) - 1\right] + \mathrm{e}^{-ik_0 z}\mathrm{e}^{2ik_0(d+z_1)} & \text{for } z_1 \leq z \leq z_1 + d, \\ \mathrm{e}^{+ik_0 z} 2ik_0 d & \text{for } z > z_1 + d. \end{cases} \tag{5.12b}$$

$$U_2(z) = \frac{\Delta\varepsilon_r^2}{16} \times \begin{cases} \mathrm{e}^{-ik_0 z}\mathrm{e}^{2ik_0 z_1}\left[-(\mathrm{e}^{2ik_0 d} - 1) + 2ik_0 d\mathrm{e}^{2ik_0 d}\right] & \text{for } z < z_1, \\ \mathrm{e}^{+ik_0 z}\left[(1 + \frac{1}{2}\mathrm{e}^{2ik_0 d}) - 2ik_0(z - z_1) - k_0^2(z - z_1)^2\right] & \\ \quad + \mathrm{e}^{-ik_0 z}\mathrm{e}^{2ik_0(z_1+d)}\left[-\frac{3}{2} + ik_0(z_1 + 2d - z)\right] & \text{for } z_1 \leq z \leq z_1 + d, \\ \mathrm{e}^{+ik_0 z}\left[-\frac{1}{2}(1 - \mathrm{e}^{2ik_0 d}) - ik_0 d - k_0^2 d^2\right] & \text{for } z > z_1 + d. \end{cases} \tag{5.12c}$$

When considering that the $\ell = 0$ term is the incident field while the $\ell > 0$ terms represent the scattered field, we expect that the $\ell > 0$ terms are radiating outward for $|z| \to \infty$. This is indeed the case for Eq. (5.12). Furthermore it can be checked that each $U_\ell(z)$ and $\mathrm{d}U_\ell(z)/\,\mathrm{d}z$ is continuous at the interfaces $z = z_1$ and $z = z_1 + d$.

An important difference between these Born terms and the analytical solution (5.5) is that in the region inside the slab, $z_1 \leq z \leq z_1 + d$, the analytical solution is expressed in terms of plane waves with wave number $k = k_0 n$ while the Born terms are corrections consisting of plane waves with wave number k_0. This is due to the perturbation series being an expansion in terms of $\Delta\varepsilon_r$ while the wave number $k = k_0 n$ depends on $\Delta\varepsilon_r$ through n.

In Section 2.2.3 we introduced the parameter $\Gamma^{(n)}_{\text{Born}}$ (where n stands for numerical), namely Eq. (2.25), which characterizes the strength of the scattering and is an indicator of the degree of convergence of the Born series. This parameter is calculated from numerical results of the Born series. From the analytical expressions of the Born series, we can deduce a related parameter $\Gamma^{(a)}_{\text{Born}}$. The ratio between the second and first, and first and zero-th perturbation orders is of the order

$$\Gamma^{(a)}_{\text{Born}} = \frac{\pi}{2}\left|\frac{\Delta\varepsilon_r d}{\lambda}\right|, \tag{5.13}$$

where the superscript (a) denotes that it is deduced analytically. This parameter characterizes the strength of the scattering as well: if $\pi/2 \cdot |\Delta\varepsilon_r d/\lambda| > 1$, the series might be diverging. It is not a hard limit, but mostly an indication of the series approaching the divergence condition. In general, this parameter shows that the Born series tends to diverge for large values of the thickness and/or the relative permittivity contrast of the slab.

5.3 Implementation

5.3.1 Implementation of the analytical solution

We compute the analytical solution, as presented in Section 5.2.1, in MATLAB in order to use it as the baseline for comparison with the Padé method. The solution is computed on a spatial grid for each of the three intervals separately. All of the computational steps make use of basic MATLAB functions.

MATLAB app for the analytical solution

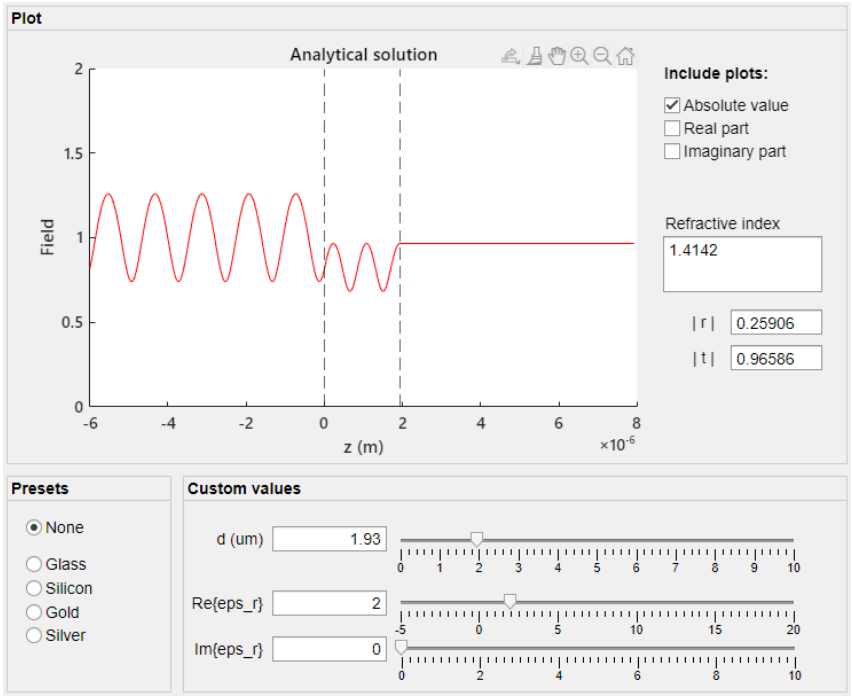

Figure 5.2: MATLAB app that calculates the analytical solution of the scattering by a 1D slab problem. Among its features are choosing a preset object medium and varying the thickness and permittivity with sliders.

We additionally created a MATLAB app with which the analytical solution is plotted in an interactive manner. The app consists of an interface with a plot of the analytical solution and sliders for varying different parameters. An example of the interface is shown in Fig. 5.2. Other features are plotting the real and imaginary parts of the analytical solution and selecting a preset material for the object. This app can be useful for future education purposes since one can play around with different parameters using the sliders, which helps to acquire a visual understanding of the problem.

5.3.2 Implementation of the Born series

The Born series is computed on a 1D spatial grid. The terms are recurrently obtained by repeated numerical integration using Eq. (5.11b) and starting with $U_0(z)$ as the zero-th order

term.

The calculation might seem computationally intensive at first sight, since for each z, we have to evaluate a different integral according to Eq. (5.10). However, we in fact have only two integrals with an integrand that does not change, while only the upper or lower limit differs per value of z. Here, the MATLAB function `cumtrapz`, which calculates the integral cumulatively, is an outcome because it effectively calculates values of an integral of which one of the limits varies.

The most important parameter that influences the accuracy and performance is the grid spacing. Among others the accuracy of the trapezoidal method is heavily affected by it. In all of the cases that are studied in this chapter, we use a resolution of $\Delta z = \lambda/20$.

Generalization to any 1D object

This implementation of the Born series can be generalized for any (bounded) object in 1D, with a possibly varying permittivity $\Delta\varepsilon_r(z)$ as long as it is sufficiently smooth (or piece-wise smooth with finite jumps) and bounded. This also allows for multiple objects. The recurrence relation for the Born series is then,

$$U_{\ell+1}(z) = k_0^2 \int_{z_1}^{z_2} G_0(z; z')\Delta\varepsilon_r(z')U_\ell(z')\,\mathrm{d}z' \quad \text{for } \ell = 0, 1, 2, \ldots \tag{5.14}$$

with again $U_0(z) = U_i(z)$. Like in Eq. (5.11b), the integral is split in one integral over all source points z' to the left of the considered z and one integral over all z' to the right, i.e., for the cases $z' > z$ and $z' < z$, respectively.

5.3.3 Implementation of the Padé approximants

When $2N + 1$ terms of the Born series have been computed, we can calculate the Padé approximant of order $[N/N]$ using the procedure presented in Section 3.6. The Padé coefficients are different for different points in space, so the computation has to be done separately for each point in space. This is done with a loop over all different points. With the $2N + 1$ computed terms of the Born series the approximants $[0/0]$, $[1/1]$, $[2/2], \ldots$, $[N - 1/N - 1]$ can be calculated as well.

5.3.4 Cases and materials

To test the Born-Padé method we consider several cases. We use $\lambda = 400\,\mathrm{nm}$ and consider slabs with a thickness d of $600\,\mathrm{nm}$ and $200\,\mathrm{nm}$ whose left side is located at $z_1 = 0$. Furthermore, we consider three values of ε_r, namely that of a weak-scattering material, a metal and a semiconductor: $\varepsilon_r = 1.2$, $\varepsilon_r = -4.42 + 0.210i$ and $\varepsilon_r = 30.8 + 4.30$, which correspond to a fictitious material, silver and silicon at $\lambda = 400\,\mathrm{nm}$. The latter two have non-vanishing imaginary part, which means they are absorbing materials. In total we consider all combinations of the values of d and ε_r, resulting in six different cases. The wavelength in vacuum is $\lambda = 400\,\mathrm{nm}$ and since the integrands in Eq. (5.11) are complex exponentials that oscillate like a sine function with wave number k_0, we choose to use a resolution of 20 points per wavelength $\lambda = 2\pi/k_0$. Therefore, the grid spacing is set to $\Delta z = 20\,\mathrm{nm}$.

5.4 Results

5.4.1 Analytical solution

The absolute value of the analytical solution is shown in Fig. 5.3 for all six cases. The field for $z < 0$ consists of an incident and reflected wave, according to Eq. (5.5). This causes $|U(z)|$ to be sinusoidal to the left of the slab. Right of the slab, for $z > d$, the field is only a wave propagating to the right, so that $|U(z)|$ is constant. Absorption effects can be seen for the cases of silver and silicon, due to the non-vanishing imaginary component of the relative permittivity.

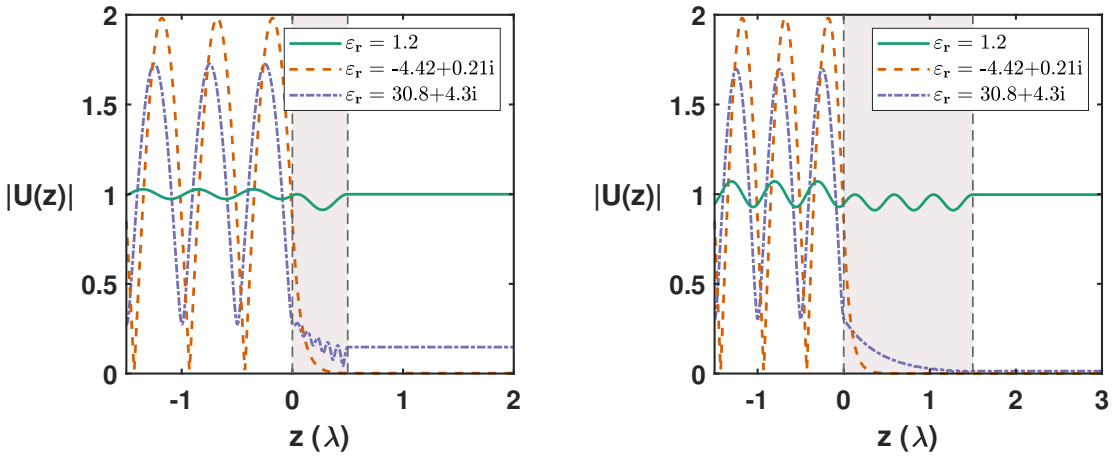

(a) Analytical solution for a slab with $d = 200\,\mathrm{nm}$. **(b)** Analytical solution for a slab with $d = 600\,\mathrm{nm}$.

Figure 5.3: The absolute value of the analytical solution $|U(z)|$ of the 1D slab problem for the six configurations, where the green solid, the orange dotted and the purple dash-dot lines correspond to the weak-scattering material, silver and silicon, respectively. The shaded area bounded by the dotted lines represents the slab. The vacuum wavelength is $\lambda = 400\,\mathrm{nm}$.

5.4.2 Born series

The Born series are calculated for each of the six cases. As an example, we show the first eight terms of the case of a silver slab of $d = 600\,\mathrm{nm}$ in Fig. 5.4. The parameters $\Gamma^{(a)}_{\text{Born}}$ and $\Gamma^{(n)}_{\text{Born}}$, defined by Eq. (5.13) and Eq. (2.25), respectively, characterize the scattering strength for this case $\Gamma^{(a)}_{\text{Born}} = 12.8$ and $\Gamma^{(n)}_{\text{Born}} = 11.7$. This means the Born series strongly diverges, which is clearly seen in the amplitudes of the terms in Fig. 5.4, which increase exponentially. Term U_4 for instance is already of order 10^3 times larger than the incident field. We recall that in Section 2.2.2 it was discussed that for homogeneous objects the permittivity contrast only influences the amplitudes of the terms in the Born series. As a result, the terms shown in Fig. 5.4 are exactly the same for the other cases considered here, up to an overall scalar factor per term. If $\Gamma^{(n)}_{\text{Born}} < 1$, the terms decrease in size and consequently the Born series converges.

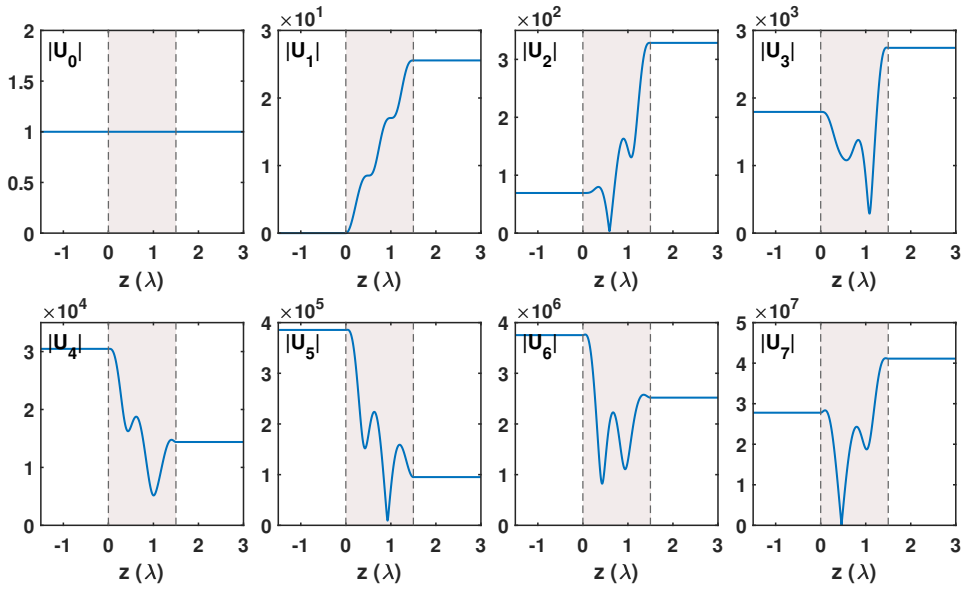

Figure 5.4: The absolute value of each of the first eight terms in the Born series for a slab of silver ($\varepsilon_r = -4.42 + 0.210i$) and for $d = 600\,\mathrm{nm}$ and $\lambda = 400\,\mathrm{nm}$. The shaded area bounded by the gray dotted lines is the slab. Note that the terms increase exponentially.

Convergence

The values of $\Gamma^{(a)}_{\text{Born}}$ and $\Gamma^{(n)}_{\text{Born}}$ for each of the cases are listed in Table 5.1, calculated with Eqs. (2.25) and (5.13), respectively. We consider $\Gamma^{(n)}_{\text{Born}}$ to be a more reliable indicator of the degree of convergence, because $\Gamma^{(a)}_{\text{Born}}$ is a strong simplification of analytical expressions of the first few terms of the Born series, while $\Gamma^{(n)}_{\text{Born}}$ directly follows from numerical calculations of many terms. Still, $\Gamma^{(n)}_{\text{Born}}$ can be larger than 1, but that does not mean the series diverges for *all* points. These parameters indicate that the two cases with permittivity $\varepsilon_r = 1.2$ are in the weak-scattering regime, while the four other cases are indicated to be in the strong-scattering regime. The case whose Born series most strongly diverges is case VI with $\Gamma^{(n)}_{\text{Born}} = 64.7$.

Table 5.1: The six simulated configurations of a 1D slab. The parameters $\Gamma^{(a)}_{\text{Born}}$ and $\Gamma^{(n)}_{\text{Born}}$ give an indication of the degree of convergence of the Born series of each case, where values larger than 1 indicate that the Born series (possibly) diverges.

Case	Material	$\mathrm{Re}(\varepsilon_r)$	$\mathrm{Im}(\varepsilon_r)$	d (nm)	$\Gamma^{(a)}_{\text{Born}}$	$\Gamma^{(n)}_{\text{Born}}$
I	*Fictitious*	1.20	0	200	0.157	0.227
II	Silver	−4.42	0.210	200	4.26	6.15
III	Silicon	30.8	4.30	200	23.6	34.2
IV	*Fictitious*	1.2	0	600	0.471	0.431
V	Silver	−4.42	0.210	600	12.8	11.7
VI	Silicon	30.8	4.30	600	70.9	64.7

The divergence of the Born series in cases II, III, V and VI is clearly seen in Fig. 5.5, where the maximum of the absolute value of the perturbation orders $A_\ell = \max_{\mathbf{r}\in\Omega} |U_\ell(\mathbf{r})|$ are plotted for each of the cases. In Fig. 5.5a, the cases with a slab of thickness $d = 200\,\mathrm{nm}$ are shown, while in Fig. 5.5b the cases with $d = 600\,\mathrm{nm}$ are shown.

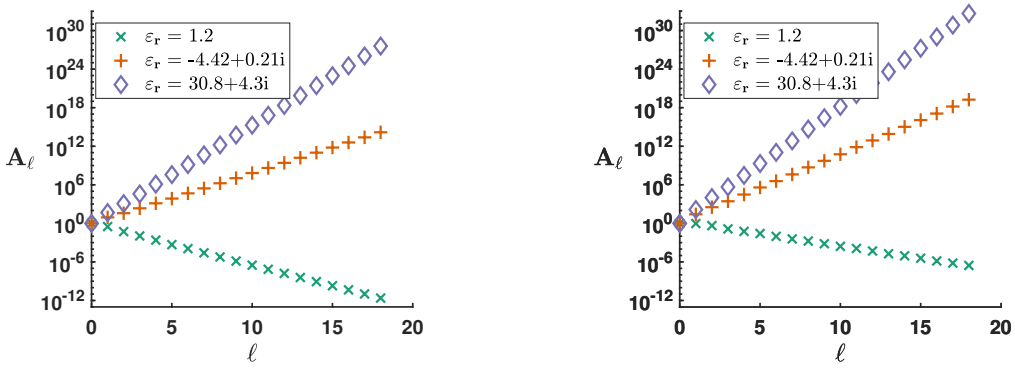

(a) A_ℓ for a slab with $d = 200\,\mathrm{nm}$. **(b)** A_ℓ for a slab with $d = 600\,\mathrm{nm}$.

Figure 5.5: Logarithmic plots of A_ℓ, the maximum of the absolute value of $|U_\ell(\mathbf{r})|$ of the terms in the Born series in order to show the exponential behaviour of the series. The green crosses, the orange pluses and the purple diamonds correspond to slabs of the weak-scattering material, silver and silicon, respectively.

5.4.3 Padé approximation

For each of the cases in Table 5.1, the symmetric Padé approximants $[N/N]$ are calculated up to order $N = 10$. Any order N can be calculated by the algorithm, but in practice it is limited by computer memory and computational time. As an example, we present in Fig. 5.6 the approximants P_1^1 up to P_8^8 for case VI. (We omit P_0^0 because it is the incident field.) For increasing order N the approximants approach the analytical solution, which is the dash-dot orange line, increasingly better. Taking into account that for this case $\Gamma_{\text{Born}}^{(n)}$ is 11.7 and therefore the Born series strongly diverges, it follows that one can extract a useful result from a diverging series by using Padé approximants.

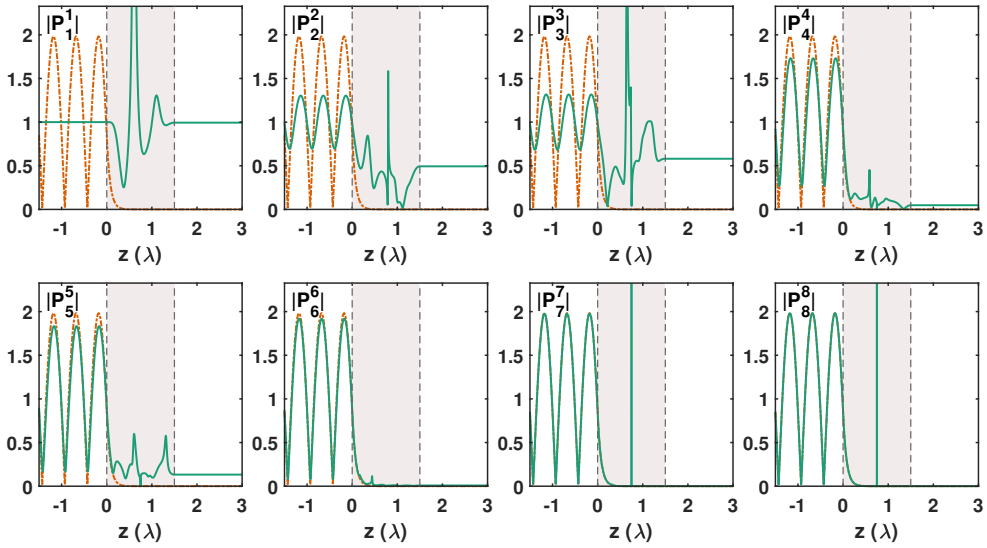

Figure 5.6: The absolute value of the Padé approximants P_N^N, $N = 1, 2, \ldots, 8$, for $d = 600\,\mathrm{nm}$ and the permittivity of silver ($\varepsilon_r = -4.42 + 0.210i$). The dash-dot orange line is the analytical solution and the shaded area bounded by the gray dotted lines is the slab.

To assess how well a certain Padé approximant approximates the analytical solution, we determine the relative error, using the total electric energy inside the slab as norm, i.e.,

$$e_N = \frac{\int_\Omega \mathrm{Re}(\varepsilon_r)|U_{\text{analytical}}(z) - P_N^N(z)|^2 \,\mathrm{d}z}{\int_\Omega \mathrm{Re}(\varepsilon_r)|U_{\text{analytical}}(z)|^2 \,\mathrm{d}z}, \tag{5.15}$$

where Ω is the slab. Also, we define the absolute error of a Padé approximant at a certain point in space, as follows

$$e_{\text{abs},N}(z) = |U_{\text{analytical}}(z) - P_N^N(z)|. \tag{5.16}$$

Acceleration of the convergence of the Born series in the weak-scattering regime

In Section 3.1.1 we discussed the two uses of Padé approximants of which one is accelerating the rate of convergence of converging series. Cases I and IV are in the weak-scattering regime and therefore have a converging Born series, as seen in Fig. 5.5. We use these two cases to show that the Padé approximants can indeed be used to accelerate the convergence. In Fig. 5.7 we compare the Padé approximation with simply summing the (in this case converging) Born series. The relative error, as defined in Eq. (5.15), is plotted for the partial sum of the Born series $U^{[J]}$ and for the Padé approximant $P_{J/2}^{J/2}$. Here, $J = 2N$ and is the highest-order of the Born series that is used when calculating either of the two methods. In Fig. 5.7, $P_{J/2}^{J/2}$ is only included for even J, because that corresponds to integer N. In this way, the accuracy of the two methods can be directly compared. From the figure we see that although the two methods start off equally accurate, the Padé approximant has a lower error for increasing J. At a certain point the decrease in error levels off and the two methods perform equally well. The approximant of the J for which the relative error is minimum is taken as the best approximant.

The cause of this stagnation in the error is not directly understood, but it behaves as if there is a fixed error in the numerical integration, because the error stagnates in both $U^{[J]}$ and $P_{J/2}^{J/2}$. It could be caused by the `cumtrapz` function for instance.

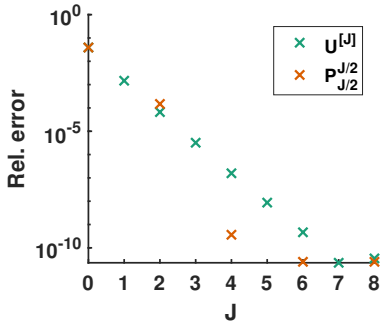

(a) A slab with $d = 200\,\mathrm{nm}$ and $\varepsilon_r = 1.2$.

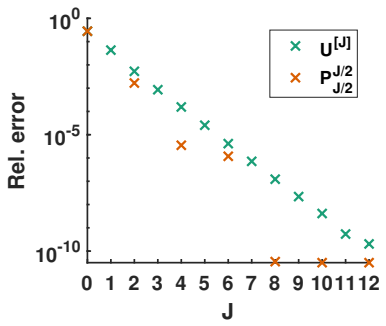

(b) A slab with $d = 600\,\mathrm{nm}$ and $\varepsilon_r = 1.2$.

Figure 5.7: The relative errors of partial sums of the Born series $U^{[J]}$ and of Padé approximants $P_{J/2}^{J/2}$ (for even J). Here, J refers to the highest-order term of the Born series that is used to calculate either $U^{[J]}$ or $P_{J/2}^{J/2}$.

Analytic continuation in the strong-scattering regime

Cases II, III, V and VI are in the strong-scattering regime and have a diverging Born series. In Fig. 5.6 we already saw that the Padé approximants for case VI approximate the exact solution increasingly well for increasing order N. This concerns the other type of use of Padé approximants discussed in Section 3.1, namely that of analytic continuation of a Taylor series. For all four strong-scattering cases we selected the best approximant by determining which approximant has the lowest relative error e_N compared to the analytical solution. For each of the cases, the analytical solution and the best Padé approximant are plotted in Fig. 5.8. Also, the absolute error $e_{\text{abs},N}$ of that approximant is shown as function of z and the relative error e_N is shown per approximant. In the plots we can see that the optimum Padé approximant is very close to the analytical solution in case II with absolute errors less than 10^{-3}. In cases III, V and VI the method retrieves a result with a lower accuracy, but it is still an accurate result considering that the Born series strongly diverges. In cases V and VI a higher-order approximant is required to achieve the same accuracy as in case III. The use of higher-order approximants is hindered by numerical instabilities in all cases.

Numerical instabilities From the e_N plots we observe first a steady decrease of the error for increasing N in both the $d = 200\,\text{nm}$ and $d = 600\,\text{nm}$ cases, but at a certain order the error starts increasing again. For the $d = 200\,\text{nm}$ cases this happens at P_6^6 and for $d = 600\,\text{nm}$ at P_{10}^{10}. This is due to numerical instabilities that arise as the approximants start showing noise-like features. The precise source is not known, but this could among others be caused by round-off errors. In Ref. [8, p. 372] Bender mentions that nonlinear sequence transformations, such as the Shanks transformation, suffer from amplification of round-off errors on computers. In particular he states: "This loss of accuracy becomes compounded in the computation of the iterated Shanks transformations because they converge so rapidly. High-precision computation must be used for their computation. Typically, if the computer arithmetic is accurate to k digits, the results of Shanks transformations will be affected by roundoff error when convergence to only $k/2$ digits is achieved."

Determining the best approximant In Section 3.5.2 we addressed the problem of determining the accuracy of Padé approximants when no analytical solution is available. With the proposed method the difference $e_{\text{consec},N}$ between two subsequent Padé approximants P_{N-1}^{N-1} and P_N^N is computed, as defined in Eq. (3.33). The minimum of $e_{\text{consec},N}$ is supposed to indicate at which order N a higher-order approximant does not offer an improvement anymore. This method returns the correct order N of the actual best approximant for cases II and III. For both cases V and VI the method returns $N = 5$ as the best approximant, which is lower than the the actual best one of order $N = 6$. This is indirectly seen in the plots of e_N in Fig. 5.8, since the error does not decrease in steps that are decreasing in size. If no numerical instabilities were present, we would hope that the approximants would keep converging towards the correct solution, such that finding the best approximant by finding the minimum of $e_{\text{consec},N}$ would be more effective.

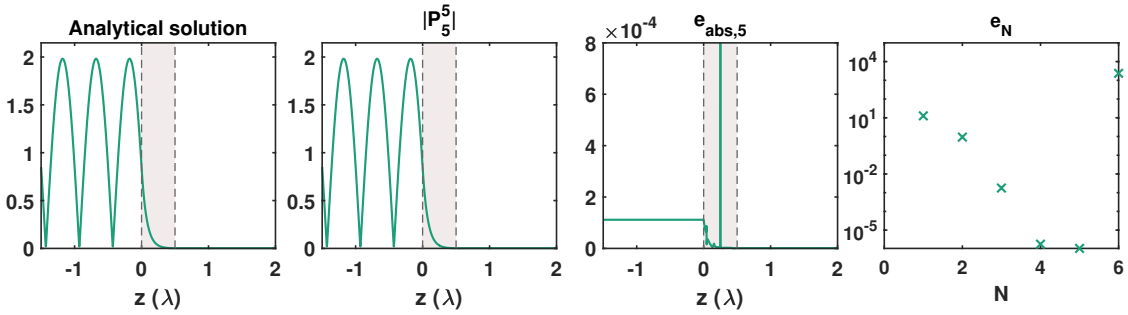

(a) Slab with $d = 200\,\mathrm{nm}$ and the relative permittivity of silver ($\varepsilon_r = -4.42 + 0.210i$).

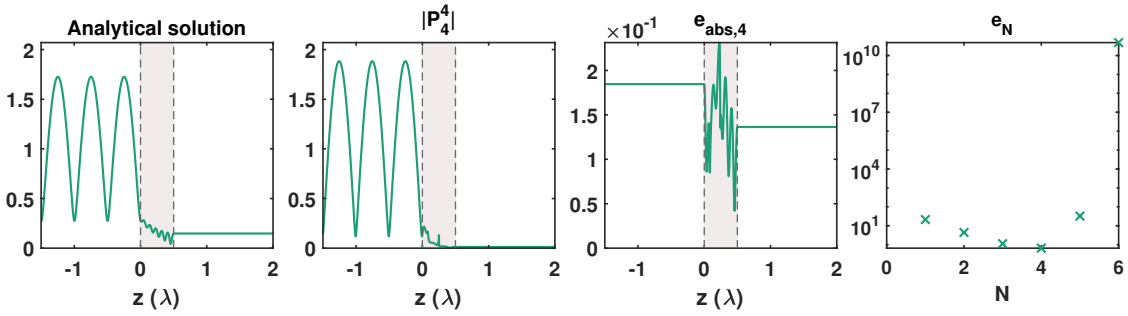

(b) Slab with $d = 200\,\mathrm{nm}$ and the relative permittivity of silicon ($\varepsilon_r = 30.8 + 4.30i$).

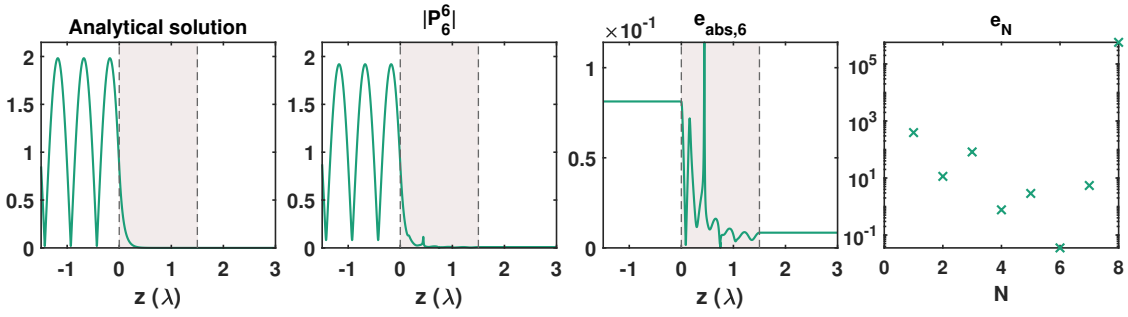

(c) Slab with $d = 600\,\mathrm{nm}$ and the relative permittivity of silver ($\varepsilon_r = -4.42 + 0.210i$).

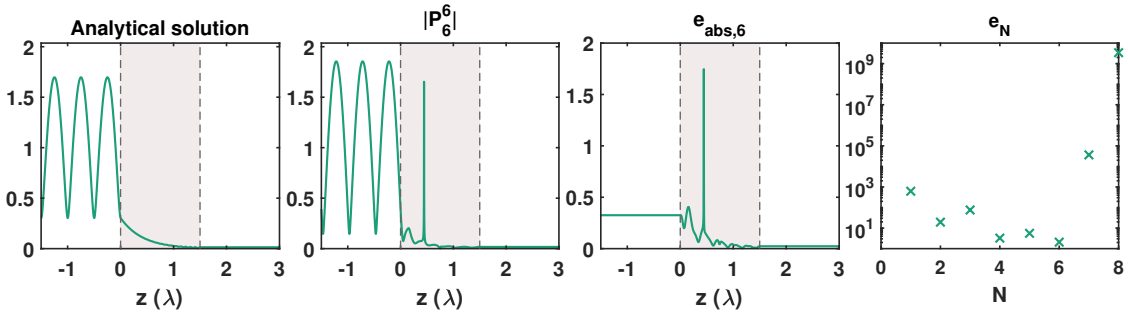

(d) Slab with $d = 600\,\mathrm{nm}$ and the relative permittivity of silicon ($\varepsilon_r = 30.8 + 4.30i$).

Figure 5.8: For the four strong-scattering cases the absolute value of the analytical solution, the best Padé approximant and its local absolute error $e_{\mathrm{abs},N}$ are shown as function of z and in the rightmost figures the relative error Eq. (5.15) is shown for every computed approximant.

CHAPTER 6

2D scattering problem for an infinitely long cylinder

6.1 Scattering by an infinitely long cylinder

In this chapter we turn our attention to a two-dimensional problem. We will consider the scattering of an incident field by an infinitely long cylinder of radius R because, also for this case, an analytical solution exists. The incident field consists of a plane wave, with the direction of propagation perpendicular to the axis of the cylinder. The background permittivity is again that of vacuum ε_0, while the cylinder is homogeneous and made of an isotropic material with (possibly complex) relative electric permittivity ε_r. Hence, the relative permittivity contrast $\Delta\varepsilon_r = \varepsilon_r - 1$ is constant within the cylinder and zero outside.

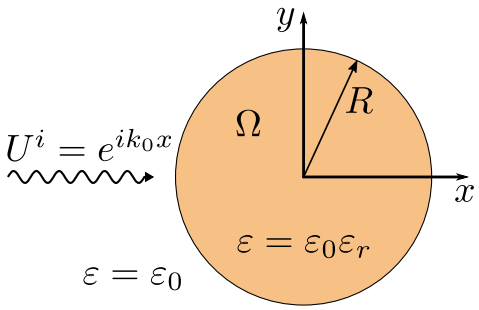

Figure 6.1: Geometry of the two-dimensional problem. The incident plane wave U_i represents either the z-component of the electric field, E_z, or the z-component of the magnetic field, H_z. We will only consider the TM polarization case (namely the E_z case).

We choose a Cartesian coordinate system such that the z-axis coincides with the axis of the cylinder. If the electric and magnetic fields, $\mathbf{E}$ and $\mathbf{H}$, do not depend on z, it can be shown from the source-free Maxwell's equations that two uncoupled Helmholtz equations can be

obtained, one for E_z and one for H_z [56]. The boundary conditions for the fields are then uncoupled as well. Therefore, two polarization states, TM and TE, can be distinguished, where E_z and H_z are parallel to the z-axis, respectively. Here, we will consider TM polarization and we choose the incident field to be a plane wave with $E_z^i(x,y) = \mathrm{e}^{ik_0 x}$, which propagates in the positive x-direction, as illustrated by Fig. 6.1. In TM polarization, the total E_z satisfies the equation

$$\nabla^2 E_z(x,y) + k_0^2 \varepsilon_r(x,y) E_z(x,y) = 0, \tag{6.1}$$

both inside and outside of the cylinder and such that E_z and the normal derivative $\partial E_z/\partial r$ are both continuous at the boundary $r = R$ of the cylinder. Here, $\varepsilon_r(x,y)$ is a scalar function

$$\varepsilon_r(x,y) = \begin{cases} \varepsilon_r, & x^2 + y^2 < R, \\ 1, & x^2 + y^2 > R. \end{cases} \tag{6.2}$$

The total field can be written as the sum of the incident and the scattered field, i.e., $E_z(x,y) = E_z^i(x,y) + E_z^s(x,y)$. Because $E_z^i(x,y)$ is a solution to the Helmholtz equation in vacuum, the scattered part of the field satisfies:

$$\nabla^2 E_z^s(x,y) + k_0^2 E_z^s(x,y) = -k_0^2 \Delta\varepsilon_r(x,y)[E_z^i(x,y) + E_z^s(x,y)], \tag{6.3}$$

as well as the radiation condition at infinity:

$$\lim_{r\to\infty} r^{1/2} \left(\frac{\partial E_z^s}{\partial r} - ik_0 E_z^s \right) = 0. \tag{6.4}$$

The 2D free-space Green's function is:

$$G_0(\mathbf{r};\mathbf{r}') = \frac{i}{4} H_0^{(1)}(k_0|\mathbf{r} - \mathbf{r}'|), \tag{6.5}$$

where $H_0^{(1)}(r)$ is the Hankel function of the first kind. This is the solution which radiates outwards, in contrast to the analogous Green's function with the Hankel function of the second kind $H_0^{(2)}(r)$ which radiates inwards. $H_0^{(1)}(r)$ has a singularity for $r = r'$ that behaves as [57]:

$$H_0^{(1)}(r) \sim \frac{2i}{\pi} \ln(r) \quad \text{as } r \to 0. \tag{6.6}$$

In Section 6.2 we derive the analytical solution of the formulated scattering problem. We then proceed with deriving the analytical expression for the first-order Born approximation in Section 6.3. Subsequently, in Section 6.4 we describe the implementation of the Born series and of the Padé approximants in MATLAB. We test this implementation on a number of cases and we show the results in Section 6.5.

6.2 Analytical solution

The analytical solution of E_z, which satisfies Eq. (6.1), and the boundary conditions will be derived concisely since the derivation can be found in electromagnetic theory textbooks such as Refs. [58, 59], although the notations might differ. Also Ref. [60] provides a general

solution for incoming plane waves under any angle. We use polar coordinates (r, φ) and expand E_z in a Fourier series as function of φ:

$$E_z(r,\varphi) = \sum_{m=-\infty}^{+\infty} \hat{E}_z(r,m)\mathrm{e}^{im\varphi}, \tag{6.7}$$

$$\hat{E}_z(r,m) = \frac{1}{2\pi}\int_0^{2\pi} E_z(r,\varphi)\mathrm{e}^{-im\varphi}\,\mathrm{d}\varphi, \tag{6.8}$$

where $\hat{E}_z(r,m)$ are the Fourier coefficients. Substituting the series in the differential equation (6.1) written in polar coordinates yields Bessel's equation for every $\hat{E}_z(r,m)$:

$$r\frac{\partial}{\partial r}\left(\frac{1}{r}\frac{\partial \hat{E}_z(r,m)}{\partial r}\right) + \left(k_0^2\varepsilon_r - \frac{m^2}{r^2}\right)\hat{E}_z(r,m) = 0. \tag{6.9}$$

Incident field The incident field $E_z^i(x,y)$ can be written as a Fourier series

$$E_z^i(r,\varphi) = \sum_{m=-\infty}^{+\infty} \hat{E}_z^i(r,m)\mathrm{e}^{im\varphi}, \tag{6.10}$$

whose Fourier coefficients $\hat{E}_z^i(r,m)$ are given by Eq. (6.8) and satisfy Bessel's equation (6.9) in the case that the relative permittivity ε_r is set to 1. Bessel's equation has two linearly independent solutions and since the incident field should be finite for all r it should be proportional to $J_m(k_0\sqrt{\varepsilon_r}r)$; the Bessel function of the first kind of order m. For the incident plane wave with unit amplitude we get [61, Ch. 4]:

$$\hat{E}_z^i(r,m) = i^m J_m(k_0 r). \tag{6.11}$$

Scattered field The Hankel function of the first and second kind $H_m^{(1,2)}(k_0 r)$ of order m are the solution to Eq. (6.3). Since the time dependence of E_z is $\mathrm{e}^{-i\omega t}$ and because $\omega > 0$, the Hankel function of the first kind $H_m^{(1)}(k_0 r)$ is the solution that satisfies Eq. (6.4) and thus radiates outwards. Therefore, for the scattered field we have

$$\hat{E}_z^s(r,m) = B_m H_m^{(1)}(k_0 r), \tag{6.12}$$

where the coefficient B_m is to be determined by the boundary conditions.

Field inside the cylinder The solution should be finite, so for $r < R$ we have

$$\hat{E}_z(r,m) = C_m J_m(k_0\sqrt{\varepsilon_r}r), \tag{6.13}$$

where the coefficient C_m is also to be determined.

Total field Putting together the expressions for the incident and scattered field, the total field becomes

$$\hat{E}_z(r,m) = \begin{cases} \hat{E}_z^i(r,m) + \hat{E}_z^s(r,m) = i^m J_m(k_0 r) + B_m H_m^{(1)}(k_0 r) & \text{for } r > R, \\ \hat{E}_z(r,m) = C_m J_m(k_0\sqrt{\varepsilon_r}r) & \text{for } r < R. \end{cases} \tag{6.14}$$

The coefficients B_m and C_m have to be chosen such that the boundary conditions

$$\hat{E}_z(r,m) \quad \text{and} \quad \frac{\partial \hat{E}_z}{\partial r}(r,m) \quad \text{are continuous for } r = R \tag{6.15}$$

are satisfied. This results in the following expressions:

$$B_m = -i^m \frac{J_m(k_0\sqrt{\varepsilon_r}R)J_{m+1}(k_0R) - \sqrt{\varepsilon_r}J_{m+1}(k_0\sqrt{\varepsilon_r}R)J_m(k_0R)}{J_m(k_0\sqrt{\varepsilon_r}R)H^{(1)}_{m+1}(k_0R) - \sqrt{\varepsilon_r}J_{m+1}(k_0\sqrt{\varepsilon_r}R)H^{(1)}_m(k_0R)}, \tag{6.16a}$$

$$C_m = \frac{-2i^{m+1}}{\pi k_0 R} \cdot \frac{1}{J_m(k_0\sqrt{\varepsilon_r}R)H^{(1)}_{m+1}(k_0R) - \sqrt{\varepsilon_r}J_{m+1}(k_0\sqrt{\varepsilon_r}R)H^{(1)}_m(k_0R)}. \tag{6.16b}$$

6.3 Born series

In this section we treat the Born series analytically to find closed-form expressions for the first-order Born approximation of E_z. Initially we do this in the spatial domain, but we also make a connection to the Fourier domain and how to calculate higher-order terms of the Born series in that domain. This lays the foundation for the numerical calculation of the Born series.

6.3.1 Recurrence relation and the Hankel addition theorem

The Born series is obtained by a perturbation expansion of the Lippmann-Schwinger equation (2.9) and the perturbation orders are obtained by a recurrence relation that is derived from this expansion. This recurrence relation is, now denoting E_z by U:

$$U_0(\mathbf{r}) = U_i(\mathbf{r}) = \mathrm{e}^{+ik_0x} = \mathrm{e}^{+ik_0r\cos\varphi} \tag{6.17a}$$

$$U_{\ell+1}(\mathbf{r}) = k_0^2 \int_\Omega G_0(\mathbf{r};\mathbf{r}')U_\ell(\mathbf{r}')\Delta\varepsilon_r(\mathbf{r}')\,\mathrm{d}\mathbf{r}' \tag{6.17b}$$

where Ω is the cylinder and $G_0(\mathbf{r};\mathbf{r}')$ is given by Eq. (6.5). The integrand has a singularity for $r' = r$ due to the Hankel function. One way to compute the integral is by using the addition theorem [61]:

$$H_0^{(1)}(k_0|\mathbf{r}-\mathbf{r}'|) = \begin{cases} \displaystyle\sum_{m=-\infty}^{+\infty} J_m(k_0r)H_m^{(1)}(k_0r')\mathrm{e}^{im(\varphi-\varphi')}, & r \le r', \quad (6.18a) \\ \displaystyle\sum_{m=-\infty}^{+\infty} J_m(k_0r')H_m^{(1)}(k_0r)\mathrm{e}^{im(\varphi-\varphi')}, & r \ge r', \quad (6.18b) \end{cases}$$

which expresses the Hankel function, corresponding to a source at $\mathbf{r} = \mathbf{r}'$, in terms of a sum of Hankel functions with a singularity at the origin. This theorem requires us to distinguish between the cases $r \le r'$ and $r \ge r'$, just like in Chapter 5 where we had to distinguish between source points to the left ($z' < z$) and to the right ($z' > z$) of the point z under consideration.

6.3.2 Analytical calculation of the Born approximation

Although all terms in the Born series can be calculated by numerical integration, we compute the first order of the Born series analytically in order to validate the results of the numerical calculation. The case of a homogeneous cylinder is simple and it is therefore possible to find closed-form expressions for the first-order Born approximation $U_{\text{Born},1} = U_0(\mathbf{r}) + U_1(\mathbf{r})$ using Eq. (6.17b). We derive $U_1(\mathbf{r})$ in this section by distinguishing two regions, namely, $r > R$ and $r < R$, corresponding to points outside and inside the cylinder, respectively.

Region 1: points outside the cylinder

Outside the cylinder we have $r \geq r'$. By substituting Eq. (6.5) and Eq. (6.17a) in Eq. (6.17b) we get

$$U_1(\mathbf{r}) = \frac{ik_0^2 \Delta\varepsilon_r}{4} \int_0^R \int_0^{2\pi} H_0^{(1)}(k_0|\mathbf{r} - \mathbf{r}'|) \mathrm{e}^{ik_0 r' \cos\varphi'} r' \,\mathrm{d}\varphi' \,\mathrm{d}r'. \tag{6.19}$$

Because $r \geq r'$, we substitute Eq. (6.18b):

$$U_1(\mathbf{r}) = \frac{ik_0^2 \Delta\varepsilon_r}{4} \sum_{m=-\infty}^{+\infty} \mathrm{e}^{im\varphi} H_m^{(1)}(k_0 r) \int_0^R r' J_m(k_0 r') \int_0^{2\pi} \mathrm{e}^{ik_0 r' \cos\varphi' - im\varphi'} \,\mathrm{d}\varphi' \,\mathrm{d}r', \tag{6.20}$$

where $\Delta\varepsilon_r(\mathbf{r})$ has been taken outside the integral because it is constant. For the integral over φ' we use the following integral representation [57]:

$$J_m(x) = \frac{1}{2\pi i^m} \int_0^{2\pi} \mathrm{e}^{i(x\cos\tau - m\tau)} \,\mathrm{d}\tau. \tag{6.21}$$

Therefore,

$$U_1(\mathbf{r}) = \frac{i\pi k_0^2 \Delta\varepsilon_r}{2} \sum_{m=-\infty}^{+\infty} i^m \mathrm{e}^{im\varphi} H_m^{(1)}(k_0 r) \int_0^R r' J_m^2(k_0 r') \,\mathrm{d}r'. \tag{6.22}$$

The remaining integral over r is equal to [62]:

$$\int r' J_m^2(k_0 r') \,\mathrm{d}r' = \frac{1}{2} r^2 [J_m^2(k_0 r) - J_{m-1}(k_0 r) J_{m+1}(k_0 r)]. \tag{6.23}$$

Hence,

$$U_1(\mathbf{r}) = \frac{i\pi k_0^2 \Delta\varepsilon_r R^2}{2} \sum_{m=-\infty}^{+\infty} i^m \mathrm{e}^{im\varphi} H_m^{(1)}(k_0 r) \Big[J_m^2(k_0 R) - J_{m-1}(k_0 R) J_{m+1}(k_0 R) \Big] \quad \text{for } r > R. \tag{6.24}$$

This result expresses $U_1(\mathbf{r})$ for $r > R$ in terms of Hankel functions $H_m^{(1)}(k_0 r)$, which satisfy the radiation condition for $r \to \infty$. Although Hankel functions have a singularity at $r = 0$, none of the terms in the series of $U_1(\mathbf{r})$ have a singularity for $r > R$.

Region 2: points inside the cylinder

The computation of $U_1(\mathbf{r})$ is more complicated for $r \leq R$. For a certain point (r, φ) inside the cylinder we have to distinguish between source points (r', φ') closer to and farther away from the origin than (r, φ), corresponding to $r \geq r'$ and $r \leq r'$, respectively. This distinction

results in two integrals over r', one from 0 to r and the other from r to R, in which we use Eq. (6.18a) and Eq. (6.18b), respectively. We find

$$U_1(\mathbf{r}) = \frac{ik_0^2\Delta\varepsilon_r}{4}\int_0^R\int_0^{2\pi} H_0^{(1)}(k_0|\mathbf{r}-\mathbf{r}'|)\mathrm{e}^{ik_0r'\cos\varphi'}r'\,\mathrm{d}\varphi'\,\mathrm{d}r' \tag{6.25a}$$

$$\begin{aligned} &= \frac{i\pi k_0^2\Delta\varepsilon_r}{2}\sum_{m=-\infty}^{+\infty} i^m\mathrm{e}^{im\varphi}\Bigg[H_m^{(1)}(k_0r)\int_0^r r'J_m^2(k_0r')\,\mathrm{d}r' \\ &\qquad + J_m(k_0r)\int_r^R r'H_m^{(1)}(k_0r')J_m(k_0r')\,\mathrm{d}r'\Bigg]. \end{aligned} \tag{6.25b}$$

The first integral in Eq. (6.25b) follows from Eq. (6.23). The second integral is given by [62]:

$$\int J_m(x)H_m^{(1)}(x)x\,\mathrm{d}x = \frac{x^2}{4}\left[2J_m(x)H_m^{(1)}(x) - J_{m+1}(x)H_{m-1}^{(1)}(x) - J_{m-1}(x)H_{m+1}^{(1)}(x)\right]. \tag{6.26}$$

Further simplification of the expression yields:

$$\begin{aligned} U_1(\mathbf{r}) = \frac{i\pi k_0^2\Delta\varepsilon_r}{2}\sum_{m=-\infty}^{+\infty} i^m\mathrm{e}^{im\varphi}\times\Bigg\{&\frac{r}{i\pi k_0}J_m'(k_0r) \\ &+\frac{R^2}{2}J_m(k_0r)\left[J_{m-1}(k_0R)H_m^{(1)\prime}(k_0R) - J_m(k_0R)H_{m-1}^{(1)\prime}(k_0R)\right]\Bigg\} \text{ for } r<R, \end{aligned} \tag{6.27}$$

for which we refer to Appendix D.1 for more details. Here, the prime $'$ denotes a derivative with respect to the argument k_0R. It is seen that all terms of the series are smooth functions of r. It can be checked that the two expressions (6.24) and (6.27) and the normal derivatives of these expressions are equal for $r = R$.

Validity of the first Born approximation

In Section 2.2.1 we discussed the validity of the first Born approximation. When applied to this 2D case of a cylinder with diameter $a = 2R$, the validity criterion reads

$$4k_0^2R^2\,|\Delta\varepsilon_r| \ll 1 \quad \text{for } 2k_0R \ll 1, \tag{6.28a}$$

$$2k_0R\,|\Delta\varepsilon_r| \ll 1 \quad \text{for } 2k_0R \gg 1. \tag{6.28b}$$

For a cylinder with wavelength equal to the diameter $2R$ this implies that $|\Delta\epsilon_r| < \pi/2$.

6.3.3 Born series in the Fourier domain

The Born series can also be computed in terms of the Fourier series. This leads to simpler formulae than in the spatial domain because of the circular symmetry that we can exploit. We can express the field or a term in the Born series in a Fourier series like we did for the analytical solution in Section 6.2, namely,

$$U_\ell(r,\varphi) = \sum_{m=-\infty}^{+\infty}\hat{U}_\ell(r,m)\mathrm{e}^{im\varphi}. \tag{6.29}$$

We recall that the Fourier coefficients of the incident field $U_i(r,\varphi) = \mathrm{e}^{+ik_0 r\cos\varphi}$ are $\hat{U}_i(r,m) = i^m J_m(k_0 r)$. We can substitute the Fourier expansion of term $U_\ell(r,\varphi)$ of the Born series in recurrence relation (6.17b):

$$U_{\ell+1}(r,\varphi) = \frac{ik_0^2\Delta\varepsilon_r}{4}\int_0^R\int_0^{2\pi} H_0^{(1)}(k_0|\mathbf{r}-\mathbf{r}'|)\sum_{m=-\infty}^{+\infty}\hat{U}_\ell(r',m)\mathrm{e}^{im\varphi'}r'\,\mathrm{d}\varphi'\,\mathrm{d}r'. \tag{6.30}$$

We will evaluate this expression for the cases $r > R$ and $r < R$, to be used to (numerically) calculate any term in the Born series.

Region 1: points outside the cylinder

For $r > R$, we always have $r \geq r'$ holds. We substitute Eq. (6.18b) into Eq. (6.30) to obtain

$$U_{\ell+1}(r,\varphi) = \frac{ik_0^2\Delta\varepsilon_r}{4}\sum_{n,m=-\infty}^{+\infty}\mathrm{e}^{in\varphi}H_n^{(1)}(k_0 r)\int_0^R J_n(k_0 r')\hat{U}_\ell(r',m)r'\,\mathrm{d}r'\int_0^{2\pi}\mathrm{e}^{i(m-n)\varphi'}\,\mathrm{d}\varphi'. \tag{6.31}$$

The integral over φ' reduces to $2\pi\delta_{mn}$, where δ is the kronecker delta and hence the following single sum remains:

$$U_{\ell+1}(r,\varphi) = \frac{i\pi k_0^2\Delta\varepsilon_r}{2}\sum_{m=-\infty}^{+\infty}\mathrm{e}^{im\varphi}H_m^{(1)}(k_0 r)\int_0^R J_m(k_0 r')\hat{U}_\ell(r',m)r'\,\mathrm{d}r'. \tag{6.32}$$

The integral is the inner product (or in a sense the overlap) of Fourier coefficient $\hat{U}_\ell(r',m)$ and the Bessel function $J_m(k_0 r')$. This expression is again a Fourier series of the form of Eq. (6.29) with Fourier coefficients

$$\hat{U}_{\ell+1}(r,m) = \frac{i\pi k_0^2\Delta\varepsilon_r}{2}H_m^{(1)}(k_0 r)\int_0^R J_m(k_0 r')\hat{U}_\ell(r',m)r'\,\mathrm{d}r' \quad \text{for } r > R. \tag{6.33}$$

This result is useful because it is a recurrence relation for every Fourier term m separately which contains only an integral over r'. Furthermore, after computing all the integrals over r' corresponding to all the Fourier coefficients m, we can use Eq. (6.32) for any $r > R$. We see that the Fourier coefficients $\hat{U}_{\ell+1}(r,m)$ are outward-radiating Hankel functions in the radial coordinate.

Region 2: points inside the cylinder

We can use the same approach for $r < R$. As in Section 6.3.2, we need to distinguish between source points closer to and farther away from the origin than $\mathbf{r}$, corresponding to $r > r'$ and $r < r'$. We get two integrals and in each we use either Eq. (6.18a) or Eq. (6.18b). The result is

$$\begin{aligned} U_{\ell+1}(r,\varphi) = \frac{i\pi k_0^2\Delta\varepsilon_r}{2}\sum_{m=-\infty}^{+\infty}\mathrm{e}^{im\varphi}\Bigg[&H_m^{(1)}(k_0 r)\int_0^r J_m(k_0 r')\hat{U}_\ell(r',m)r'\,\mathrm{d}r' \\ &+ J_m(k_0 r)\int_r^R H_m^{(1)}(k_0 r')\hat{U}_\ell(r',m)r'\,\mathrm{d}r'\Bigg]. \end{aligned} \tag{6.34}$$

From this we conclude that the Fourier coefficients $\hat{U}_{\ell+1}(r,m)$ are

$$\hat{U}_{\ell+1}(r,m) = \frac{i\pi k_0^2 \Delta\varepsilon_r}{2} \left[H_m^{(1)}(k_0 r) \int_0^r J_m(k_0 r') \hat{U}_\ell(r',m) r' \,\mathrm{d}r' + J_m(k_0 r) \int_r^R H_m^{(1)}(k_0 r') \hat{U}_\ell(r',m) r' \,\mathrm{d}r' \right] \quad \text{for } r < R. \tag{6.35}$$

Note that now the limits of integration depend on r. However, if one would compute the integrals in order of increasing r, one can use the result of the integral of the previous $\tilde{r} < r$ and only compute the integrals over the interval $\tilde{r} < r' < r$.

Coefficients of the first Born term

Taking again a look at the analytical expressions of the first order term $U_1(\mathbf{r})$ in Eqs. (6.24) and (6.27), we see that those expressions are already Fourier expansions and we can simply read off the Fourier coefficients for the $r > R$ and $r < R$ cases separately.

Computing higher-order terms in the Born series

Higher-order terms are found with the two recurrence relations (6.33) and (6.35) in the Fourier domain, of which the former is used to find term $\hat{U}_{\ell+1}(r,m)$ for points outside the cylinder and the latter for points inside the cylinder. Each term can afterwards be inverse Fourier transformed to the spatial domain with Eq. (6.29). In both recurrence relations, the integrals use only the Fourier coefficient of one order lower *inside* the cylinder to calculate the Fourier coefficient of the next order.

Analytical calculation of higher-order Born terms It is possible to analytically calculate higher-order terms of the Born series for this problem, but then one has to resort to hypergeometric functions in order to evaluate the integrals, which however becomes quite cumbersome.

6.4 Implementation

6.4.1 Computation of analytical expressions

Analytical solution

The analytical solution to plane-wave scattering by a cylinder, as described in Section 6.2, is used as a benchmark for the Born-Padé method. Although the solution (6.14) is analytical, it is an infinite series. As a rough estimate, $m_{\text{max}} \approx k_0 r_{\text{max}}$ cylindrical waves are needed for the calculation, where r_{max} is the maximum value of r of the points on which the analytical solution is calculated [63]. For instance, if we calculate the solution for a cylinder of $R = 0.25\lambda$ on a square grid that is 2.5λ wide, r_{max} is approximately 1.77λ (corresponding to one of the corners of the square), which gives $m_{\text{max}} \approx 11$. This number can be taken with a safety margin. The computation of the analytical solution involves no other notable settings.

Analytical expressions of the first-order Born approximation

The analytical expressions for $U_1(\mathbf{r})$ that are derived in Section 6.3.2 are used to validate the numerical integration method of the Born series. We again use the estimate made in the previous paragraph to determine the number of cylindrical waves that are required to include in the calculation.

6.4.2 Implementation of the Born series

In Section 6.3.3 we showed that calculating terms in the Born series using Fourier series is more efficient than repeated integration over the cylinder. Our implementation follows that method and consists of roughly two steps.

Integration The terms in the Born series are calculated by recurrent integration on a grid that is rectangular in (r, φ) coordinates. To determine the required resolution in the radial direction, we consider that the Bessel functions $J_m(k_0 r)$ in the integrands approximately oscillate as a sine with wave number k_0 (which is that in vacuum) [57]. Therefore, we have a radial resolution $\Delta r = \lambda/20$, taking 20 points per vacuum wavelength λ. Concerning the number of cylindrical wave functions, we include the Bessel modes from $m = -m_{\text{max}}$ to $m = +m_{\text{max}}$ in the calculation, where m_{max} is determined as described in Section 6.4.1. We use the trapezoidal method for the integrals and as in Chapter 5, we actually use the `cumtrapz` function in MATLAB instead of `trapz` because of computational efficiency. In future versions of this MATLAB routine, a more efficient integration method can be considered which makes use of a variable grid. This is further discussed in Chapter 7.

Inverse Fourier transform In order to apply the Padé approximation, we have to sum the Fourier series for every order. As a result, every Born order is given on a grid that is rectangular in (r, φ) coordinates. Hence, the final step is interpolating the terms to a rectangular grid in the (x, y) coordinate system. The MATLAB function `interp2` is used with the `spline` method for the interpolation.

Generalization to any 2D geometry

The complexity of the calculations of the Born series is reduced by exploiting the cylindrical symmetry of the considered geometry. However, this is only possible for objects with a circularly symmetric $\varepsilon_r(\mathbf{r})$ profile. We refer to Appendix D.2 for the general recurrence relation for calculating the Born series for any infinitely long cylinder with a possibly non-circular cross-section. If $\varepsilon_r(\mathbf{r})$ is not circularly symmetric, calculating even a few terms in the Born series can become computationally expensive, especially for larger scatterers. This is because for every point of interest $\mathbf{r}$ an integral over the scatterer has to be computed with an integrand that is singular. Possibilities for improving the efficiency of the numerical integration that can be calculated are: performing the convolution as a multiplication in Fourier domain, using stochastic integration as presented in Ref. [64], or treating the singularity separately, such as done in [65].

6.4.3 Implementation of the Padé approximants

We choose to calculate the Padé approximants—and therefore also the Born series—for points both inside and outside the cylinder. Referring to the discussion in Section 3.1.1, we choose for the second option, because it appears to yield more accurate results in simulations. We suspect that the reason is that in the first option a Padé approximation is used for the total field inside the scatterer when evaluating the Lippmann-Schwinger integral. Due to the field inside the scatterer being approximated, the integral magnifies the error of this approximation in the case of strong scattering. Furthermore the computation of the Padé approximants follows the same procedure as for the 1D slab problem in Chapter 5.

6.4.4 Cases and materials

In order to assess the performance of the Born-Padé method, we consider cylinders of different sizes and materials. In all cases we use a wavelength of $\lambda = 400\,\mathrm{nm}$ in vacuum. The materials that we consider are a metal, a semiconductor and a fictitious material. For the latter we choose a permittivity of $\varepsilon_r = 1.35$ and this will be used to simulate relatively weak-scattering cases. For the metal and the semiconductor we choose silver and silicon, respectively, which have a larger relative permittivity. The corresponding values are $\varepsilon_{r,\mathrm{Ag}} = -4.42 + 0.201i$ for silver [66] and $\varepsilon_{r,\mathrm{Si}} = 30.8 + 4.30i$ for silicon [67]. For each material, we perform the calculations for two cylinder radii, namely $R = 100\,\mathrm{nm}$ and $R = 400\,\mathrm{nm}$, which means the cylinder has a diameter of either $\lambda/2$ or 2λ. In total six different configurations are investigated, one for each combination of size and relative permittivity. The cases are listed in Table 6.1.

6.5 Results

6.5.1 Born series

For each of the cases, we calculate the values of two parameters, $\Gamma^{(a)}_{\mathrm{Born}}$ and $\Gamma^{(n)}_{\mathrm{Born}}$ to have a useful indication of the degree of convergence or divergence of a Born series. The latter parameter is calculated numerically as defined by Eq. (2.25) and the former is defined by:

$$\Gamma^{(a)}_{\mathrm{Born}} = \frac{\pi R|\Delta\varepsilon_r|}{\lambda}. \tag{6.36}$$

Here, $\Gamma^{(a)}_{\mathrm{Born}}$ is obtained by considering its definition (5.13) in the 1D slab case, but replacing the thickness d of the slab by the characteristic size of the scatterer in the 2D problem; the diameter $2R$ of the cylinder. The parameter $\Gamma^{(a)}_{\mathrm{Born}}$ serves as an indication of the transition between the weak- and strong-scattering regime. It indicates that the Born series converges or diverges when $\Gamma^{(a)}_{\mathrm{Born}} < 1$ or $\Gamma^{(a)}_{\mathrm{Born}} > 1$, respectively, but is no guarantee for either, as discussed in Section 2.2.3. The parameter $\Gamma^{(n)}_{\mathrm{Born}}$ is determined from the numerical calculations of the Born terms and therefore gives a more realistic indication of the divergence of the series compared to Eq. (6.36). The values of the radii and relative permittivities and the corresponding values of $\Gamma^{(a)}_{\mathrm{Born}}$ and $\Gamma^{(n)}_{\mathrm{Born}}$ are listed for all cases in Table 6.1.

Table 6.1: Specifications of the six simulated configurations in the 2D case. The wavelength is $400\,\mathrm{nm}$ in vacuum.

Case	Material	ε_r	R (nm)	$\Gamma^{(a)}_{\text{Born}}$	$\Gamma^{(n)}_{\text{Born}}$
I	*Fictitious*	1.35	100	0.274	0.365
II	Silver	$-4.42 + i\,0.210$	100	4.26	5.67
III	Silicon	$30.8 + i\,4.30$	100	23.7	31.5
IV	*Fictitious*	1.35	400	1.10	0.938
V	Silver	$-4.42 + i\,0.210$	400	17.0	14.9
VI	Silicon	$30.8 + i\,4.30$	400	94.7	83.0

6.5.2 Padé approximation

Since we also calculate the analytical solution, the quality of the solution obtained through Padé approximants can be assessed by determining the relative error of the Padé approximants, using the total electric energy inside the cylinder as norm,

$$e_N = \frac{\iint_\Omega \mathrm{Re}(\varepsilon_r)|E_{z,\text{analytical}} - P_N^N|^2 \,\mathrm{d}x\,\mathrm{d}y}{\iint_\Omega \mathrm{Re}(\varepsilon_r)|E_{z,\text{analytical}}|^2 \,\mathrm{d}x\,\mathrm{d}y}, \tag{6.37}$$

where Ω is the cylinder. Also, we define the absolute error of a Padé approximant per point, as compared to the analytical solution, as follows

$$e_{\text{abs},N}(\mathbf{r}) = |E_{z,\text{analytical}}(\mathbf{r}) - P_N^N(\mathbf{r})|. \tag{6.38}$$

These two error metrics are analogous to those in Chapter 5.

Acceleration of the convergence of the Born series in the weak-scattering regime

Cases I and IV are weak-scattering cases and the corresponding Born series are convergent. We compare in this case the relative error (6.37) of Padé approximant P_N^N with the analogous relative error with P_N^N replaced by the partial sum of the Born series using $2N+1$ terms. This partial sum is $U^{[2N]}$ as denoted in Eq. (2.23). Note that to compute the Padé approximant P_N^N, $2N+1$ terms of the Born series are needed. The two relative errors are shown in Fig. 6.2 as function of J, which is defined as $J = 2N$. We see that although the Born series is convergent and hence that the partial sums converge to the analytical solution, the Padé approximants outperform the partial sums for the same number of perturbation orders. In case I for example, for both P_3^3 and $U^{[6]}$ we used 7 terms in the Born series to calculate them and the relative error of the Padé approximant is only $e_3 = 3.40 \times 10^{-7}$, while for the partial sum it is 6.96×10^{-5}. In particular case IV has a slowly converging Born series and the Padé approximants achieve errors that are several orders of magnitude smaller. The accuracy saturates at a a certain order, as seen in both Figs. 6.2a and 6.2b. It can among others be caused by the non-vanishing error of the integrals for calculating the terms in the Born series.

Analytic continuation in the strong-scattering regime

The cases II, III, V and VI correspond to cylinders made of silver and silicon, which have a considerably larger relative permittivity than the permittivity in cases I and IV. In Table 6.1 it is

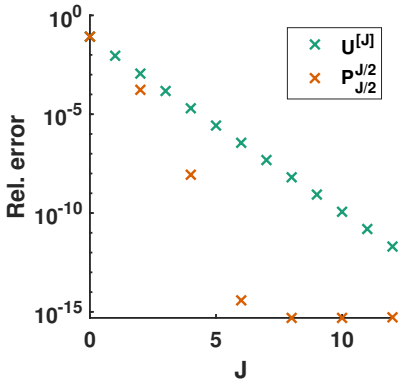

(a) A cylinder with $R = 100\,\mathrm{nm}$ and $\varepsilon_r = 1.35$.

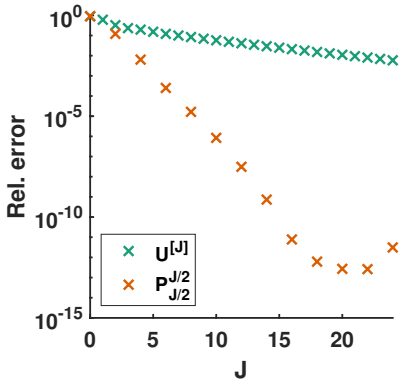

(b) A cylinder with $R = 400\,\mathrm{nm}$ and $\varepsilon_r = 1.35$.

Figure 6.2: The relative errors of partial sums of the Born series $U^{[J]}$ and of Padé approximants $P^{J/2}_{J/2}$ (for even J). Here, J refers to the highest-order term of the Born series that is used to calculate either $U^{[J]}$ or $P^{J/2}_{J/2}$.

seen that configurations II, III, V and VI have values $\Gamma^{(a)}_{\text{Born}}$ and $\Gamma^{(n)}_{\text{Born}}$ that indicate that they are far into the strong-scattering regime. Numerical calculations of the Born terms indeed confirm that in all four cases the series diverges strongly. In Fig. 6.3 we show $A_\ell = \max_{\mathbf{r}} |U_\ell(\mathbf{r})|$ per perturbation order ℓ.

By choosing the N for which (6.37) is minimum, the best Padé approximant of E_z is selected for every case. In Fig. 6.4, the modulus of the analytical solution is shown together with the best Padé approximant and the corresponding absolute error (6.38). Note that the incident field has unit amplitude. Also, a plot of e_N as a function of order N of the approximant is included.

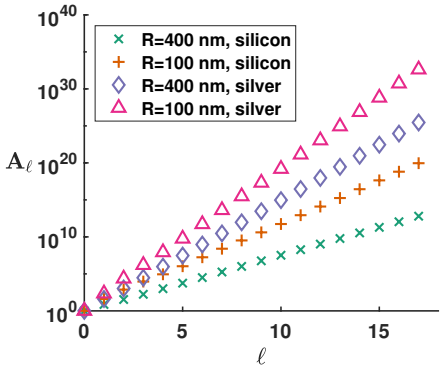

Figure 6.3: The values of $A_\ell = \max_{\mathbf{r}} |U_\ell(\mathbf{r})|$ for $\ell = 0$ to $\ell = 17$ for cases II, III, V and VI of Table 6.1, showing exponential growth.

For all four strong-scattering cases, we observe that the best Padé approximant is similar to the analytical solution, although the error increases for higher values of $\Gamma^{(n)}_{\text{Born}}$ as expected. For instance, the best approximant for case II is P^5_5 and it approximates the analytical solution quite accurately although $\Gamma^{(n)}_{\text{Born}} = 5.67$ which implies that this case is well inside the strong-scattering regime. The maximum of the absolute error $e_{\text{abs},5}(\mathbf{r})$ is 1.3×10^{-4}. Even for the

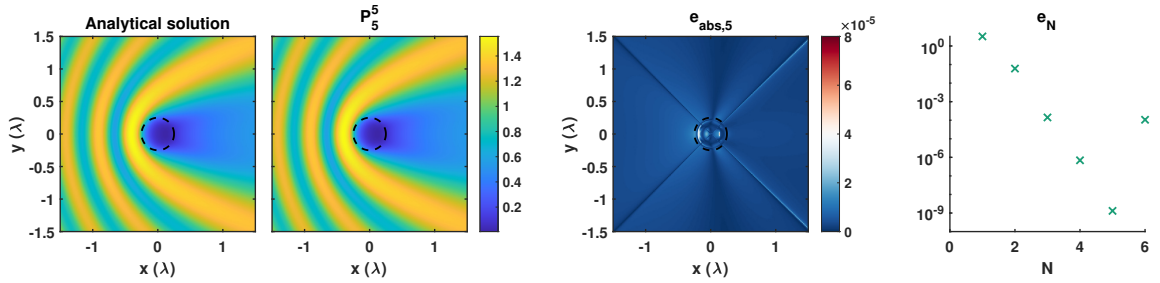

(a) Cylinder with $R = 100\,\mathrm{nm}$ and made of silver.

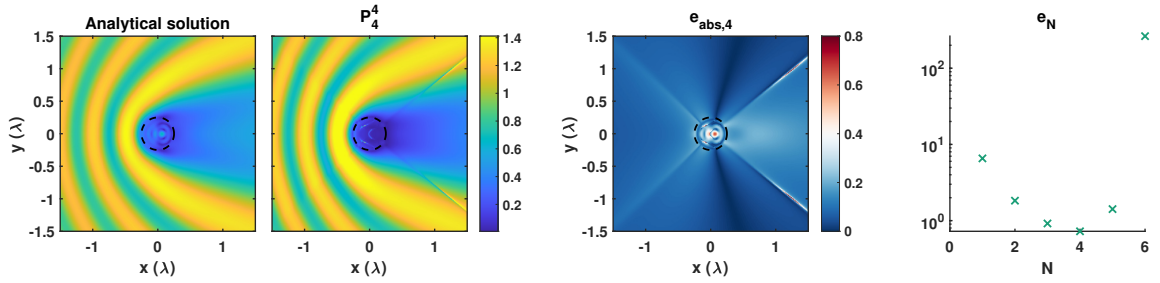

(b) Cylinder with $R = 100\,\mathrm{nm}$ and made of silicon.

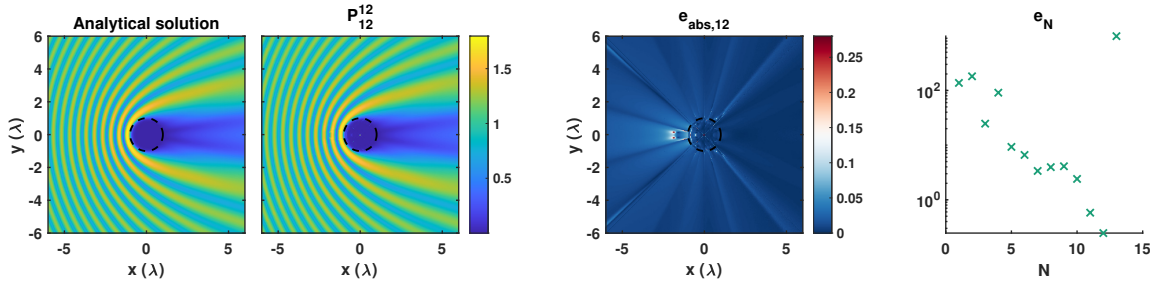

(c) Cylinder with $R = 400\,\mathrm{nm}$ and made of silver.

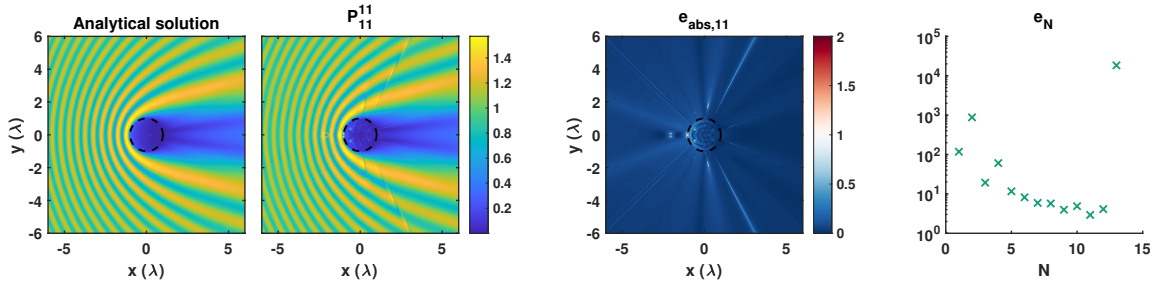

(d) Cylinder with $R = 400\,\mathrm{nm}$ and made of silicon.

Figure 6.4: For the four strong-scattering cases the modulus of the analytical solution, the modulus of the best Padé approximant and its absolute error $e_{\mathrm{abs},N}$, and the relative error e_N per approximant are shown.

configuration with the highest $\Gamma^{(n)}_{\mathrm{Born}}$, case IV, the Padé approximant P^{11}_{11} is still able to retrieve E_z from the first 22 terms of the diverging Born series. Remarkably, the difference between A_0 and A_{22}, the maximum of the modulus of the lowest- and the highest-order Born term, is of order 1×10^{42}. In the majority of cases, the largest point-wise errors (6.38) are found near or within the scattering cylinder.

We remark that the error metric e_N that we use to select the best Padé approximant only takes points inside the cylinder into account. As a consequence, it explains why it is possible that the P_{12}^{12} approximant is more accurate for points outside the cylinder than P_{11}^{11} but has a higher error e_N than P_{11}^{11} has.

Furthermore, in Section 3.5 we mentioned the case of Stieltjes series for which the sequences of $[N/N]$ and $[N/N-1]$ Padé approximants enclose the exact solution. Such an enclosure would give the error of the approximant. Unfortunately, preliminary simulations indicate that the Born series in this problem is not a Stieltjes series.

Numerical instabilities From the plots of e_N we observe that for increasing order N of the approximant, the error decreases quite consistently initially. However, from a certain order, the approximants start to show numerical instabilities and artifacts with noisy features start to dominate. This is the same kind of instability that is observed in the 1D slab problem in Chapter 5. The order N at which this happens, appears to depend mostly on the radius of the cylinder relative to the wavelength λ in vacuum. For $R = 100\,\mathrm{nm}$ this happens from $N = 6$, while for $R = 400\,\mathrm{nm}$ it begins at $N = 13$. A larger relative permittivity increases the amplitude of the noisy features. In numerically stable Padé approximants, often line-like artifacts arising from the cylinder can be observed, as in Fig. 6.4b for instance. These artifacts exist independent of the number of Fourier coefficients.

Determining the best approximant In the case of a cylinder we have the analytical solution at our disposal to determine which Padé approximant is most accurate. According to the idea discussed in Section 3.5.2, we can possibly predict which approximant of order N_{best} is most accurate by computing the difference between consecutive approximants. This approach actually returns the same N for cases II, III and V as when comparing it to the analytical solution. However, for case IV this approach gives $N_{\text{best}} = 12$ instead of $N = 11$.

CHAPTER 7

Conclusions

7.1 Conclusions

Padé approximation can improve results obtained by using the Born series in electromagnetic scattering problems in two ways: convergence acceleration of an already converging Born series and analytic continuation of a series outside its region of convergence. We have applied this method to three electromagnetic scattering problems and we have successfully seen both effects in practice in all three problems.

For an infinitely thin slab in 1D, the Born series is a geometric series that can readily be analytically continued into a function of the form $1/(1-x)$. Padé approximation yields the same result when applied to the Born series of the total field. The $[1/1]$ approximant already retrieves the exact solution, while using only three terms in the series. Also, Padé approximation can retrieve the correct Green's function of the problem when applied to the Dyson expansion.

For the 1D slab of finite thickness and for the 2D cylinder, we considered both weak- and strong-scattering cases. For weak-scattering cases, the approximants yield results sometimes several orders of magnitude more accurate than partial sums of the Born series while using the same number of terms of the Born series. This demonstrates a strongly accelerated rate of convergence. In strong-scattering cases, Padé approximation is able to retrieve a correct result from a number of terms of a strongly diverging series. The accuracy of the results mostly depends on the degree of divergence. We have for instance simulated the case of a cylinder for which the Born series strongly diverges, i.e., with $\Gamma_{\text{Born}}^{(n)} = 5.67$, but for which the Padé approximant of order $N = 5$ has a local absolute error that does not surpass 1×10^{-5}. Under more extreme strong-scattering conditions, such as the case of a cylinder where $\Gamma_{\text{Born}}^{(n)} = 83.0$, the results are still fairly accurate with local errors up to about the order of magnitude of the exact solution, i.e., errors of about 100%.

In general, the local absolute errors of the Padé approximants are larger in points within or near the scattering object. Hence, the Padé method is more accurate when aiming to compute the field in the far-field regime. In all cases, the approximants are increasingly accurate

for increasing order N until the decrease in error stalls at N_{best}, although the error does not always decrease monotonically. Under strong-scattering conditions, numerical instabilities arise at a certain order, depending on the geometry. While it is possible to keep calculating approximants of a higher order, these instabilities preclude us from observing whether higher-order approximants further converge towards the exact solution. In future research the cause of these instabilities should be studied. Possible causes are numerical round-off errors, degeneracy of the system of equations that determine the Padé coefficients and/or the fact that analytic continuation can in general be unstable.

An advantage of Padé approximation over numerical solvers is that the latter are fundamentally limited in accuracy by the resolution of the discretized grid. Padé approximation, in principle, can be computed in any point and can achieve any accuracy, if the scattering integrals are computed with arbitrary precision and the sequence of approximants converges to the correct solution. When using the Fourier series in the case of a cylinder, the accuracy depends on the accuracy of the evaluation of the numerical integrals over radius and on the number of Fourier coefficients taken into the Fourier series.

7.2 Recommendations for further research

We give four recommendations for future research.

More advanced applications First of all, the method can be applied to a 3D problem, such as scattering by a sphere, which is a straightforward extension of the problem of scattering by a cylinder. We have specifically chosen to limit this study to scalar electromagnetic problems, but due to the vectorial nature of electrodynamics, it is highly interesting and almost obligatory to extend the research to vectorial problems. One of the challenges that this would involve, is working with the dyadic Green's function, which has a rather larger singularity. This implies that special care is needed in evaluating the integrals over the scatterers. Ultimately, the application of Padé approximants in measurements techniques should be investigated as a possible way to achieve higher resolutions.

Computational improvements We distinguish between three improvements. The first is making the numerical integration over the scatterers more efficient, for instance by using Fourier transforms or having a grid with possibly varying spacing by making use of interpolation of the numeric data. The second is, as previously mentioned, investigating the cause of the instabilities and its dependence on the properties of the scatterers. Specifically, numerical round-off errors should be investigated, as well as the behaviour of the system of equations for the Padé coefficients. Third, the implementation of the Padé approximation could be made more efficient by employing known recurrence relations between Padé approximants or Padé coefficients of different orders, such as in Section 3.2.4.

Mathematical improvements There are extensions of Padé approximants, such as two-point Padé approximants, so-called type-II approximants, Padé-Fourier and Padé-Laurent approximants. An overview of such extensions is found in Ref. [28], for example. These can be investigated for further improvement of the method and to possibly extend the region of convergence even beyond that of the Padé approximants.

Mathematical understanding As briefly discussed throughout this thesis, the convergence properties of Padé approximants are poorly understood. While the convergence of a sequence of symmetric Padé approximants to the correct solution has been proven for some problems in quantum-mechanical scattering, future research should point out whether this is also the case for (scalar) electromagnetic scattering. It would be particularly nice if the Born series for these electromagnetic scattering problems happened to be a Stieltjes series. Preliminary simulations indicate that this is not the case, unfortunately.

APPENDIX A

Perturbation solution of the Green's function of the Helmholtz equation

A.1 The Green's function of the Helmholtz equation

The scattering problem introduced in Chapter 2 can also be approached from the point of view of the so-called full Green's function of the problem. To start, we consider the Helmholtz equation (2.6) and by using that the incident field $U_i(\mathbf{r})$ satisfies the Helmholtz equation in vacuum (2.4) we get:

$$\left[\nabla^2 + k_0^2 \varepsilon_r(\mathbf{r})\right] U_s(\mathbf{r}) = -k_0^2 \Delta\varepsilon_r(\mathbf{r}) U_i(\mathbf{r}). \tag{A.1}$$

This is an inhomogeneous equation for the scattered field in which the source term contains the incident field only and is therefore known, contrary to Eq. (2.8). Mathematically the same is done in the integral formulation in the step from Eq. (2.9) to Eq. (2.10). Now, we can distinguish between the differential operators $L_0 = [\nabla^2 + k_0^2]$ and $L = [\nabla^2 + k_0^2 \varepsilon_r(\mathbf{r})]$. The free-space operator L_0 is associated with the free-space Green's function (satisfying Eq. (2.5)), while the operator L is associated with the 'full' Green's function of the problem $G(\mathbf{r};\mathbf{r}')$, which satisfies

$$LG(\mathbf{r};\mathbf{r}') = [\nabla^2 + k_0^2 \varepsilon_r(\mathbf{r})] G(\mathbf{r};\mathbf{r}') = -\delta(\mathbf{r} - \mathbf{r}'). \tag{A.2}$$

Since the right-hand side of Eq. (A.1) is a source term, the scattered field can be found with $G(\mathbf{r};\mathbf{r}')$ as follows

$$U_s(\mathbf{r}) = k_0^2 \int_\Omega G(\mathbf{r};\mathbf{r}') \Delta\varepsilon_r(\mathbf{r}') U_i(\mathbf{r}') \, \mathrm{d}\mathbf{r}'. \tag{A.3}$$

Hence, if the Green's function $G(\mathbf{r};\mathbf{r}')$ can be found, the scattered field immediately follows from the incident field. Naturally, the total field is then

$$U(\mathbf{r}) = U_i(\mathbf{r}) + k_0^2 \int_\Omega G(\mathbf{r};\mathbf{r}') \Delta\varepsilon_r(\mathbf{r}') U_i(\mathbf{r}') \, \mathrm{d}\mathbf{r}'. \tag{A.4}$$

A.2 Perturbation expansion

A perturbation expansion also exists for $G(\mathbf{r};\mathbf{r}')$. Namely, when writing each term in the Born series as a repeated integration, we get

$$\begin{aligned} U(\mathbf{r}) = U_i(\mathbf{r}) &- \int_{\mathbf{r}_1} G_0(\mathbf{r};\mathbf{r}_1)V(\mathbf{r}_1)U_i(\mathbf{r}_1)\,\mathrm{d}\mathbf{r}_1 \\ &+ \int_{\mathbf{r}_1}\int_{\mathbf{r}_2} G_0(\mathbf{r};\mathbf{r}_1)V(\mathbf{r}_1)G_0(\mathbf{r}_1;\mathbf{r}_2)V(\mathbf{r}_2)U_i(\mathbf{r}_2)\,\mathrm{d}\mathbf{r}_2\,\mathrm{d}\mathbf{r}_1 - \ldots, \end{aligned} \tag{A.5}$$

where we switched to the notation $V(\mathbf{r}) = -k_0^2\Delta\varepsilon_r(\mathbf{r})$. Interestingly, this can be rewritten (by renaming integration variables) as

$$\begin{aligned} U(\mathbf{r}) = U_i(\mathbf{r}) \\ - \int_{\mathbf{r}_1}\left[G_0(\mathbf{r};\mathbf{r}_1) - \int_{\mathbf{r}_2} G_0(\mathbf{r};\mathbf{r}_2)V(\mathbf{r}_2)G_0(\mathbf{r}_2;\mathbf{r}_1)\,\mathrm{d}\mathbf{r}_2 + \ldots\right]V(\mathbf{r}_1)U_i(\mathbf{r}_1)\,\mathrm{d}\mathbf{r}_1. \end{aligned} \tag{A.6}$$

This equation is very similar to Eq. (A.4) and we can conclude that the terms between the square brackets correspond to an expansion of the full Green's function $G(\mathbf{r};\mathbf{r}')$. This expansion also follows from expanding the so-called Dyson equation—or actually a special case of it—which reads [30]:

$$G(\mathbf{r};\mathbf{r}') = G_0(\mathbf{r};\mathbf{r}') - \int_{\mathbf{r}_1} G_0(\mathbf{r};\mathbf{r}_1)V(\mathbf{r}_1)G(\mathbf{r}_1;\mathbf{r}')\,\mathrm{d}\mathbf{r}_1. \tag{A.7}$$

The Dyson equation for $G(\mathbf{r};\mathbf{r}')$ is analogous to the Lippmann-Schwinger equation for $U(\mathbf{r})$ and is the integral formulation of Eq. (A.2). Explicitly, the series expansion of $G(\mathbf{r};\mathbf{r}')$ reads [68]:

$$\begin{aligned} G(\mathbf{r};\mathbf{r}') = G_0(\mathbf{r};\mathbf{r}') &- \int_{\mathbf{r}_1} G_0(\mathbf{r};\mathbf{r}_1)V(\mathbf{r}_1)G_0(\mathbf{r}_1;\mathbf{r}')\,\mathrm{d}\mathbf{r}_1 \\ &- \int_{\mathbf{r}_2}\int_{\mathbf{r}_1} G_0(\mathbf{r};\mathbf{r}_1)V(\mathbf{r}_1)G_0(\mathbf{r}_1;\mathbf{r}_2)V(\mathbf{r}_2)G_0(\mathbf{r}_2;\mathbf{r}')\,\mathrm{d}\mathbf{r}_1\,\mathrm{d}\mathbf{r}_2 + \ldots \end{aligned}$$

and is known as the resolvent identity. Just like in the perturbation expansion of the field, a perturbation parameter σ can be introduced, such that the series reads

$$G^{(\sigma)}(\mathbf{r};\mathbf{r}') = \sum_{\ell=0}^{\infty} G_\ell(\mathbf{r};\mathbf{r}')\sigma^\ell. \tag{A.8}$$

The terms are recurrently calculated by the following set of equations

$$G_0(\mathbf{r};\mathbf{r}') = G_0(\mathbf{r};\mathbf{r}'), \tag{A.9a}$$

$$G_1(\mathbf{r};\mathbf{r}') = k_0^2\int_\Omega G_0(\mathbf{r};\mathbf{r}_1)\Delta\varepsilon_r(\mathbf{r}_1)G_0(\mathbf{r}_1;\mathbf{r}')\,\mathrm{d}\mathbf{r}_1, \tag{A.9b}$$

$$G_2(\mathbf{r};\mathbf{r}') = k_0^2\int_\Omega G_0(\mathbf{r};\mathbf{r}_1)\Delta\varepsilon_r(\mathbf{r}_1)G_1(\mathbf{r}_1;\mathbf{r}')\,\mathrm{d}\mathbf{r}_1, \tag{A.9c}$$

$$\vdots$$

$$G_{\ell+1}(\mathbf{r};\mathbf{r}') = k_0^2\int_\Omega G_0(\mathbf{r};\mathbf{r}_1)\Delta\varepsilon_r(\mathbf{r}_1)G_\ell(\mathbf{r}_1;\mathbf{r}')\,\mathrm{d}\mathbf{r}_1, \tag{A.9d}$$

where each subsequent iteration is a higher-order correction to the free-space Green's function $G_0(\mathbf{r};\mathbf{r}')$. The equations are likewise analogous to the equations in Eq. (2.20). Once a sufficient number of corrections has been computed, the series can be substituted in Eq. (A.4) to find the total field $U(\mathbf{r})$.

Concluding, we see that the perturbation approach can be equivalently applied to the field and the Green's function, because they both follow from Eq. (A.5). An advantage of the latter is that the result is independent of the incident field, and therefore the scattered field can be calculated for any incident field chosen (though $U_i(\mathbf{r})$ should always satisfy the homogeneous Helmholtz equation). A disadvantage of the Green's function is that it is a function of both $\mathbf{r}$ and $\mathbf{r}'$ and that each term $G_\ell(\mathbf{r};\mathbf{r}')$ has to be calculated for any combination of $\mathbf{r}$ and $\mathbf{r}'$.

APPENDIX B

Computation of Padé approximants for the 1D infinitely thin slab problem

In this appendix we show how to compute the first few symmetric Padé approximants for the problem of scattering by a 1D infinitely thin slab. This is an addition to Section 4.3.3.

Case N=0 For $N = 0$, we have one unknown in the approximant P_0^0, which is equal to the first term in the series. The approximant is simply

$$P_0^0(\sigma) = \frac{A_0^{(0)}}{1} = U_0 = \mathrm{e}^{ik_0 x}. \tag{B.1}$$

Case N=1 We use Eq. (3.13) to calculate the $N = 1$ Padé approximant in terms of the terms of the Born series $U_\ell(x)$ given by Eq. (4.18):

$$P_1^1(\sigma = 1) = U_0 + U_1 \frac{U_1}{U_1 - U_2} \tag{B.2a}$$

$$= \mathrm{e}^{ik_0 x} + \frac{i\Delta\varepsilon_r k_0}{2} \mathrm{e}^{ik_0|x|} \frac{\frac{i\Delta\varepsilon_r k_0}{2} \mathrm{e}^{ik_0|x|}}{\mathrm{e}^{ik_0|x|}\left[\frac{i\Delta\varepsilon_r k_0}{2} - \left(\frac{i\Delta\varepsilon_r k_0}{2}\right)^2\right]} \tag{B.2b}$$

$$= \mathrm{e}^{ik_0 x} - \mathrm{e}^{ik_0|x|} \frac{\Delta\varepsilon_r k_0}{2i + \Delta\varepsilon_r k_0}, \tag{B.2c}$$

which is exactly the analytic solution of $U(x)$.

Case N=2 Now we have to find the coefficients $A_n^{(2)}$ and $B_n^{(2)}$ of

$$P_2^2(\sigma) = \frac{A_0^{(2)} + A_1^{(2)}\sigma + A_2^{(2)}\sigma^2}{1 + B_1^{(2)}\sigma + B_2^{(2)}\sigma^2}. \tag{B.3}$$

The $B_n^{(2)}$ coefficients are calculated using Eq. (3.15) by substituting the expressions for U_ℓ. As a result, the denominators of both $B_1^{(2)}$ and $B_2^{(2)}$ are 0, which is due to the system of equations being singular. The Padé approximant P_2^2 is thus undetermined.

APPENDIX C

General analytical solution of the problem of scattering by a slab

C.1 Analytical solution for any position of the slab

In Chapter 5 we provided the analytical solution of scattering by a slab for the case $z_1 = 0$ in terms of Fresnel coefficients. Here we provide expression for the analytical solution that are valid for any z_1. If we denote by $\Delta\varepsilon_r$ the scalar value of the relative permittivity contrast of the slab and by $n = \sqrt{\Delta\varepsilon_r}$ the refractive index, the analytical solution of this problem reads

$$U(z) = \begin{cases} \mathrm{e}^{ik_0 z} + a_1^- \mathrm{e}^{-ik_0 z} & \text{for } z < z_1, \\ a_2^+ \mathrm{e}^{ik_0 n z} + a_2^- \mathrm{e}^{-ik_0 n z} & \text{for } z_1 \leq z \leq z_1 + d, \\ a_3^+ \mathrm{e}^{ik_0 z} & \text{for } z > z_1 + d, \end{cases} \tag{C.1}$$

where the coefficients a_1^-, a_2^+, a_2^- and a_3^+ are

$$a_1^- = \frac{ik_0}{D}\left[-C^+(n-1)\mathrm{e}^{+ik_0(n+1)z_1} + C^-(n+1)\mathrm{e}^{-ik_0(n-1)z_1}\right], \tag{C.2}$$

$$a_2^\pm = a_3^+ C^\pm, \tag{C.3}$$

$$a_3^+ = \frac{2ik_0}{D}, \tag{C.4}$$

where the coefficients C^+, C^- and D are

$$C^\pm = \frac{(n \pm 1)}{2n}\mathrm{e}^{ik_0(1\mp n)(z_1+d)}, \tag{C.5}$$

$$D = C^+ ik_0(n+1)\mathrm{e}^{+ik_0(n-1)z_1} - C^- ik_0(n-1)\mathrm{e}^{-ik_0(n+1)z_1}. \tag{C.6}$$

APPENDIX D

Additional material related to the 2D infinitely long cylinder problem

D.1 Derivation of the first Born order for points inside the cylinder

In this section we present a more elaborate derivation of the first term $U_1(\mathbf{r})$ of the Born series for points inside the cylinder. In Section 6.3.2, we found after applying the Hankel addition theorem (6.18) that

$$U_1(\mathbf{r}) = \frac{i\pi k_0^2 \Delta\varepsilon_r}{2} \sum_{m=-\infty}^{+\infty} i^m \mathrm{e}^{im\varphi} \left[H_m^{(1)}(k_0 r) \int_0^r r' J_m^2(k_0 r')\,\mathrm{d}r' + J_m(k_0 r) \int_r^R r' H_m^{(1)}(k_0 r') J_m(k_0 r')\,\mathrm{d}r' \right]. \tag{D.1}$$

Using Eq. (6.23) and Eq. (6.26) to evaluate the integrals, we get

$$U_1(\mathbf{r}) = \frac{ik_0^2 \Delta\varepsilon_r}{4} \sum_{m=-\infty}^{+\infty} 2\pi i^m \mathrm{e}^{im\varphi} \left(H_m^{(1)}(k_0 r) \frac{r^2}{2} \left[\underbrace{J_m^2(k_0 r)}_{I} \underbrace{- J_{m-1}(k_0 r) J_{m+1}(k_0 r)}_{II} \right] + J_m(k_0 r) \left\{ \frac{R^2}{4} \left[\underbrace{2J_m(k_0 R) H_m^{(1)}(k_0 R) - J_{m+1}(k_0 R) H_{m-1}^{(1)}(k_0 R) - J_{m-1}(k_0 R) H_{m+1}^{(1)}(k_0 R)}_{III} \right] - \frac{r^2}{4} \left[\underbrace{2J_m(k_0 r) H_m^{(1)}(k_0 r)}_{I} \underbrace{- J_{m+1}(k_0 r) H_{m-1}^{(1)}(k_0 r) - J_{m-1}(k_0 r) H_{m+1}^{(1)}(k_0 r)}_{II} \right] \right\} \right) \tag{D.2}$$

This expression can be simplified by first cancelling the terms denoted by I. Secondly, the terms underlined by II can be reduced by applying the Wronskian [57]:

$$\mathcal{W}\{J_m(x), H_m^{(1)}(x)\} = J_{m+1}(x)H_m^{(1)}(x) - H_{m+1}^{(1)}(x)J_m(x) = \frac{2i}{\pi x}. \tag{D.3}$$

Namely, we use it to find the following identity, where we leave out the dependency (x) for brevity:

$$\begin{aligned}
&- H_m^{(1)}J_{m-1}J_{m+1} + \frac{1}{2}J_m\left(J_{m+1}H_{m-1}^{(1)} + J_{m-1}H_{m+1}^{(1)}\right) && \text{(D.4a)}\\
&= \quad \frac{1}{2}J_{m+1}\left(J_mH_{m-1}^{(1)} - H_m^{(1)}J_{m-1}\right) + \frac{1}{2}J_{m-1}\left(J_mH_{m+1}^{(1)} - H_m^{(1)}J_{m+1}\right) && \text{(D.4b)}\\
&= \frac{i}{\pi x}(J_{m+1} - J_{m-1}) = \frac{-2i}{\pi x}J_m', && \text{(D.4c)}
\end{aligned}$$

where the derivative

$$J_m'(x) = \frac{1}{2}(J_{m-1}(x) - J_{m+1}(x)) \tag{D.5}$$

is used [57]. Third, for the terms underlined by III we use the following recurrence relations for Bessel functions [57]:

$$J_m(x) = \frac{x}{2m}(J_{m+1}(x) + J_{m-1}(x)), \tag{D.6}$$

$$J_m'(x) = J_{m-1}(x) - \frac{m}{x}J_m(x). \tag{D.7}$$

The terms denoted by III can thus be simplified as follows, again leaving out the dependency (x) for brevity:

$$\begin{aligned}
&2J_mH_m^{(1)} - J_{m+1}H_{m-1}^{(1)} - J_{m-1}H_{m+1}^{(1)} && \text{(D.8a)}\\
&= 2J_mH_m^{(1)} - (\frac{2m}{x}J_m - J_{m-1})H_{m-1}^{(1)} - (\frac{2m}{x}H_m^{(1)} - H_{m-1}^{(1)})J_{m-1} && \text{(D.8b)}\\
&= 2J_m(H_m^{(1)} - \frac{m}{x}H_{m-1}^{(1)}) + 2J_{m-1}(H_{m-1}^{(1)} - \frac{m}{x}H_m^{(1)}) && \text{(D.8c)}\\
&= 2(J_{m-1}H_m^{(1)\prime} - J_mH_{m-1}^{(1)\prime}). && \text{(D.8d)}
\end{aligned}$$

Hence, after applying these three steps, we arrive at:

$$\begin{aligned}
U_1(\mathbf{r}) = \frac{ik_0^2\Delta\varepsilon_r}{4}\sum_{m=-\infty}^{+\infty} 2\pi i^m \mathrm{e}^{im\varphi}\Bigg\{&\frac{r}{i\pi k_0}J_m'(k_0r)\\
&+\frac{R^2}{2}J_m(k_0r)\left[J_{m-1}(k_0R)H_m^{(1)\prime}(k_0R) - J_m(k_0R)H_{m-1}^{(1)\prime}(k_0R)\right]\Bigg\},
\end{aligned} \tag{D.9a}$$

which is equal to Eq. (6.27) in the main text.

D.2 Implementation of the Born series for an infinitely long cylinder with any cross-section

Here we give the expressions for the implementation of the Born series for scattering by an infinitely long cylinder with any cross-section—also non-circular. Any term in the Born

series can be calculated in a recurrent manner using numerical integration. Starting with $U_0(\mathbf{r}) = U_i(\mathbf{r})$, the higher-order terms become:

$$U_{\ell+1}(\mathbf{r}) = k_0^2 \int_\Omega G_0(\mathbf{r};\mathbf{r}')U_\ell(\mathbf{r}')\Delta\varepsilon_r(\mathbf{r}')\,\mathrm{d}\mathbf{r}' \tag{D.10a}$$

$$= \frac{ik_0^2\Delta\varepsilon_r}{4}\int_0^R\int_0^{2\pi} H_0^{(1)}(k_0|\mathbf{r}-\mathbf{r}'|)U_\ell(\mathbf{r}')r'\,\mathrm{d}\varphi'\,\mathrm{d}r'. \tag{D.10b}$$

As in Section 6.3.2, we distinguish between points inside and outside the cylinder and accordingly apply the Hankel addition theorem (6.18).

Outside the cylinder For all points outside the cylinder $r \geq r'$ holds, hence by applying the Hankel addition theorem (6.18) one finds:

$$U_{\ell+1}(\mathbf{r}) = \frac{ik_0^2\Delta\varepsilon_r}{4}\int_0^R\int_0^{2\pi}\sum_{m=-\infty}^{+\infty} J_m(k_0r')H_m^{(1)}(k_0r)\mathrm{e}^{im(\varphi-\varphi')}U_\ell(\mathbf{r}')r'\,\mathrm{d}\varphi'\,\mathrm{d}r' \tag{D.11a}$$

$$= \frac{ik_0^2\Delta\varepsilon_r}{4}\sum_{m=-\infty}^{+\infty} H_m^{(1)}(k_0r)\mathrm{e}^{im\varphi}\int_0^R\int_0^{2\pi} J_m(k_0r')\mathrm{e}^{-im\varphi'}U_\ell(\mathbf{r}')r'\,\mathrm{d}\varphi'\,\mathrm{d}r'. \tag{D.11b}$$

The last double integral can be evaluated numerically.

Inside the cylinder Inside the cylinder, both regimes of the Hankel addition theorem apply. Therefore the integral over r is split into two; one from 0 to r and one from r to R:

$$\begin{aligned} U_{\ell+1}(\mathbf{r}) = \frac{ik_0^2\Delta\varepsilon_r}{4}\sum_{m=-\infty}^{+\infty}\mathrm{e}^{im\varphi}\Bigg[&H_m^{(1)}(k_0r)\int_0^r\int_0^{2\pi} J_m(k_0r')\mathrm{e}^{-im\varphi'}U_\ell(\mathbf{r}')r'\,\mathrm{d}\varphi'\,\mathrm{d}r' \\ &+\; J_m(k_0r)\int_r^R\int_0^{2\pi} H_m^{(1)}(k_0r')\mathrm{e}^{-im\varphi'}U_\ell(\mathbf{r}')r'\,\mathrm{d}\varphi'\,\mathrm{d}r'\Bigg]. \end{aligned} \tag{D.12}$$

Here as well the integration should be performed numerically.

D.3 Fourier decomposition of a 2D plane wave

Plane wave propagating in +x-direction

A plane wave e^{ik_0x} propagating in the x-direction can be expressed as a sum of cylindrical waves. As discussed in Section 6.2, this expansion in terms of Bessel functions of the first kind J_m reads:

$$\mathrm{e}^{ik_0x} = \mathrm{e}^{ik_0r\cos\varphi} = \sum_{m=-\infty}^{\infty} i^m J_m(k_0r)\mathrm{e}^{im\varphi}. \tag{D.13}$$

General case

For the general case of a plane wave $\mathrm{e}^{i\mathbf{k_0}\cdot\mathbf{r}}$ of which $\mathbf{k_0}$ makes an angle ψ with respect to the positive x-axis, we can write

$$\mathrm{e}^{i\mathbf{k_0}\cdot\mathbf{r}} = \mathrm{e}^{i(k_xx+k_yy)} = \mathrm{e}^{ik_0r(\cos\varphi\cos\psi+\sin\varphi\sin\psi)} = \mathrm{e}^{ik_0r\cos(\varphi-\psi)}, \tag{D.14}$$

with $k_x = k_0 \cos\psi$ and $k_y = k_0 \sin\psi$. We can find the Fourier expansion by replacing φ in the $\psi = 0$ case (D.13) by $\varphi - \psi$:

$$\mathrm{e}^{i\mathbf{k_0}\cdot\mathbf{r}} = \sum_{m=-\infty}^{\infty} i^m \mathrm{e}^{-im\psi} J_m(k_0 r)\mathrm{e}^{im\varphi} = \sum_{m=-\infty}^{\infty} \mathrm{e}^{-im(\psi-\frac{\pi}{2})} J_m(k_0 r)\mathrm{e}^{im\varphi}. \tag{D.15}$$

The Fourier coefficients are therefore

$$\mathrm{e}^{-im(\psi-\frac{\pi}{2})} J_m(k_0 r). \tag{D.16}$$

The sum (D.15) can alternatively be written in terms of Hankel functions by using the following property [57]:

$$J_m(k_0 r) = \frac{1}{2}\left[H_m^{(1)}(k_0 r) + H_m^{(2)}(k_0 r)\right]. \tag{D.17}$$

Substituting this in Eq. (D.15) gives:

$$\mathrm{e}^{i\mathbf{k_0}\cdot\mathbf{r}} = \sum_{m=-\infty}^{\infty} \frac{i^m}{2} \mathrm{e}^{-im\psi} H_m^{(1)}(k_0 r)\mathrm{e}^{im\varphi} + \sum_{m=-\infty}^{\infty} \frac{i^m}{2} \mathrm{e}^{-im\psi} H_m^{(2)}(k_0 r)\mathrm{e}^{im\varphi}. \tag{D.18}$$

Bibliography

[1] D. L. Colton and R. Kress, *Inverse Acoustic and Electromagnetic Scattering Theory*. Heidelberg: Springer, 2nd ed., 1998.

[2] M. N. O. Sadiku, *Numerical techniques in electromagnetics with MATLAB*. CRC press, 2018.

[3] A. Taflove and S. C. Hagness, *Computational electrodynamics: the finite-difference time-domain method*. Artech House antennas and propagation library, Boston, MA: Artech House, 3rd ed., 2005.

[4] M. G. Moharam and T. K. Gaylord, "Rigorous coupled-wave analysis of planar-grating diffraction," *Journal of the Optical Society of America*, vol. 71, p. 811, 7 1981.

[5] S. Weinberg, "Quasiparticles and the Born series," *Physical Review*, vol. 131, no. 1, pp. 440–460, 1963.

[6] M. Born and E. Wolf, *Principle of optics*. Cambridge: Cambridge University Press, 7th ed., 2003.

[7] A. S. Bereza, A. V. Nemykin, S. V. Perminov, L. L. Frumin, and D. A. Shapiro, "Light scattering by dielectric bodies in the Born approximation," *Physical Review A*, vol. 95, no. 6, pp. 1–6, 2017.

[8] C. Bender and S. Orszag, "Summation of Series," in *Advanced Mathematical Methods for Scientists and Engineers I: Asymptotic Methods for Scientists and Engineers*, ch. 8, New York: Springer, 1999.

[9] M. Znojil, "Iterative solutions of the Lippmann-Schwinger–type equations," *Physical Review A*, vol. 34, pp. 2697–2705, 10 1986.

[10] D. J. Kouri and A. Vijay, "Inverse scattering theory: Renormalization of the Lippmann-Schwinger equation for acoustic scattering in one dimension," *Physical Review E - Statistical Physics, Plasmas, Fluids, and Related Interdisciplinary Topics*, vol. 67, no. 4, p. 12, 2003.

[11] R. E. Kleinman, G. F. Roach, and P. M. van den Berg, "Convergent Born series for large refractive indices," *Journal of the Optical Society of America A*, vol. 7, no. 5, p. 890, 1990.

[12] S. Roy, S. F. Pereira, H. P. Urbach, X. Wei, and O. El Gawhary, "Exploiting evanescent-wave amplification for subwavelength low-contrast particle detection," *Physical Review A*, vol. 96, p. 013814, 7 2017.

[13] O. E. Gawhary, M. C. Dheur, S. F. Pereira, and J. J. Braat, "Extension of the classical Fabry-Perot formula to 1D multilayered structures," *Applied Physics B: Lasers and Optics*, vol. 111, pp. 637–645, 6 2013.

[14] S. Roy, O. El Gawhary, N. Kumar, S. F. Pereira, and H. P. Urbach, "Scanning effects in coherent fourier scatterometry," *Journal of the European Optical Society*, vol. 7, 2012.

[15] F. Simonetti, "Multiple scattering: The key to unravel the subwavelength world from the far-field pattern of a scattered wave," *Physical Review E*, vol. 73, p. 036619, 3 2006.

[16] F. Simonetti, L. Huang, N. Duric, and O. Rama, "Imaging beyond the Born approximation: An experimental investigation with an ultrasonic ring array," *Physical Review E*, vol. 76, p. 036601, 9 2007.

[17] F.-C. Chen and W. C. Chew, "Experimental verification of super resolution in nonlinear inverse scattering," *Applied Physics Letters*, vol. 72, pp. 3080–3082, 6 1998.

[18] S. Tani, "Padé approximant in potential scattering," *Physical Review*, vol. 139, no. 4B, 1965.

[19] S. Tani, "Complete continuity of kernel in generalized potential scattering: I. Short range interaction without strong singularity," *Annals of Physics*, vol. 37, no. 3, pp. 411–450, 1966.

[20] S. Tani, "Complete continuity of kernel in generalized potential scattering: II. Generalized fourier series expansion," *Annals of Physics*, vol. 37, no. 3, pp. 451–486, 1966.

[21] J. L. Gammel and F. A. McDonald, "Application of the padé approximant to scattering theory," *Physical Review*, vol. 142, pp. 1245–1254, 2 1966.

[22] J. S. Chisholm, "Solution of linear integral equations using Padé approximants," *Journal of Mathematical Physics*, vol. 4, no. 12, pp. 1506–1510, 1963.

[23] S. Caser, C. Piquet, and J. Vermeulen, "Padé approximants for a Yukawa potential," *Nuclear Physics B*, vol. 14, no. 1, pp. 119–132, 1969.

[24] J. L. Basdevant and B. W. Lee, "Padé approximation and bound states: Exponential potential," *Nuclear Physics B*, vol. 13, no. 1, pp. 182–188, 1969.

[25] J. A. Tjon, "Padé approximants in three-body calculations," *Physical Review D*, vol. 1, no. 7, pp. 2109–2112, 1970.

[26] W. M. Kloet and J. A. Tjon, "Elastic neutron-deuteron scattering with local potentials," *Annals of Physics*, vol. 79, no. 2, pp. 407–440, 1973.

[27] G. A. Baker, *Essentials of Padé approximants*. New York: Academic Press, 1975.

[28] G. A. Baker and P. Graves-Morris, *Padé Approximants*. Cambridge University Press, 2nd ed., 1996.

[29] T. A. van der Sijs, O. El Gawhary, and H. P. Urbach, "Electromagnetic scattering beyond the weak regime: Solving the problem of divergent Born perturbation series by Padé approximants," *Physical Review Research*, vol. 2, p. 013308, 3 2020.

[30] E. N. Economou, *Green's Functions in Quantum Physics*, vol. 7. Springer Science & Business Media, 2006.

[31] B. A. van Tiggelen and E. Kogan, "Analogies between light and electrons: Density of states and Friedel's identity," *Physical Review A*, vol. 49, pp. 708–713, 2 1994.

[32] D. J. Griffiths and D. F. Schroeter, *Introduction to quantum mechanics*. Cambridge University Press, 2018.

[33] A. Lagendijk and B. A. Van Tiggelen, "Resonant multiple scattering of light," *Physics Report*, vol. 29, no. 3, pp. 143–215, 1996.

[34] T. M. Habashy, R. W. Groom, and B. R. Spies, "Beyond the Born and Rytov approximations: A nonlinear approach to electromagnetic scattering," *Journal of Geophysical Research: Solid Earth*, vol. 98, no. B2, pp. 1759–1775, 1993.

[35] M. Sancer and A. Varvatsis, "A comparison of the Born and Rytov methods," *Proceedings of the IEEE*, vol. 58, no. 1, pp. 140–141, 1970.

[36] K. Iwata and R. Nagata, "Calculation of Refractive Index Distribution from Interferograms Using the Born and Rytov's Approximation," *Japanese Journal of Applied Physics*, vol. 14, p. 379, 1 1975.

[37] M. Slaney, A. C. Kak, and L. E. Larsen, "Limitations of Imaging with First-Order Diffraction Tomography," *IEEE Transactions on Microwave Theory and Techniques*, vol. 32, no. 8, pp. 860–874, 1984.

[38] B. Chen and J. J. Stamnes, "Validity of diffraction tomography based on the first Born and the first Rytov approximations," *Applied Optics*, vol. 37, no. 14, p. 2996, 1998.

[39] G. Osnabrugge, S. Leedumrongwatthanakun, and I. M. Vellekoop, "A convergent Born series for solving the inhomogeneous Helmholtz equation in arbitrarily large media," *Journal of Computational Physics*, 2016.

[40] M. S. Zhdanov and S. Fang, "Quasi-linear series in three-dimensional electromagnetic modeling," *Radio Science*, vol. 32, no. 6, pp. 2167–2188, 1997.

[41] G. Gao and C. Torres-Verdin, "High-Order Generalized Extended Born Approximation for Electromagnetic Scattering," *IEEE Transactions on Antennas and Propagation*, vol. 54, pp. 1243–1256, 4 2006.

[42] H. W. Tseng, K. H. Lee, and A. Becker, "3D interpretation of electromagnetic data using a modified extended Born approximation," *Geophysics*, vol. 68, no. 1, pp. 127–137, 2003.

[43] W. Tarantino and S. Di Sabatino, "Diagonal Padé approximant of the one-body Green's function: A study on Hubbard rings," *Physical Review B*, vol. 99, 2 2019.

[44] C. R. Garibotti and M. Villani, "Continuation in the coupling constant for the total K andT matrices," *Il Nuovo Cimento A (1965-1970)*, vol. 59, no. 1, pp. 107–123, 1969.

[45] C. R. Garibotti and M. Villani, "Padé approximant and the Jost function," *Il Nuovo Cimento A (1965-1970)*, vol. 61, no. 4, pp. 747–754, 1969.

[46] J. H. McGuire, J. E. Golden, and J. Nuttall, "Solution of the schödinger equation using Padé approximants to sum asymptotic series," *Rocky Mountain Journal of Mathematics*, vol. 4, no. 2, pp. 375–376, 1974.

[47] P. Graves-Morris, "Padé Approximants for Linear Integral Equations?," *IMA Journal of Applied Mathematics*, vol. 21, pp. 375–378, 6 1978.

[48] I. R. Lapidus, "Phase Shifts for Scattering by a One-Dimensional Delta-Function Potential," *American Journal of Physics*, vol. 37, pp. 930–931, 9 1969.

[49] R. M. Cavalcanti, "Exact Green's functions for delta-function potentials and renormalization in quantum mechanics," *Revista Brasileira de Ensino de Física*, vol. 21, pp. 336–340, 9 1999.

[50] P. Boonserm and M. Visser, "Quasi-normal frequencies: Key analytic results," *Journal of High Energy Physics*, vol. 2011, no. 3, pp. 1–28, 2011.

[51] J. Boos, V. P. Frolov, and A. Zelnikov, "Quantum scattering on a delta potential in ghost-free theory," *Physics Letters, Section B: Nuclear, Elementary Particle and High-Energy Physics*, vol. 782, pp. 688–693, 2018.

[52] I. R. Lapidus, "Born Series for Scattering by a One-Dimensional Delta-Function Potential," *American Journal of Physics*, vol. 37, pp. 1064–1065, 10 1969.

[53] J. Gilewicz and M. Pindor, "Padé approximants and noise: A case of geometric series," *Journal of Computational and Applied Mathematics*, vol. 87, no. 2, pp. 199–214, 1997.

[54] S. H. Patil and A. S. Roy, "Two-centre double delta-function potential in one dimension," *Physica A: Statistical Mechanics and its Applications*, vol. 253, pp. 517–529, 5 1998.

[55] S.-L. Nyeo, "Regularization methods for delta-function potential in two-dimensional quantum mechanics," *American Journal of Physics*, vol. 68, no. 6, pp. 571–575, 2000.

[56] J. J. Bowman, T. B. A. Senior, and P. L. E. Uslenghi, *Electromagnetic and acoustic scattering by simple shapes*. New York: Hemisphere, 1987.

[57] M. Abramowitz and I. A. Stegun, *Handbook of mathematical functions with formulas, graphs, and mathematical tables*, vol. 55. US Government printing office, 1948.

[58] M. Kerker, *The scattering of light and other electromagnetic radiation*. Academic Press, New York, 2013.

[59] R. F. Harrington, *Time-Harmonic Electromagnetic Fields*. New York: IEEE, 2001.

[60] F. Frezza, F. Mangini, and N. Tedeschi, "Introduction to electromagnetic scattering: tutorial," *Journal of the Optical Society of America A*, vol. 35, p. 163, 1 2018.

[61] C. A. Balanis, *Advanced Engineering Electromagnetics*. John Wiley & Sons, 1999.

[62] Y. L. Luke, *Integrals of Bessel functions*. Courier Corporation, 2014.

[63] W. J. Wiscombe, "Improved Mie scattering algorithms," *Applied Optics*, vol. 19, no. 9, p. 1505, 1980.

[64] M. Sadiku, *Monte Carlo Methods for Electromagnetics*. Boca Raton: CRC Press, 2009.

[65] G. Gao, C. Torres-Verdín, and T. M. Habashy, "Analytical techniques to evaluate the integrals of 3D and 2D spatial dyadic Green's functions," *Progress in Electromagnetics Research*, vol. 52, pp. 47–80, 2005.

[66] P. B. Johnson and R. W. Christry, "Optical Constants of the Noble Metals," *Physical Review B*, vol. 6, no. 12, pp. 4370–4379, 1972.

[67] D. E. Aspnes and A. A. Studna, "Dielectric functions and optical parameters of Si, Ge, GaP, GaAs, GaSb, InP, InAs, and InSb from 1.5 to 6.0 eV," *Physical Review B*, vol. 27, pp. 985–1009, 1 1983.

[68] I. Starshynov, *Quantum and classical correlations of multiply scattered light*. PhD thesis, University of Exeter, 2018.